NSF/ENG-88007

日
米

U.S. - JAPAN COORDINATED PROGRAM
FOR
MASONRY BUILDING RESEARCH

REPORT NO. 4.1-1

SEISMIC BEHAVIOR OF FLANGED MASONRY SHEAR WALLS

by

HE LIMIN
and
M.J. NIGEL PRIESTLEY

MAY 1988

supported by:

NATIONAL SCIENCE FOUNDATION

GRANT NO. CES-8722864

DEPARTMENT OF APPLIED MECHANICS & ENGINEERING SCIENCES
UNIVERSITY OF CALIFORNIA, SAN DIEGO, CA

PREFACE

The work reported herein was supported by the New Zealand Ministry of Works and Development, the University of Canterbury, National Science Foundation Grant No. CES-8722864, and UCSD Academic Senate Grant RM-1179.

Any opinions, findings, or conclusions or recommendations expressed in this document are those of the author and do not necessarily reflect the views of the National Science Foundation and the U.S. Government.

50272-101

REPORT DOCUMENTATION PAGE	1. REPORT NO. NSF/ENG-88007	2.	3. Recipient's Accession No. PB89 147987 AS

4. Title and Subtitle
Seismic Behavior of Flanged Shear Walls (U.S.-Japan Coordinated Program for Masonry Building Research)

5. Report Date
May 1988

6.

7. Author(s)
H. Limin; M.J.N. Priestley

8. Performing Organization Rept. No.
4.1-1

9. Performing Organization Name and Address
University of California at San Diego
Department of Applied Mechanics and
Engineering Sciences
San Diego, CA 92110

10. Project/Task/Work Unit No.

11. Contract(C) or Grant(G) No.
(C)
(G) CES8722864

12. Sponsoring Organization Name and Address
Directorate for Engineering (ENG)
National Science Foundation
1800 G Street, N.W.
Washington, DC 20550

13. Type of Report & Period Covered

14.

15. Supplementary Notes

16. Abstract (Limit: 200 words)

This report summarizes the results of a research project representing preliminary studies into the flexural strength, ductility, and seismic response of T-Section Masonry Walls. The project consisted of two sections: (1) analytical studies resulting in the development of dimensionless design charts for flexural strength, stiffness and ductility capacity of unconfined and confined T-section walls loaded in the two opposite directions parallel to the web; and (2) shake table testing of a full-size wide-flange T-section wall under sinusoidal and simulated earthquake acceleration input focusing on the expected asymmetric response, and the shear lag in the flange. Results confirmed the importance of the directionality of strength and stiffness characteristics.

17. Document Analysis a. Descriptors

Masonry
Flexural strength
Stiffness
Walls
Ductility
Mechanical properties

b. Identifiers/Open-Ended Terms

Earthquake engineering
Seismic response
Shake table tests
T-section masonry walls

c. COSATI Field/Group

18. Availability Statement	19. Security Class (This Report)	21. No. of Pages
NTIS		134
	20. Security Class (This Page)	22. Price

(See ANSI-Z39.18) See Instructions on Reverse OPTIONAL FORM 272 (4-7)
(Formerly NTIS-35)
Department of Commerce

日
米

U.S. - JAPAN COORDINATED PROGRAM

FOR

MASONRY BUILDING RESEARCH

REPORT NO. 4.1-1

SEISMIC BEHAVIOR OF FLANGED MASONRY SHEAR WALLS

by

HE LIMIN
and
M.J. NIGEL PRIESTLEY

MAY 1988

supported by:

NATIONAL SCIENCE FOUNDATION

GRANT NO. CES-8722864

DEPARTMENT OF APPLIED MECHANICS & ENGINEERING SCIENCES
UNIVERSITY OF CALIFORNIA, SAN DIEGO, CA

ABSTRACT

This report summarizes the results of a research project representing preliminary studies into the flexural strength ductility and seismic response of T-Section Masonry Walls. The project consisted of two sections:

1. Analytical studies resulting in the development of dimensionless design charts for flexural strength, stiffness and ductility capacity of unconfined and confined T-section walls loaded in the two opposite directions parallel to the web.

2. Shake Table Testing of a full-size wide-flange T-section wall under sinusoidal and simulated earthquake acceleration input, in order to gain preliminary confirmation of theoretical prediction. Of interest were the expected asymmetric response, and the shear lag in the flange.

Results of the analytical and experimental phase of the project confirmed the importance of the directionality of strength and stiffness characteristics. Despite the squat nature of the test unit and the wide flange, shear lag effects were not found to be particularly significant, and predicted strength calculated on the basis of full participation of the flange agreed closely with measured values.

ACKNOWLEDGEMENTS

The research project described in this report was initiated at the University of Canterbury, New Zealand, and completed at the University of California, San Diego. Funding for the research carried out in New Zealand was provided by the New Zealand Ministry of Works and Development, and by the University of Canterbury. The research carried out at San Diego was funded in part by UCSD Academic Senate Grant RM-1179, and in part by NSF Grant No. CES-8722864 (Dr. A.J. Eggenberger cognizant NSF program official) as part of the TCCMAR coordinated masonry research program.

Experimental work was carried out in the Structures Laboratory, Dept. of Civil Engineering, University of Canterbury. The authors would particularly like to express this appreciation to G.E. Hill and G.H. Clarke for assistance and advice during the dynamic tests. Drafting by Val Grey, and typing by Gina Correia and Jan Lightsey is also gratefully acknowledged.

Any opinions, findings, conclusions, or recommendations expressed in this paper are those of the authors alone and do not necessarily reflect the view of the New Zealand Ministry of Works, the National Science Foundation, TCCMAR, or the governments of the United States or New Zealand.

TABLE OF CONTENTS

LIST OF FIGURES

LIST OF TABLES

NOMENCLATURE

A_{st}	=	Total longitudinal (flexural) steel area in section
A_v	=	Area of transverse (shear) reinforcement
d	=	Effective depth of section
E	=	Modulus of elasticity
E_m	=	Masonry modulus of elasticity
f_m	=	Masonry compression stress
f'_m	=	Masonry crushing strength
f_y	=	Reinforcement yield stress
g	=	Acceleration due to gravity; effective section parameter
h	=	Wall height
h"	=	Lateral dimension of confined core
I	=	Section moment of inertia
I_e	=	Effective moment of inertia (cracked section analysis)
K	=	Compression strength enhancement ratio resulting from confinement
ℓ	=	Wall length
ℓ_f	=	Effective length of flange
ℓ_w	=	Length of web
M	=	Moment
M_E	=	Experimentally measured moment
M_i	=	Nominal (calculated) moment capacity
M_T	=	Theoretical moment capacity
M_y	=	Yield moment of section
N	=	Axial load on section (in references)
P	=	Dimensionless mechanical reinforcement ratio parameter
P_e	=	Axial load on section (design charts, experiment)
S	=	Spacing of transverse (shear) reinforcement
S_h	=	Spacing of confinement layers (= block height)
T	=	Time
t	=	Wall thickness
t_f	=	Flange thickness
t_w	=	Web thickness
V_i	=	Ideal (nominal) shear strength

ϵ	=	Strain
ϵ_m	=	Masonry compression strain
ϵ_y	=	Yield strain of reinforcement
ϵ_{cu}	=	Masonry ultimate compression strain
ϕ_u	=	Dimensionless ultimate curvature
ϕ_y	=	Dimensionless yield curvature
ψ	=	Curvature
Δ	=	Yield displacement
Δ_u	=	Ultimate displacement
ρ	=	Reinforcement ratio
ρ_f	=	Reinforcement ratio in flange
ρ_w	=	Reinforcement ratio in web

Note: Dimensionless parameters for analysis in Chapter 2 are defined in the text.

CHAPTER 1: INTRODUCTION

In recent years, the seismic performance of rectangular section masonry structural walls has been investigated in analytical and experimental studies in some detail.[1-7] Experimental studies at the University of Canterbury by Priestley, of heavily reinforced squat walls[1] and more slender walls[2,4] loaded in-plane under simulated seismic loading have confirmed the applicability of ultimate strength design equations for masonry structural walls, and have demonstrated that ductile flexural response can result, provided capacity design procedures are applied, ensuring that shear strength exceeds the maximum feasible flexural strength. Tests at the University of California, Berkeley by Mayes et al [3] on pier elements have investigated the shear failure mode of squat elements under double bending. Priestley has carried out analytical studies in dimensionless form to produce design charts predicting the ductility capacity of unconfined and confined masonry walls of rectangular sections.[5] Dimensionless design charts for flexural strength of rectangular section walls have also recently been developed by Priestley[6], who showed that flexural strength was relatively insensitive to the fashion in which the flexural reinforcement was distributed, provided the distribution was symmetrical about the wall centerline.

Recent and continuing studies at the University of Colorado by Shing et al[7] are concentrating on defining the strength of masonry shear-resisting mechanisms, again with rectangular section walls, as part of the U.S. side of the research under the auspices of the U.S./Japan Technical Coordinating Committee on Masonry Research [TCCMAR][8].

In many practical design situations, the structural requirements for lateral strength in the two principle orthoganal directions of masonry structures will result in interesting shear walls, creating structural elements of flanged shape, such as I,

T or [section walls. Although these elements are probably more common in the 'real world' than rectangular section walls, there has been surprisingly little research emphasis to develop an understanding of the performance of such sections under seismic response.

Current work by Abrahms[9] at the University of Illinois, Urbana/Champaign involves structural testing of simple masonry structures including flanged elements. Apart from this work, which is limited in scope, there appears to have been no systematic study of the behavior of flanged masonry walls. It is of interest, and concern, that the lack of relevant experimental data on flanged walls extends to reinforced concrete shear walls, as well as masonry walls.

Of particular interest is the T-section wall shape depicted in Fig. 1-1 with acceleration parallel to the web, as shown. Such walls have different flexural strengths, stiffness and ductility capacities in the two opposite loading directions parallel to the web, as idealized, for example, in Fig. 1-2. When the flange is in tension, the flexural strength and stiffness are greater than when the flange is in compression, but the ultimate displacement, and hence the displacement ductility capacity is greatly reduced. Clearly the stiffness of such a wall relative to other lateral load resisting elements, and the contribution to lateral strength will depend on the direction of seismic attack. Although this directionality effect has been understood by many designers for some time, the effects have not previously been quantified.

There are other problems associated with T-Section walls. Flexural strength design will normally be dictated by the weak direction (that is, with the flange in compression) and web reinforcement for response parallel to the web will be based on provided adequate flexural strength in this direction of loading. Reinforcement in the flange will normally be dictated by strength

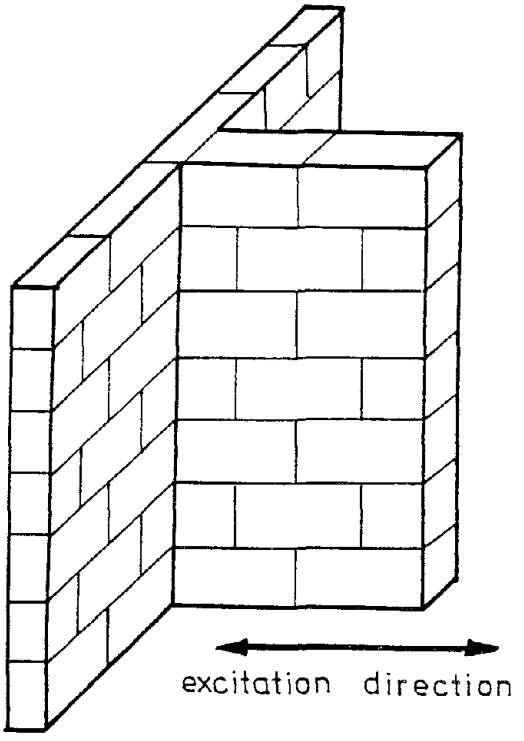

FIG. 1-1 T-SECTION WALL EXCITED PARALLEL TO WEB

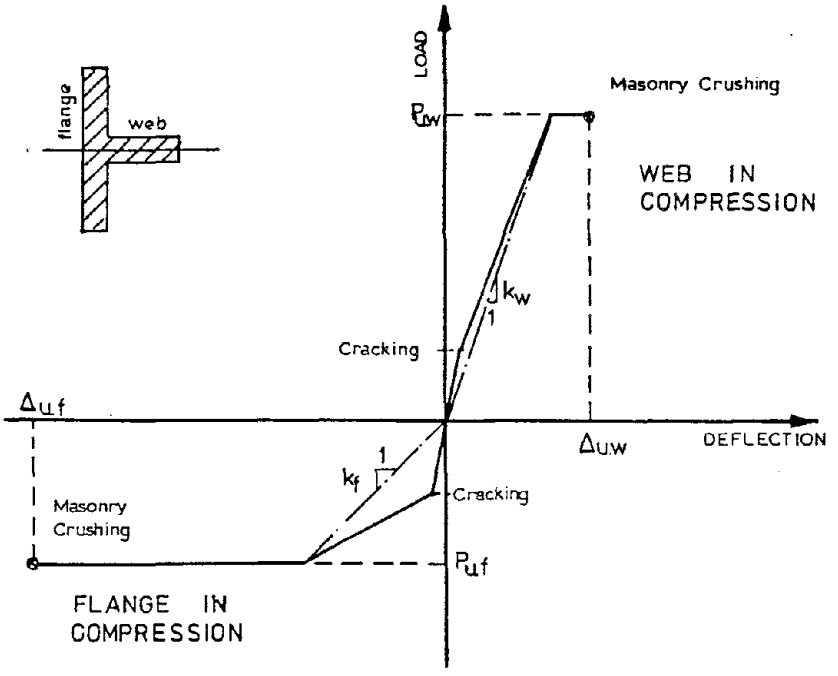

$$\frac{P_{uw}}{P_{uf}} > 1 \quad , \quad \frac{k_w}{k_f} > 1 \quad , \quad \frac{\Delta_{uw}}{\Delta_{uf}} < 1$$

FIG. 1-2 IDEALIZED MONOTONIC LOAD-DISPLACEMENT SKELETON CURVE FOR T-SECTION WALL

requirements under seismic response parallel to the flange. This reinforcement has insignificant influence on the flexural strength parallel to the web with the flange in compression, but contributes greatly to flexural strength in the opposite direction of loading, enhancing the flexural strength significantly above the required level. Assuming the structure to be designed for ductile response to the earthquake, it is the actual flexural strength that will be achieved, not the design level. The consequence can be amplification of the response shear force well above the level required to conform to code level loads. If this situation is not recognised by the designer, and appropriate capacity design measures adopted, as illustrated, for example in Fig. 1-3, shear failure can result.

Shear-lag effects in the flange are poorly understood. The extent to which the flange reinforcement contributes to flexural strength when the flange is in tension will be subject to shear lag. Although the New Zealand Masonry Design Code[10] provides some guidance on this matter, its provisions are based on the application of ACI design rules for effective flange width of T-Beam floors[11], and have not been verified experimentally. It seems probable that the extent to which the flange is effective may depend on cracking in the plane of the flange developed by previous inelastic response (if any) perpendicular to the web.

Effectiveness of the connection detail at the intersection between the flange and the web is also a matter of concern, and will depend on the block type adopted, amount of transverse reinforcement crossing the intersection, type of connection detail adopted, etc. Again, testing is needed to investigate this aspect.

Testing of squat, flanged reinforced concrete walls by Paulay et al[12] has indicated that the tendency for such walls to slide on the base in the absence of significant applied axial load levels can result in punching shear failures, where the

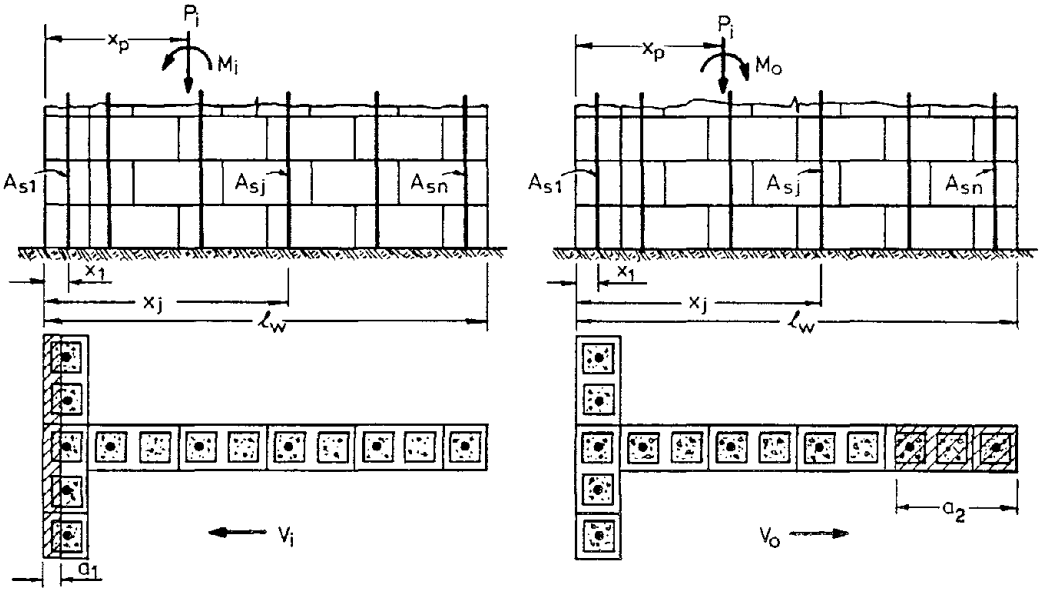

(a) Conditions for Flexural Design Web in Tension

(b) Conditions for Maximum Shear Flange in Tension

$$M_i \approx P_i\left(x_p - \frac{a_1}{2}\right) + f_y \sum_1^n A_{sj}\left(x_j - \frac{a_1}{2}\right) \geq \frac{M_c}{\phi}$$

$$M_o \approx P_i\left(\ell_w - x_p - \frac{a_2}{2}\right) + \lambda f_y \sum_1^n A_{sj}\left(\ell_w - x_p - \frac{a_2}{2}\right)$$

$$V_o = \omega \frac{M_o}{M_c} V_c$$

FIG. 1-3 CAPACITY DESIGN FOR SHEAR STRENGTH OF FLANGED WALLS (from New Zealand Masonry Design Code[10])

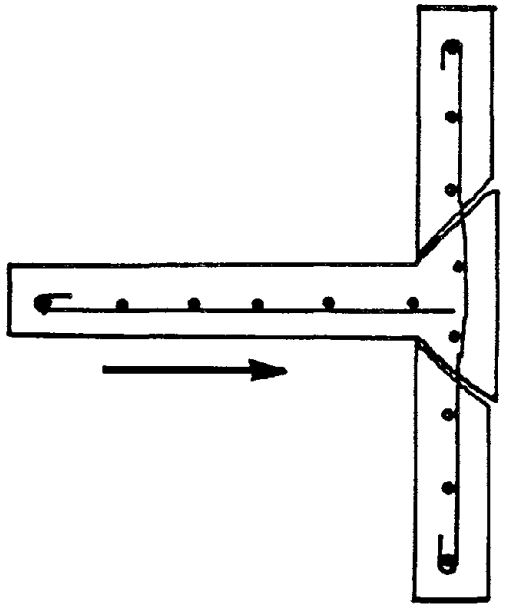

FIG. 1-4 PUNCHING SHEAR FAILURE DUE TO WEB SLIDING ON BASE

sliding web punches through the stationary flange, as illustrated in Fig. 1-4. It might be expected that flanged masonry walls, with pre-existing planes of weakness imposed by the bed and header joints might be more susceptible to this form of damage than reinforced concrete walls would be. The solution suggested by Paulay et al, of using diagonal reinforcement across the wall base to reduce base slip would seem to be impractical for hollow-unit masonry construction.

Scope of Research

This research project, initiated at the University of California, New Zealand, and completed at the University of California, San Diego represents a preliminary investigation into a number of the aspects of seismic performance of masonry shear walls noted above. It is intended that this research should act as a pilot study for a more complete experimental project to be carried out at UCSD.

The aspects covered in this project included analytical studies to extend the dimensionless design charts for strength and ductility of rectangular walls to flanged walls. The analytical background for this, and the resulting design charts are presented in Chapter 2.

Chapter 3 describes construction and shake-table testing of a wide-flange T-Section wall. Results of the testing are compared with theoretical prediction based on the analytical models developed in Chapter 2.

Finally, conclusions and recommendations for further research are included in Chapter 4.

CHAPTER 2: STRENGTH, STIFFNESS AND DUCTILITY OF T-SECTION MASONRY WALLS

2.1 INTRODUCTION

In Chapter 1, it was established that the flexural strength, stiffness and ductility of T-Section walls loaded parallel to the web depended on the direction of load application (See Fig. 1-2). The reason for this is as follows: With the flange in tension, a high reinforcement tensile force at large lever arm is mobilized, resulting in a higher flexural strength than when the flange is in compression and the lever arm to the center of tension of force is reduced. However, as shown in Fig. 1-3, a consequence of the higher tension force and reduced compression zone width when the flange is in tension is that the distance from the extreme compression fiber to the neutral axis, c, is much greater than when the flange is in compression. This results in increased stiffness of the cracked section, and significantly reduced ultimate curvature, since the ultimate curvature ψ_u can be expressed as

$$\psi_u = \epsilon_{cu}/c \qquad [1]$$

where ϵ_{cu} is the ultimate compression strain.

It is comparatively simple to produce useful design information on the flexural strength and ductility of rectangular section walls. Expressing axial load N, moment M, flexural reinforcement content A_{st} and curvature ψ in the following dimensionless forms it is possible to generate dimensionless design charts, such as those developed by Priestley[5, 6].

$$m = \frac{M}{f'_m \ell_w^2 t} \qquad [2]$$

$$n = \frac{N}{f'_m \ell_w t} \qquad [3]$$

$$\rho = \frac{A_{st}}{\ell_w t} \quad [4]$$

and $$\phi = \psi \ell_w \quad [5]$$

where f'_m is the masonry compression strength, ℓ_w is the wall length and t is the wall thickness. Figs. 2-1 and 2-2 show examples of dimensionless design charts for flexural strength and displacement ductility capacity for rectangular section walls with distributed flexural reinforcement.

This chapter extends this dimensionless approach to the analysis of T-Section masonry walls.

2.2 ASSUMPTIONS

The basis section shape analyzed is shown in Fig. 2-3, together with critical dimensions. Note that if the total flange length is $\ell_f = 0$, the wall section reverts to a rectangular wall of section ℓ_w x t, where t is the web thickness.

The following assumptions are made:

1. Plane section of the wall remain plane up to the ultimate state.

2. The discrete reinforcement pattern indicated by Fig. 2-3a can be replaced by an equivalent reinforcement laminar of equal total area as shown in Fig. 2-3b.

3. Shear lag effects are ignored. Thus all flange reinforcement is considered fully effective. (Note this assumption results directly from assumption 1.)

4. The reinforcement stress-strain curve is assumed to be elasto-plastic. Thus strain-hardening is ignored.

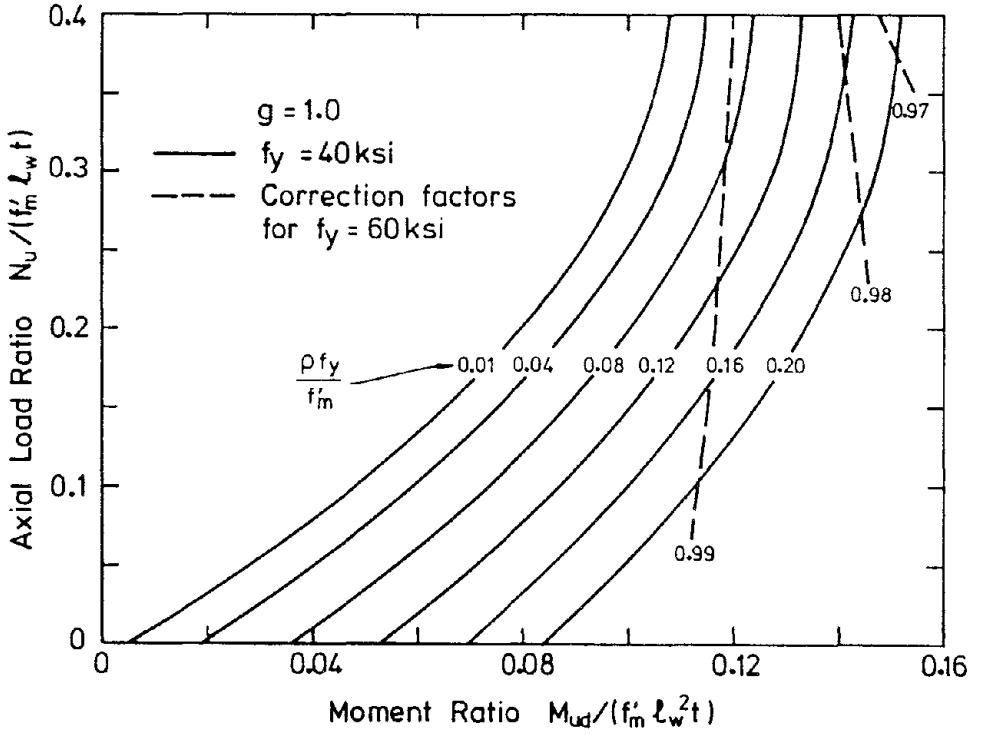

FIG. 2-1 FLEXURAL STRENGTH OF RECTANGULAR SECTION MASONRY WALL WITH DISTRIBUTED REINFORCEMENT[6]

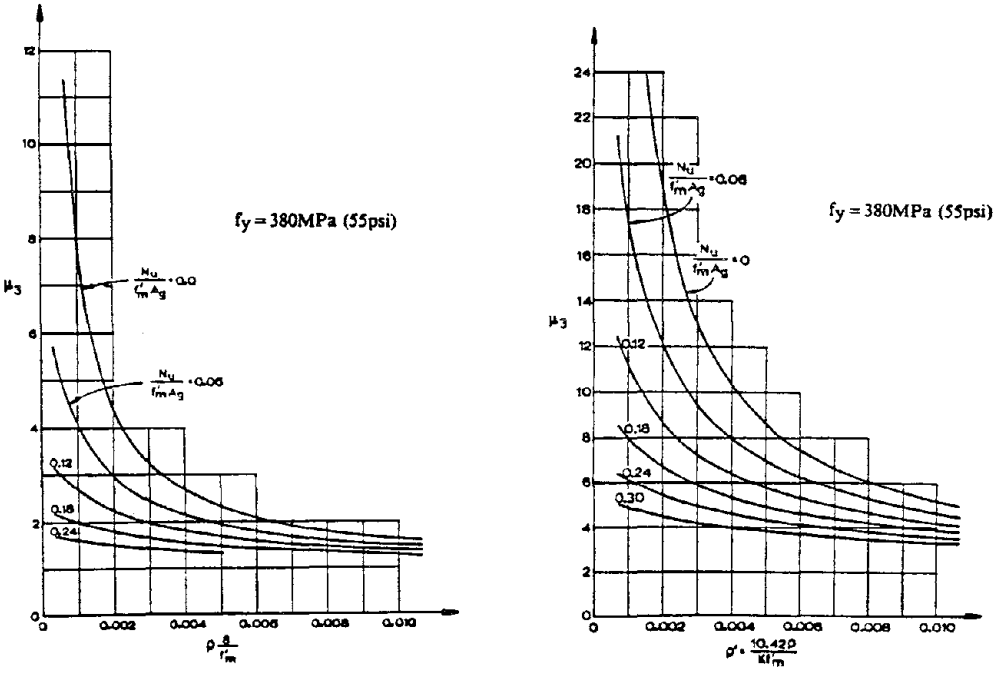

(a) Unconfined Masonry (b) Confined Masonry

FIG. 2-2 DUCTILITY CAPACITY OF RECTANGULAR WALLS WITH ASPECT RATIO $h_w/\ell_w = 3$ (5)

5. Flange and web thickness are equal, i.e. $t_f/t = 1.0$.

6. Local reinforcement ratios for the web and flange are equal, i.e. $\rho_f/\rho = 1.0$. Note that very frequently this will not be valid. However, by adjusting the flange width and using an equivalent width

$$\ell_f = \ell_f \rho_f / \rho \qquad [6]$$

the effect of different steel ratios in web and flange can be considered. This adjustment is exact when the flange is in tension. When the flange is in compression, small errors may result from the consequential adjustment to the neutral axis position to provide the correct masonry compression force. It will, however, be rare for the errors induced in strength or stiffness to exceed 1%. Ductility will be affected more significantly, but is almost never a problem when the flange is in compression.

7. The compression stress-strain characteristics for concrete masonry are those proposed by Priestley and Elder[13], and shown in Fig. 2-4. The curve is defined as follows:

Unconfined Masonry:

(i) $\epsilon_m \leq 0.0015$: $$f_m = \frac{f'_m}{0.9375} \cdot \left[\frac{2\epsilon_m}{0.002} - \left[\frac{\epsilon_m}{0.002}\right]^2\right] \qquad [7]$$

(ii) $0.0015 \leq \epsilon_m \leq 0.0025$: $$f_m = f'_m \left\{1 - Z_m(\epsilon_m - 0.0015)\right\} \qquad [8]$$

where $$Z_m = \frac{0.5}{\left\{\frac{3 + 0.29 f'_m}{145 f'_m - 1000} - 0.002\right\}} \qquad [9]$$

The ultimate compression strain for unconfined masonry is taken as 0.0025. It should be noted that this strain appears conservative for North American concrete masonry.

Confined Masonry:

Concrete masonry prisms confined with 3mm (0.12 in.)

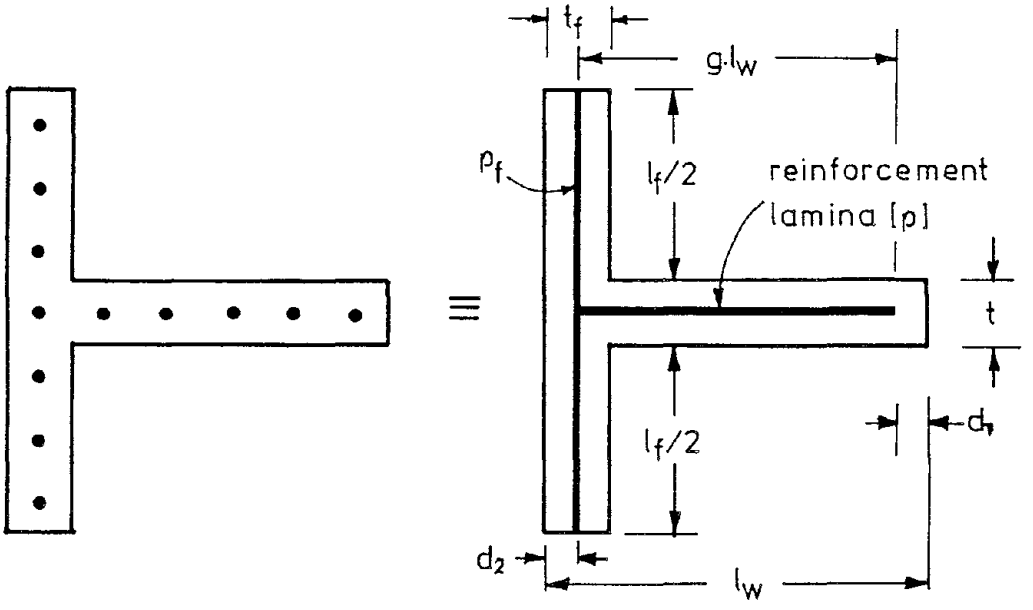

(a) Actual Section (b) Equivalent Section

FIG. 2-3 PLAN DIMENSIONS OF T-SECTION WALL

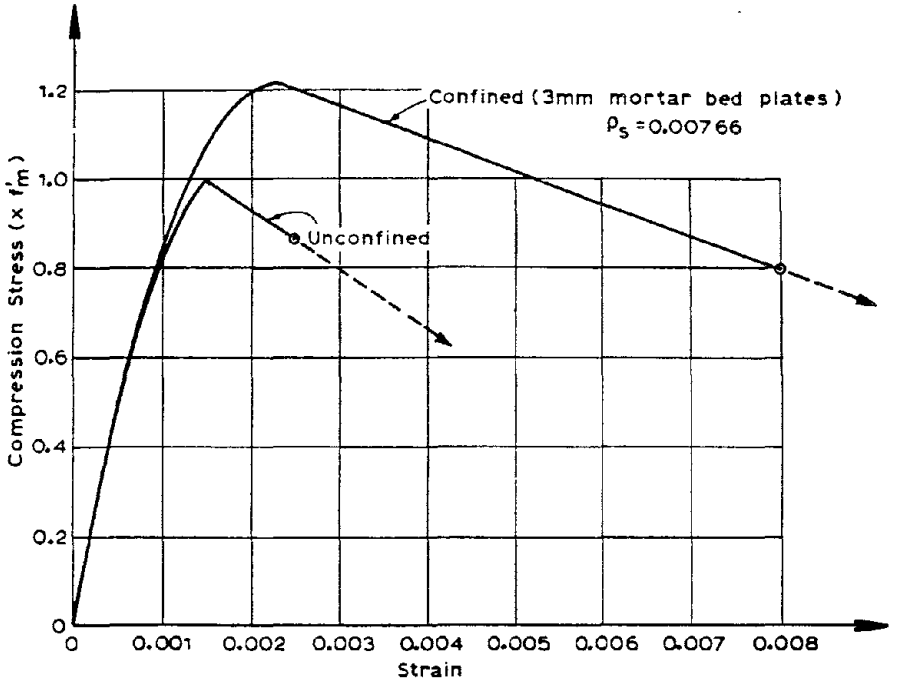

FIG. 2-4 MASONRY STRESS-STRAIN CURVES (f'_m = 16MPa)[13]

thick stainless or galvanized steel plates within the mortar beds exhibit a changed failure mode from one initiated at mortar beds by vertical splitting, to a shear/crushing failure largely within one course (13).

The plates are cut to the net shape of the masonry units so that there is no interference with the grout flues, and with a 5 mm (0.2 in.) edge allowance for pointing. Stress strain curves for the confined prisms have shown increased strength, higher strains at peak load, and a much flatter falling branch. A safe ultimate compression strain for concrete masonry confined in this fashion is estimated to be 0.008. It was found that the curve described by the following equations and included in Fig. 2-4 provide good agreement with experimental data.

(i) for $\epsilon_m \leq 0.002K$

$$f_m = K \cdot \frac{f'_m}{0.9375} \cdot \left[\frac{2\epsilon_m}{0.002K} - \left[\frac{\epsilon_m}{0.002K} \right]^2 \right]$$

where $K = 1 + \rho_s \frac{f_{yh}}{f'_m}$

ρ_s = volumetric ratio of confining steel

f_{yh} = confining steel yield strength

(ii) $0.002K < \epsilon_m \leq 0.008$

$$f_m = \frac{Kf'_m}{0.9375} \left[1 - Z_m(\epsilon_m - 0.002K) \right]$$

where

$$Z_m = \left[\frac{0.5}{\frac{3 + 0.29f'_m}{145f'_m - 1000} + \frac{3}{4} \rho_s \cdot \sqrt{\frac{h''}{S_h}} - 0.002K} \right]$$

and

h" = lateral dimension of the confined core (i.e. block width)

S_h = spacing of confining steel (i.e. block unit height)

8. Axial load is uniformly distributed across the column T-section. Thus the vertical line of action of the resultant axial load passes through the geometric center of the gross section.

2.3 VARIABLES CONSIDERED IN ANALYSIS

Shape ratio: ℓ_f/ℓ_w = 0 to 2.0 by steps of 0.25

Size ratio: g = 0.05, 0.1, 0.2 (see Fig.2.3)

Axial load ratio: $N/(f'_m A_g)$ = 0 to 0.4 by steps of 0.05

Reinforcement ratio: $\rho f_y/f'_m$ = 0.01, 0.02 to 0.2 by steps of 0.02

Yield stress: f_y = 275 MPa, 380 MPa. (40 ksi, 55 ksi)

2.4 FORMULATION OF THE DIMENSIONLESS EQUATIONS FOR T-SECTION WALLS

Fig. 2-5 presents additional terminology used in the analysis for conditions at first yield of the extreme tension reinforced, and at ultimate. Dimensionless forms of these parameters are used in the analysis as follows:

$c_{yn} = c_y/\ell_w$	(Comp. zone depth at yield)
$c_{un} = c_u/\ell_w$	(Comp. zone depth at ultimate)
$e_n = e/\ell_w$	(Distance of axial load resultant from flange edge)
$K_\ell = \ell_f/\ell_w$	
$K_t = t_f/t$	(=1. For generality, Eqns. are expressed in terms of K_t)
$\beta = t_f/\ell_w$	
$g = 1-\beta$	
$K_\rho = \rho_f/\rho$	(=1. Included for generality)
$K_A = (\ell_w t + \ell_f t_f)/\ell_w t$ $= 1 + K_\ell K_t$	
$N_A = N/f'_m A_g$	
$P = \rho f_y/f'_m$	
$\epsilon_y = f_y/2.5$	
$f_k = K_\ell K_t/\beta$	
ϵ_1 = Strain of maximum stress for masonry in compression	

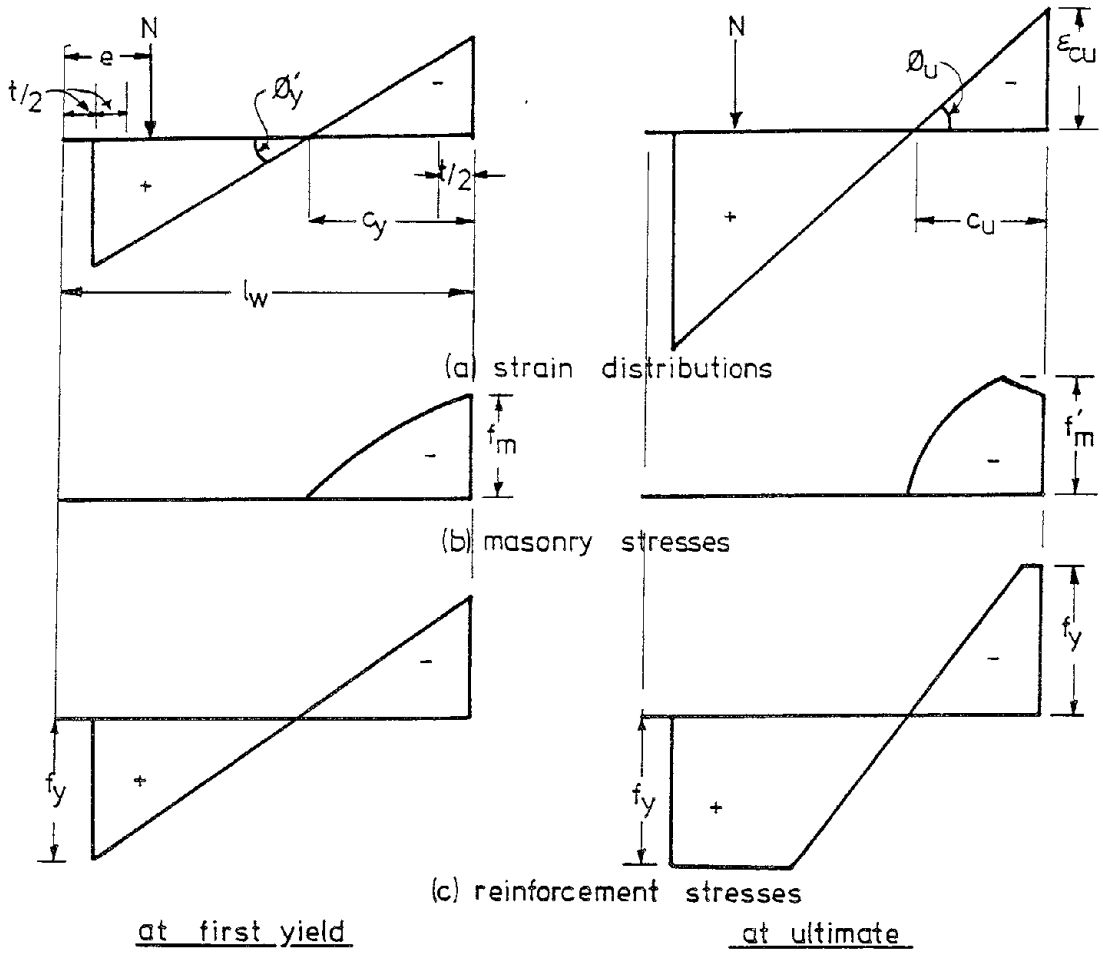

FIG. 2-5 EQUILIBRIUM CONDITIONS AT FIRST YIELD AND AT ULTIMATE

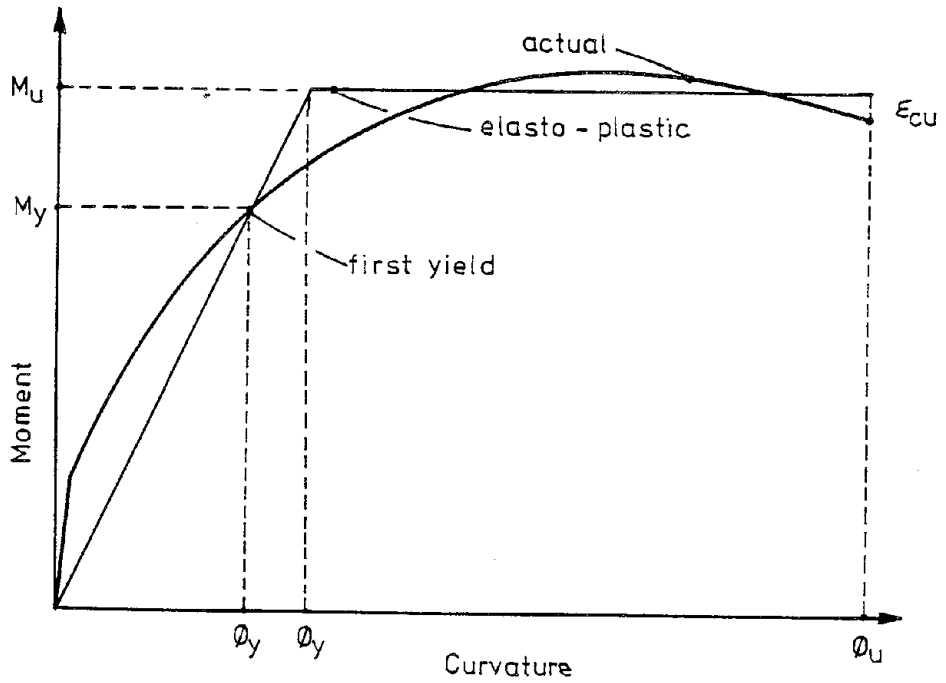

FIG. 2-6 ELASTO-PLASTIC APPROXIMATION OF MOMENT-CURVATURE RELATIONSHIP

ϵ_2 = Ultimate compression strain for masonry

R (Flag, = 0 when web in compression, = 1 when flange in compression)

Other factors appearing in the equations below relate to the masonry compression stress strain curve, as defined above.

2.4.1 Conditions at first Yield of Reinforcement

- Axial Equilibrium:

$$K_A N_A + PK_\rho K_\ell K_t(1-R) + 0.5P(1 - c_{yn} - \beta/2)/g - P_c - P_m = 0 \quad [10]$$

- Yield Moment:

$$m_{yn} = K_A N_A[(1-e_n-c_{yn})(1-R)+(e_n-c_{yn})R]+PK_\rho K_\ell K_t(1-c_{yn}-\beta/2)(1-R)+(P/3)(1-c_{yn}-\beta/2)^2/g + m_c + m_m \quad [11]$$

Equation 10 must be solved for c_{yn}, which is substituted into [11] for m_{yn}. The values of P_c (compression force in rebar in compression zone), m_c (moment of P_c about the neutral axis NA), P_m (masonry compression force), m_m (moment of P_m about NA) depend on the value of c_{yn}, as below, so an iterative solution is necessary.

- If $c_{yn} \leq 0.5$, then

$$P_c = PK_\rho K_\ell K_t(c_{yn}-\beta/2)R/(1-c_{yn}-\beta/2) + 0.5P(c_{yn}-\beta/2)^2/(g(1-c_{yn}-\beta/2)) \quad [12]$$

and

$$m_c = PK_\rho K_\ell K_t(c_{yn}-\beta/2)^2R/(1-c_{yn}-\beta/2) + (P/3)(c_{yn}-\beta/2)^3/(g(1-c_{yn}-\beta/2)) \quad [13]$$

- If $c_{yn} > 0.5$, then

$$P_c = PK_\rho K_\ell K_t R + 0.5P(1-c_{yn}-\beta/2)/g + P(2c_{yn}-1)/g \quad [14]$$

and

$$m_c = PK_\rho K_\ell K_t(c_{yn}-\beta/2)R+(P/3)(1-c_{yn}-\beta/2)^2/g + P(c_{yn}-0.5) \quad [15]$$

- If $c_{yn} \cdot \epsilon_y/(1-c_{yn}-\beta/2) \leq e_1$, and $c_{yn} \geq \beta$, then

$$P_m = P1(1 + f_kR) - Rf_kP1 \frac{(c_{yn} - \beta)\epsilon_y}{(1-c_{yn}-\beta/2)} \cdot \frac{(1 - c_{yn} - \beta/2)}{\epsilon_y}$$

and

$$m_m = Q1(1+f_kR) - Rf_kQ1 \frac{(c_{yn}-\beta)\epsilon_y}{(1-c_{yn}-\beta/2)} \cdot (1-c_{yn}-\beta/2)^2/\epsilon_y^2 \quad [17]$$

- If $c_{yn} \cdot \epsilon_y(1-c_{yn}-\beta/2) \leq e_1$ and $c_{yn} < \beta$, then

$$P_m = P1(*).(1+f_kR)(1-c_{yn}-\beta/2)/\epsilon_y \quad [18]$$

and

$$m_m = Q1(*)(1+f_kR)(1-cyn-\beta/2)^2/\epsilon y^2 \quad [19]$$

In equations 16 and 18, the function P1 ( ) is

$$P1(*) = 533.3*^2 - 8.89E4.*^3/K \quad [20]$$

where $* = cyn.\epsilon y/(1-cyn-\beta/2)$, or is specified in the ( ) [21]

In equations 17 and 19, the function Q1 ( ) is

$$Q1(*) = 355.6*^3 - 6.6E4*^4/K \quad [22]$$

- If $e_1 < cyn.\epsilon y/(1-cyn-\beta/2) \leq e_2$ and $(cyn-\beta)\epsilon_y/(1-cyn-\beta/2) \geq e_1$, then

$$Pm = (P1(e_1)+P2(*)(1+f_kR)-Rf_kP2(\#))(1-cyn-\beta/2)/\epsilon_y \quad [23]$$

and

$$m_m = (Q1(e_1)+Q2(*)(1+f_kR)-Rf_kQ2(\#))(1-cyn-\beta/2)^2/e_y^2 \quad [24]$$

- If $e_1 < cyn.\epsilon_y/(1-cyn-\beta/2) \leq e_2$ and $(cyn-\beta)\epsilon_y/(1-cyn-\beta/2) < e_1$, then

$$P_m = ((P1(e_1) + P2(*)(1+f_kR) - Rf_kP_1(\#))(1-cyn)-\beta/2)/\epsilon_y \quad [25]$$

and

$$m_m = ((Q1(e_1)+Q2(*))(1+f_kR) - Rf_kQ1(\#))(1-c_{yn}-\beta/2)^2/\epsilon_y^2 \quad [26]$$

In Equations 23-26, $P1(e_1)$ and $Q1(e_1)$ are defined by Eqns. 20 and 22, with e_1 substituted for *, and

$$P2(\#) = 1.067K_2((1 + e_1Z_m)(\# - e_1) - 0.5Z_m(\#^2 - e_1^2)) \quad [27]$$

and

$$Q2(\#) = 1.067K_2(0.5(1 + e_1Z_m)(\#^2 - e_1^2) - (Z_m/3)(\#^3 - e_1^3)) \quad [28]$$

where

$$\# = (c_{yn}-\beta)\epsilon_y/(1-c_{yn}-\beta/2)$$

and K2 = 0.9375 for confined masonry; K2 = K for confined masonry. For P2(*), Q2(*), use * from Eqn. 21 instead of # in Eqn 27, 28, etc.

- If $c_{yn}\cdot\epsilon_y/(1-c_{yn}-\beta/2) > e_2$, then crushing of the extreme compression fiber occurs before the extreme tension rebar yields, and no value for m_{yn} exists.

In the above equations, the functions P1 and P2 will be recognized as integrals of the masonry compression stress block, to obtain the total masonry compression force. Q1 and Q2 provide the moment of the total masonry stress block about the neutral axis.

2.4.2 Conditions at Ultimate Compression Strain

- Axial Equilibrium:

$$K_AN_A + P_t - P_c - P_m = 0 \quad [29]$$

- Flexural Strength:

$$m_{un} = K_AN_A((1-e_n-c_{un})(1-R) + (e_n-c_{un})R) + m_t + m_c + m_m \quad [30]$$

Eqn. 29 is solved for c_{un}, which is then substituted into Eqn. 30 to obtain the flexural strength. The values of P_T (tension force in tension rebar), P_c (compression force in compression rebar), P_m (compression force in compressed masonry) and m_t, m_c, and m_m (moments of P_T, P_c and P_m respectively about the N.A.) depend on the value of c_{un}, so again an iterative process is required.

Steel Tension Force

- If $c_{un} \cdot \epsilon_y/e_2 \leq (1 - c_{un} - \beta/2)$ then

$$P_t = PK_\rho K_\ell K_t(1-R) + P(1-c_{un}-\beta/2-c_{un}\cdot\epsilon_y/(2e_2))/g \quad [31]$$

and

$$m_t = PK_\rho K_\ell K_t(1-c_{un}-\beta/2)(1-R)+0.5P((1-c_{un}-\beta/2)^2-\frac{c_{un}^2}{3e_2^2}\epsilon_y^2)/g \quad [32]$$

- If $(1-c_{un}-\beta/2) \leq c_{un}\cdot\epsilon_y/e_2 \leq (c_{un}-1-\beta/2)$ then

$$P_t = P(c_{un}-\beta/2-c_{un}\epsilon_y/(2e_2))/g - P - PK_\rho K_\ell K_t(1-R) \quad [33]$$

and

$$m_t = -P/2((c_{un}-\beta/2)^2-c_{un}^2\epsilon_y^2/(3e_2^2))/g+P(c_{un}-1/2)+PK_\rho K_\ell K_t(c_{un}-1+\beta/2)(1-R) \quad [34]$$

- If $c_{un}\epsilon_y/e_2 > (c_{un}-1-\beta/2)$ then

$$P_t = PK_\rho K_\ell K_t(1-c_{un}-\beta/2)e_2(1-R)/(c_{un}\epsilon_y)+0.5P(1-c_{un}-\beta/2)^2e_2/c_{un}\epsilon_y g) \quad [35]$$

and

$$m_t = PK_\rho K_\ell K_t(1-c_{un}-\beta/2)^2e_2(1-R)/(c_{un}\epsilon_y)+(P/3)(1-c_{un}-\beta/2)^3 e_2/(c_{un}\epsilon_y g) \quad [36]$$

Steel Compression Force

- If $c_{un}\cdot\epsilon_y/e_2 \leq (c_{un}-\beta/2)$ then

$$P_c = PK_\rho K_\ell K_t R+P(c_{un}-\beta/2-c_{un}\epsilon_y/(2\epsilon_2))/g \quad [37]$$

and

$$m_c = PK_\rho K_\ell K_t R(c_{un}-\beta/2)+0.5P((c_{un}-\beta/2)^2-(c_{un}^2\epsilon_y^2/(3e_2^2))/g \quad [38]$$

- Else, if $c_{un} \geq \beta/2/(1 + \epsilon_y/e_2)$, then

$$P_c = PK_\rho K_\ell K_t e_2(c_{un}-\beta/2)R/(c_{un}\epsilon_y)+0.5Pe_2(c_{un}-\beta/2)^2/(c_{un}\epsilon_y g) \quad [39]$$

and

$$m_c = PK_\rho K_\ell K_t e_2 (c_{un}-\beta/2)^2 R/(c_{un}\epsilon_y)+(P/3)e_2(c_{un}-\beta/2)^3/(c_{un}\epsilon_y g) \quad [40]$$

- Else (all other cases)

$$P_c = -PK_\rho K_\ell K_t R - P + P(1-c_{un}-\beta/2-c_{un}\epsilon_y/2e_2)/g \quad [41]$$

and

$$m_c = PK_\rho K_\ell K_t(\beta/2-c_{un})R + P(1/2-c_{un}) - 0.5P[(1-c_{un}-\beta/2)^2 - c_{un}^2\epsilon_y^2/(3e_2^2)]/g \quad [42]$$

Masonry Compressive Force

(All cases except when $R = 0$ and $c_{un} \geq 1 - \beta$)

- If $e_2(c_{un} - \beta)/c_{un} \geq e_1$, then

$$P_m = (P1(e_1) + P2(e_2)(1 + f_k R) - Rf_k P2(X))c_{un}/e_2 \quad [43]$$

and

$$m_m = (Q1(e_1) + Q2(e_2)(1 + f_k R) - Rf_k Q2(X))c_{un}^2/e_2^2 \quad [44]$$

- Else, if $c_{un} \geq \beta$, then

$$P_m = ((P1(e_1) + P2(e_2))(1 + f_k R) - Rf_k P1(X))c_{un}/e_2 \quad [45]$$

and

$$m_m = ((Q1(e_1) + Q2(e_2))(1 + f_k R) - Rf_k Q1(X))c_{un}^2/e_2^2 \quad [46]$$

- Else

$$P_m = (P1(e_1) + P2(e_2))(1 + f_k R)c_{un}/e_2 \quad [47]$$

and

$$m_m = (Q1(e_1) + Q2(e_2))(1 + f_k R)c_{un}^2/e_2^2 \quad [48]$$

In equations 43-48, functions P1, P2, Q1 and Q2 are given by Eqns. 20, 27, 22, and 28 respectively using the appropriate variable, and

$$X = (c_{un}-\beta)e_2/c_{un} \quad [49]$$

When $R = 0$ and $c_{un} \geq 1 - \beta$, then special conditions apply, as follows:

- If $(c_{un}-1)/c_{un} \geq e_1/e_2$, then

$$P_m = (P2/e_2) + P2(Y)f_k - (1+f_k)P2(Z))c_{un}/e_2 \quad [50]$$

and

$$m_m = (Q2(e_2) + Q2(Y)f_k - (1+f_k)Q2(Z))c_{un}^2/e_2^2 \quad [51]$$

- Else, if $(c_{un}-1+\beta)/c_{un} \geq e_1/e_2$, then

$$P_m = (P2(e_2) + P2(Y)f_k + (1+f_k)(P1(e_1)-P1(Z)))c_{un}/e_2 \quad [52]$$

and

$$m_m = (Q2(e_2) + Q2(Y)f_k + (1+f_k)(Q1(e_1)-Q1(Z)))c_{un}^2/e_2^2 \quad [53]$$

- Else, if $c_{un} \geq 1$, then

$$P_m = (P2(e_2) + (P1(e_1) + P1(Y)f_k - (1+f_k)P1(Z))c_{un}/e_2 \quad [54]$$

and

$$m_m = (Q2(e_2) + Q1(e_1) + Q1(Y)f_k - (1+f_k)Q1(Z))c_{un}^2/e_2^2 \quad [55]$$

- Else (all other cases)

$$P_m = (P2(e_2) + P1(e_1) + P1(Y)f_k)c_{un}/e_2 \quad [56]$$

and

$$m_m = (Q2(e_2) + Q1(e_1) + Q1(Y)f_k)c_{un}^2/e_2^2 \quad [57]$$

In Eqns. 50 to 57, P1, P2, Q1 and Q2 are the previously defined functions, and the arguments Y and Z are given by

$$Y = (c_{un}-1+\beta)e_2/c_{un} \quad [58]$$

and

$$Z = (c_{un}-1)e_2/c_{un} \quad [59]$$

Solutions of the above equations directly yields the

dimensionless flexural strength. The other parameters of interest, namely the ductility and the section stiffness are then found as follows.

2.4.3 Ductility

The dimensionless curvature corresponding to onset of yield strain in the extreme tension reinforcement is given (see Fig. 2-5a) as

$$\phi'_y = \frac{\epsilon_y}{(1-c_{yn}-\beta/2)} \qquad [60]$$

At ultimate, the curvature (see Fig. 2.5b) will be

$$\phi = \epsilon_{cu}/c_{un} \qquad [61]$$

In terms of an elasto-plastic approximation of the moment-curvature relationship, the yield curvature ϕ_y needs to be related to the ultimate moment rather than the reduced moment corresponding to first yield. Extrapolating linearly, as shown in Fig. 2-6, the corrected yield curvature is thus

$$\phi_y = \phi'_y \frac{m_u}{m_y} \qquad [62]$$

The curvature ductility factor ϕ_u/ϕ_y is then found directly from Eqns 61 and 62.

For a simple cantilever shear wall, it can be shown[5] that the displacement ductility factor $\mu = \Delta u/\Delta y$ measured at the height of the resultant of the horizontal seismic forces is given by

$$\mu = 1 + 3(\phi_u/\phi_y - 1)L_p/h(1 - L_p/2h) \qquad [63]$$

where h is the height from the critical section to the resultant of the horizontal seismic forces, and L_p is the plastic hinge length at the wall base, over which the plastic curvature (ϕ_u-ϕ_y) is assumed constant.

2.4.4 Elastic Stiffness

With masonry structures, elastic stiffness parameters are primarily required for natural period calculations, and to allocate shear between lateral-load resisting elements in proportion to their stiffness. For example, the stiffness of a cantilever wall element can be expressed as

$$K = 3E_m I_e / h^3 \qquad [64]$$

where E_m is the masonry modulus of elasticity, I_e is the effective moment of inertia, and h is the height from the critical section to the resultant of the horizontal seismic forces.

The effective moment of inertia, I_e should take into account the influence of flexural cracking and shear deformation on reducing the stiffness from the uncracked, or gross value I_g. Since it is the load distribution and building period at maximum levels of lateral force that are of interest, stiffness calculations should be based on the condition of the masonry element when the extreme tension reinforcement has just reached yield strain, and thus the calculations above relative to the "first-yield" condition are appropriate.

Initially ignoring shear deformation, and assuming a linear distribution of curvature with height above the base at first yield, the yield displacement can be approximated as

$$\Delta y = \phi'_y h^2/3 = m_y h^2/3EI_e \qquad [65]$$

Thus, in dimensionless form,

$$I_e = m_{yn}/E\phi'_y \qquad [66]$$

where m_{yn} is given by Eqn. 11, and ϕ'_y is given by Eqn. 60.

The ratio of cracked-section to gross stiffness is thus given by

$$\frac{I_e}{I_g} = \frac{m_{yn}(1-c_{yn}-\beta/2)}{\epsilon_y I_g} \qquad [67]$$

where

$$I_g = (0.5 - e_n)^2 + 1/12(1 + K_\ell K_t \beta^2) + K_\ell K_t (e_n-\beta/2)^2 \qquad [68]$$

For squat cantilever walls, shear deformation further reduces the effective stiffness and a "shear adjusted" moment of inertia, I_{ev} of

$$I_{ev} = \frac{I_e}{1 + F} \qquad [69]$$

where F is the ratio of shear deformation to flexural deformation applies. An approximate value for F may be based on the uncracked relative stiffness, giving

$$F = 9I_g/(A_w h^2) \qquad [70]$$

where A_w is the web area. Eqn. 70 assumes the shear stiffness is reduced by cracking in proportion to the reduction in flexural stiffness.

2.5 DIMENSIONLESS DESIGN TABLES AND CHARTS

The equations developed above were assembled into a simple computer code written in Fortran IV, and listed in Appendix B. This code allowed design tables for flexural strength, Equivalent stiffness, and curvature ductility, to be prepared for T-Section walls of different section aspect ratio ℓ_f/ℓ_w, axial load ratio, reinforcement ratio and loading direction (i.e., flange in compression, or web in compression). These tables are listed in Appendix A, for two values of g (see Fig. 2-3 for definition of g). Values for other g values may be found with adequate accuracy by interpolation.

A selection of the resulting data have been put in graphical form to enable major trends to be emphasized. Figs. 2-7 to 2-12

present ultimate moment capacity curves, Figs. 2-13 to 2-18 present effective stiffness curves, and Figs. 2-13 to 2-23 provide information on curvature ductility.

2.5.1 Ultimate Moment Capacity

Figs. 2-7 to 2-11 present axial-load/moment capacity interaction curves for walls with ℓ_f/ℓ_w = 0, 1 and 2 respectively, for different levels of mechanical reinforcement ratio $\rho f_y/f'_m$, and for two levels of reinforcement yield stress, 275 MPa (40 ksi) indicated by broken lines, and 380 MPa (55 ksi) indicated by solid lines. The axial load ratio has been limited to $0.4f'_mA_g$ as this is felt to be a realistic upper limit to axial load on a masonry shear wall.

Fig. 2-7, with ℓ_f/ℓ_w = 0, represents the interaction curve for a rectangular wall (no flange), and hence applies for both directions of loading. It will be noted that the reinforcement yield stress does not significantly influence the moment capacity for a given axial load provided the reinforcement yield <u>force</u> ρf_y is constant. At high axial load and high $\rho f_y/f'_m$ ratios, there is up to 5% reduction in moment capacity using grade 380 rebar.

Figs. 2-8 and 2-9 show load-moment interaction curves for flanged walls with ℓ_f/f_w = 1, and the flange in compression and web in compression respectively. Considerable difference between the two direction of loading apparent. With the flange in compression, the interaction curves are almost linear, and the influence of reinforcement yield strength is insignificant. With the web in compression, the curves are strongly non-linear, have maximum moment capacity at axial loads in the range $0.1f'_mA_g$-$0.3f'_mA_g$ and display a significant influence of reinforcement yield strength. Compared with corresponding curves for flange in compression, moment capacities when the web is in compression are always higher, and for axial loads in the range $0.1f'_mA_g$ - $0.2f'_mA_g$ are typically about double. However, it is apparent that if

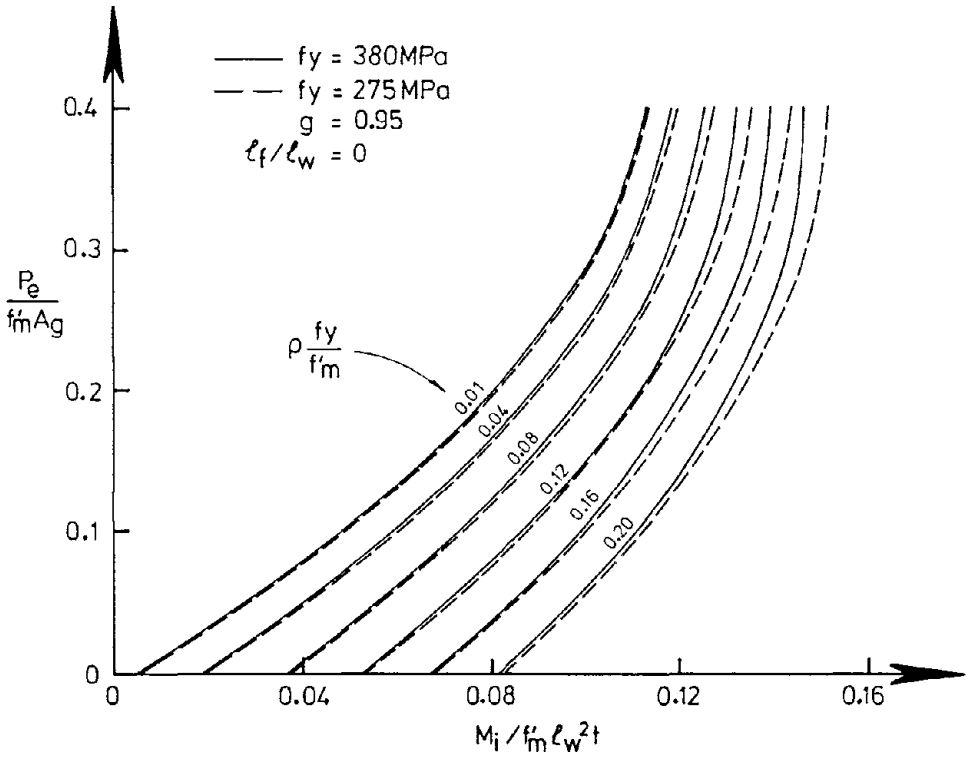

FIG. 2-7 MOMENT CAPACITY, ℓ_f/ℓ_w = 0 (Rectangular Section)

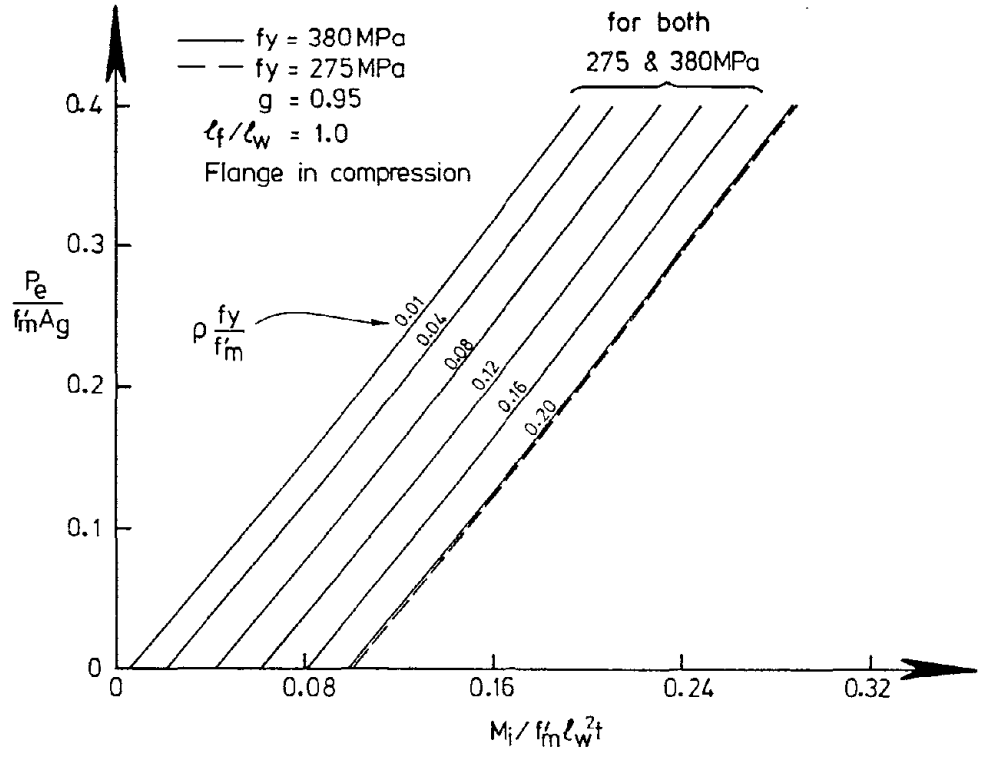

FIG. 2-8 MOMENT CAPACITY, ℓ_f/ℓ_w = 1.0 FLANGE IN COMPRESSION

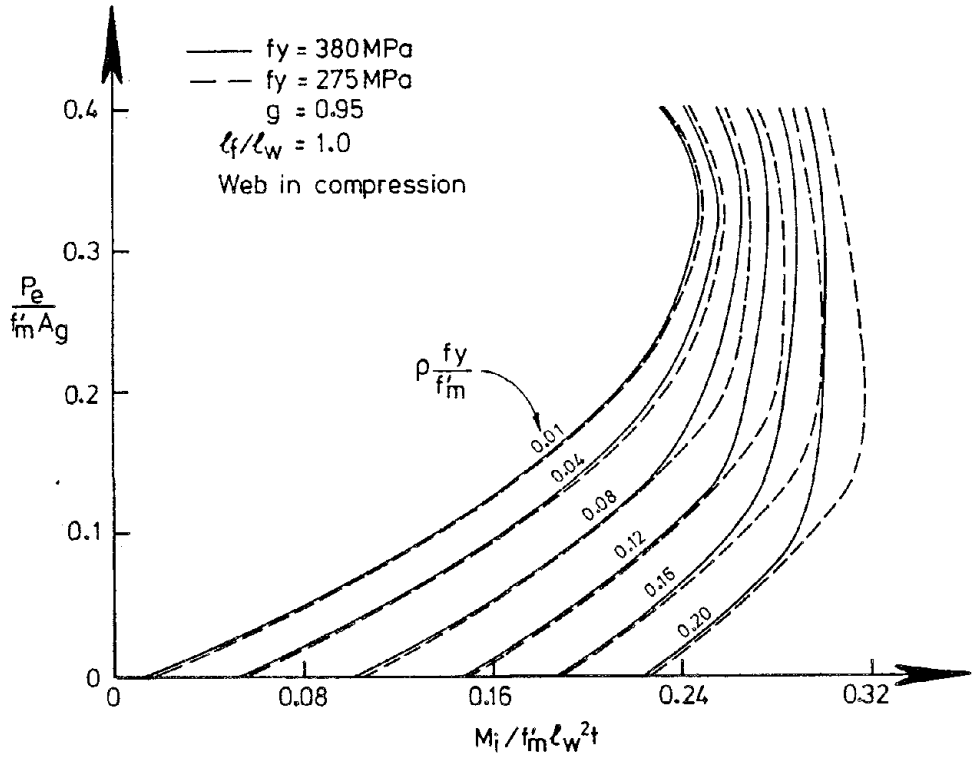

FIG. 2-9 MOMENT CAPACITY, ℓ_f/ℓ_w = 1.0 WEB IN COMPRESSION

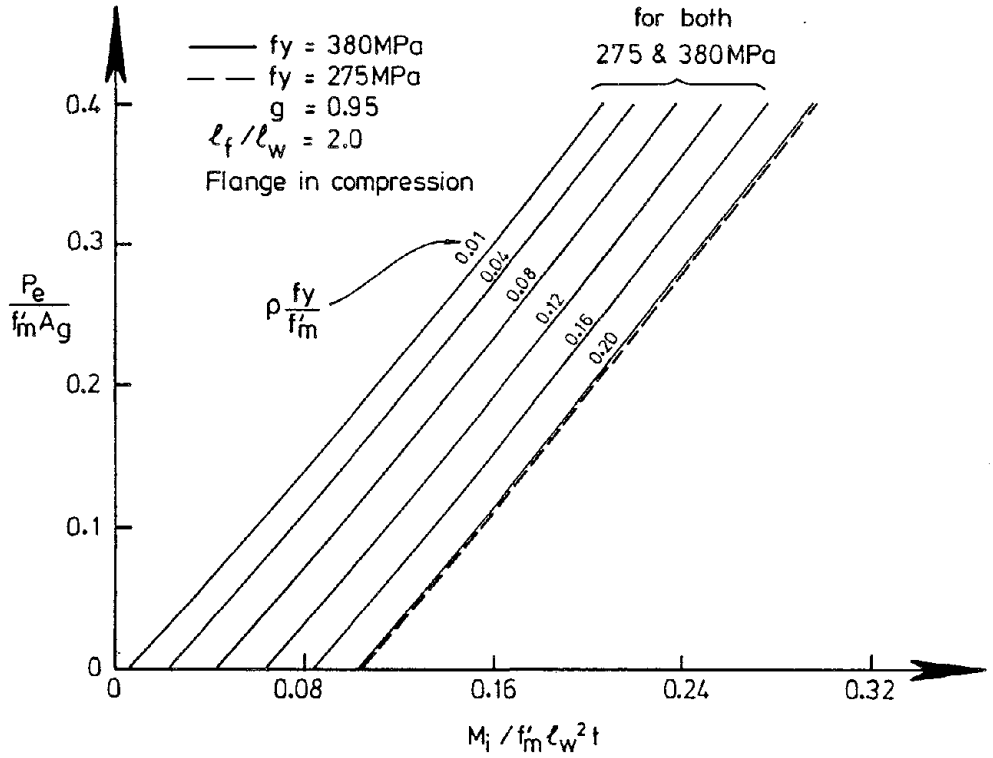

FIG. 2-10 MOMENT CAPACITY, ℓ_f/ℓ_w = 2.0 FLANGE IN COMPRESSION

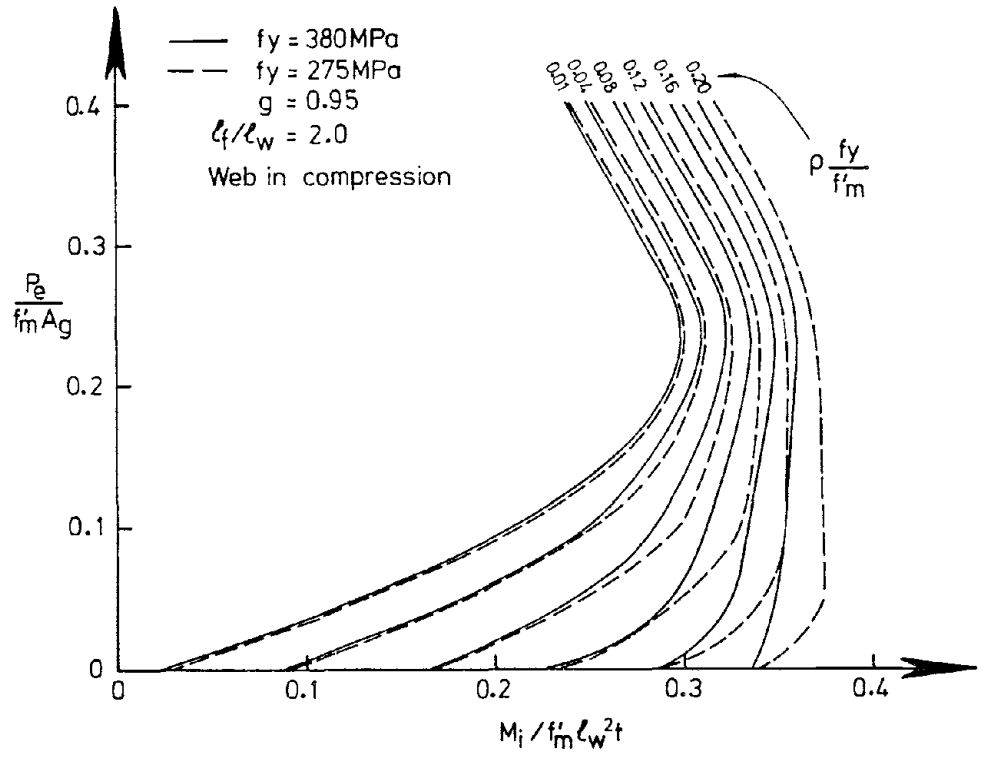

FIG. 2-11 MOMENT CAPACITY, ℓ_f/ℓ_w = 2.0 WEB IN COMPRESSION

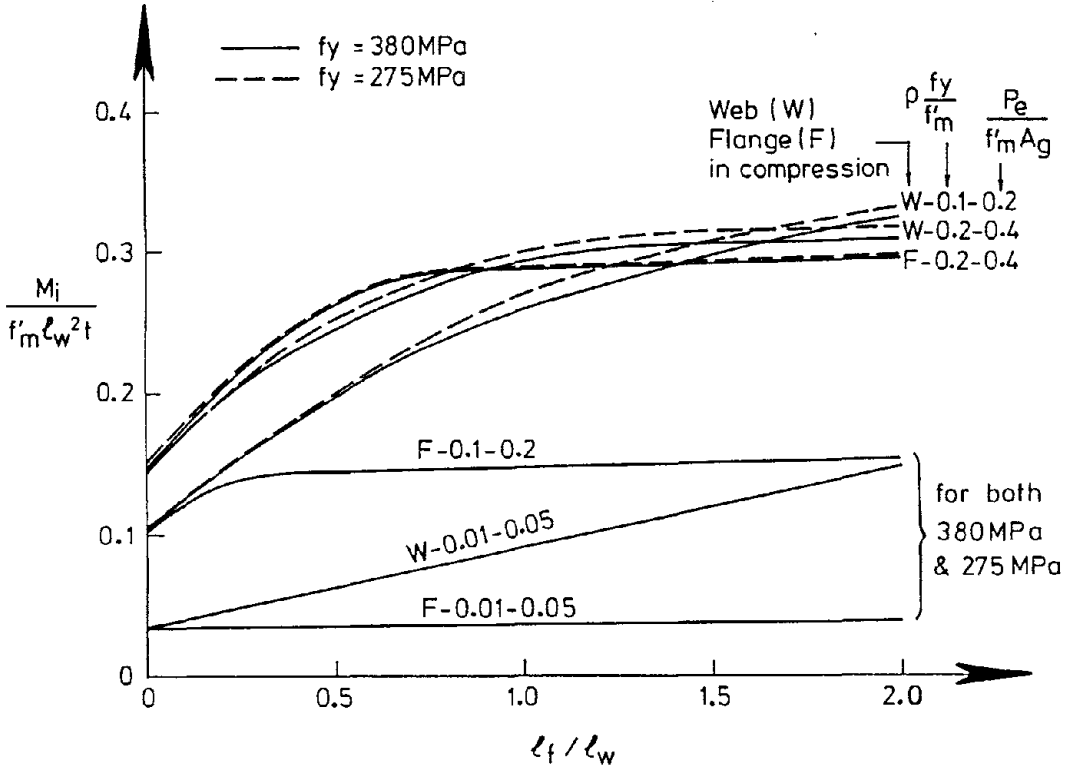

FIG. 2-12 INFLUENCE OF ℓ_f/ℓ_w, LOAD, AND REINFORCEMENT ON MOMENT CAPACITY

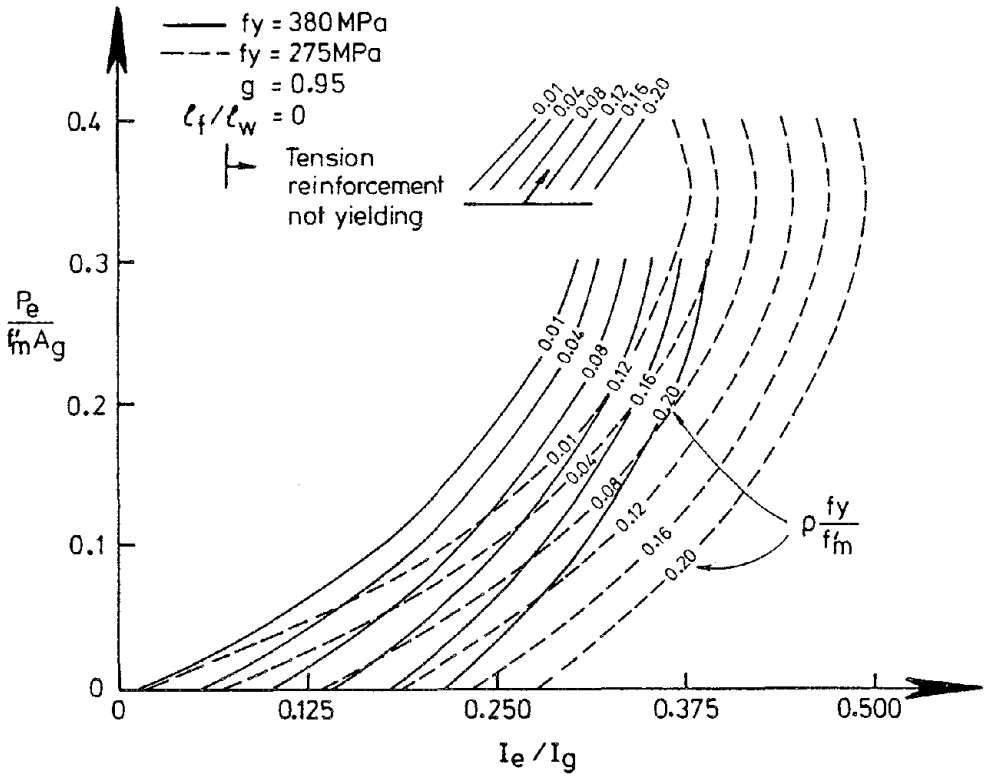

FIG. 2-13 EFFECTIVE MOMENT OF INERTIA, $\ell_f/\ell_w = 0$ (RECTANGULAR SECTION)

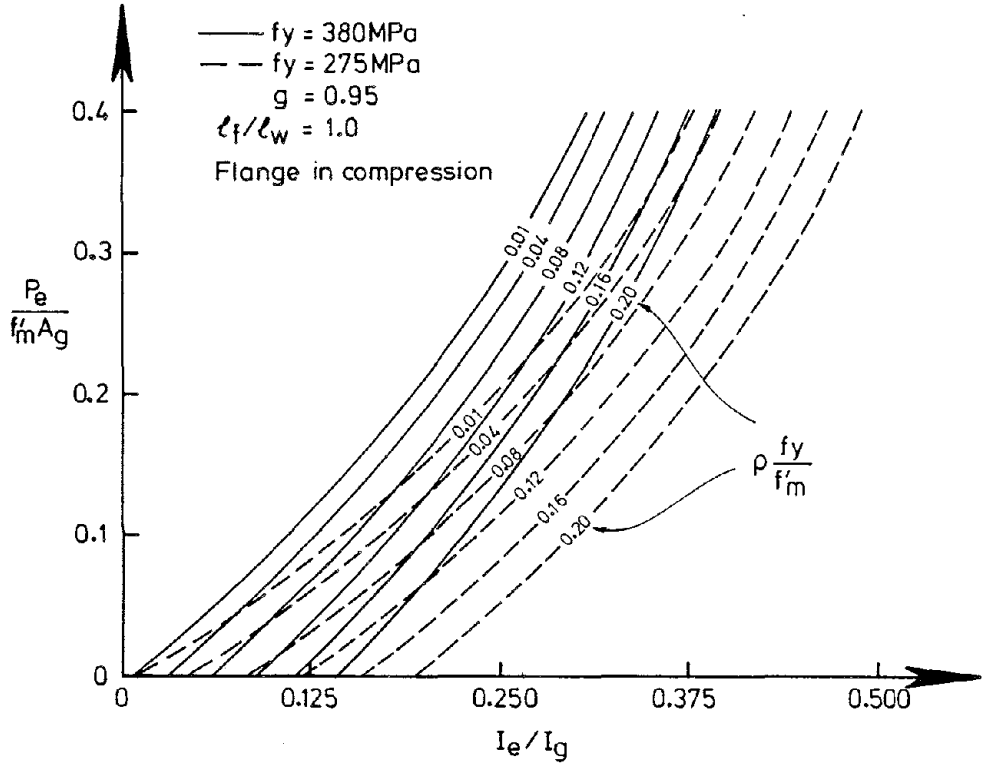

FIG. 2-14 EFFECTIVE MOMENT OF INERTIA, $\ell_f/\ell_w = 1.0$, FLANGE IN COMPRESSION

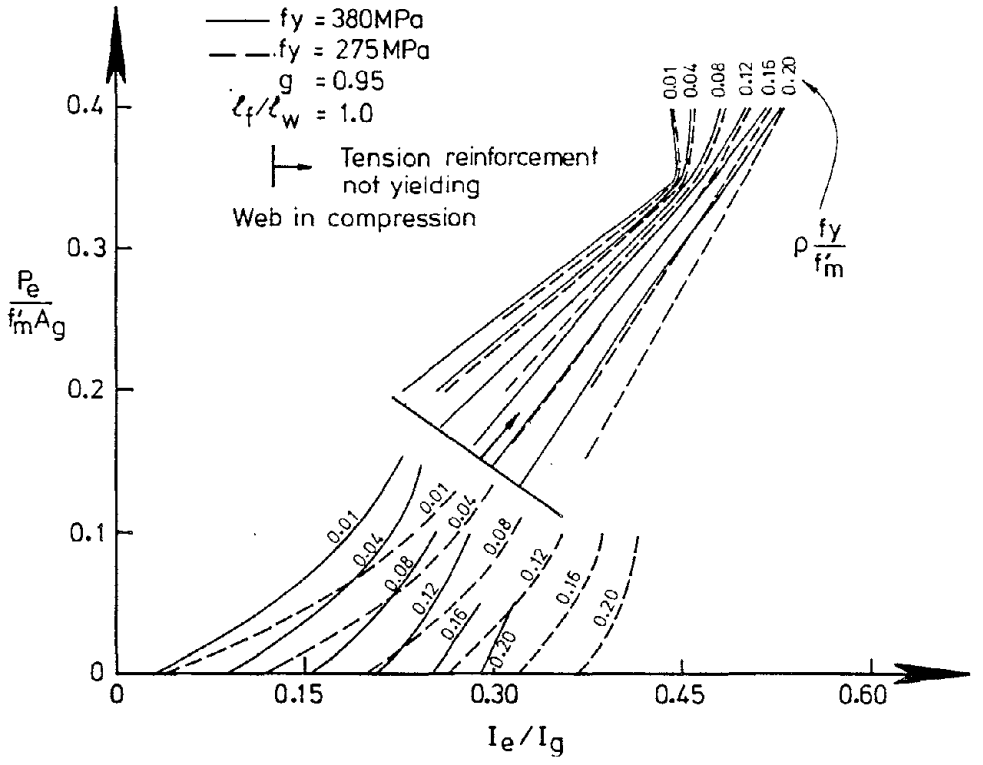

FIG. 2-15 EFFECTIVE MOMENT OF INERTIA, ℓ_f/ℓ_w = 1.0 WEB IN COMPRESSION

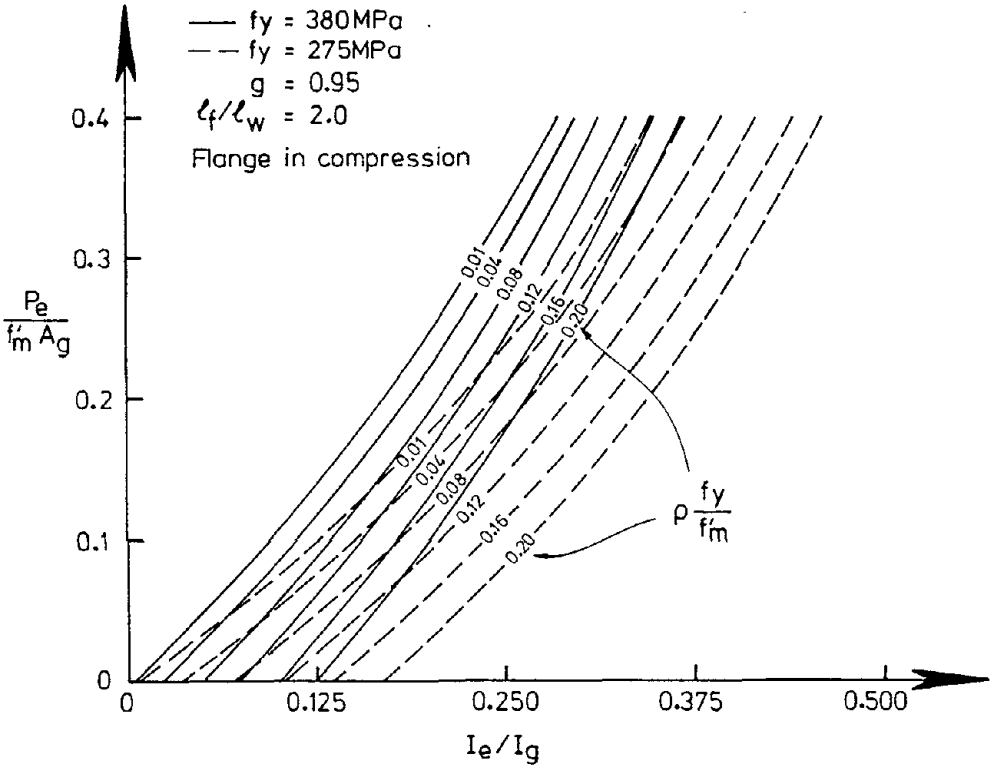

FIG. 2-16 EFFECTIVE MOMENT OF INERTIA, ℓ_f/ℓ_w = 2.0 FLANGE IN COMPRESSION

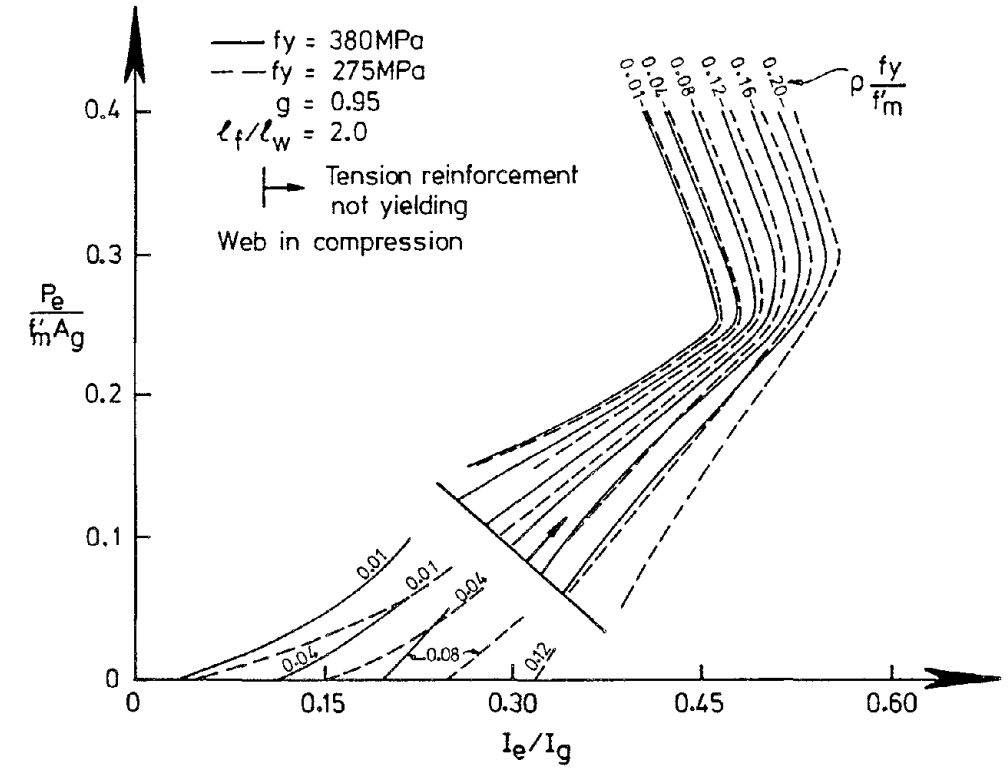

FIG. 2-17 EFFECTIVE MOMENT OF INERTIA, ℓ_f/ℓ_w = 2.0, WEB IN COMPRESSION

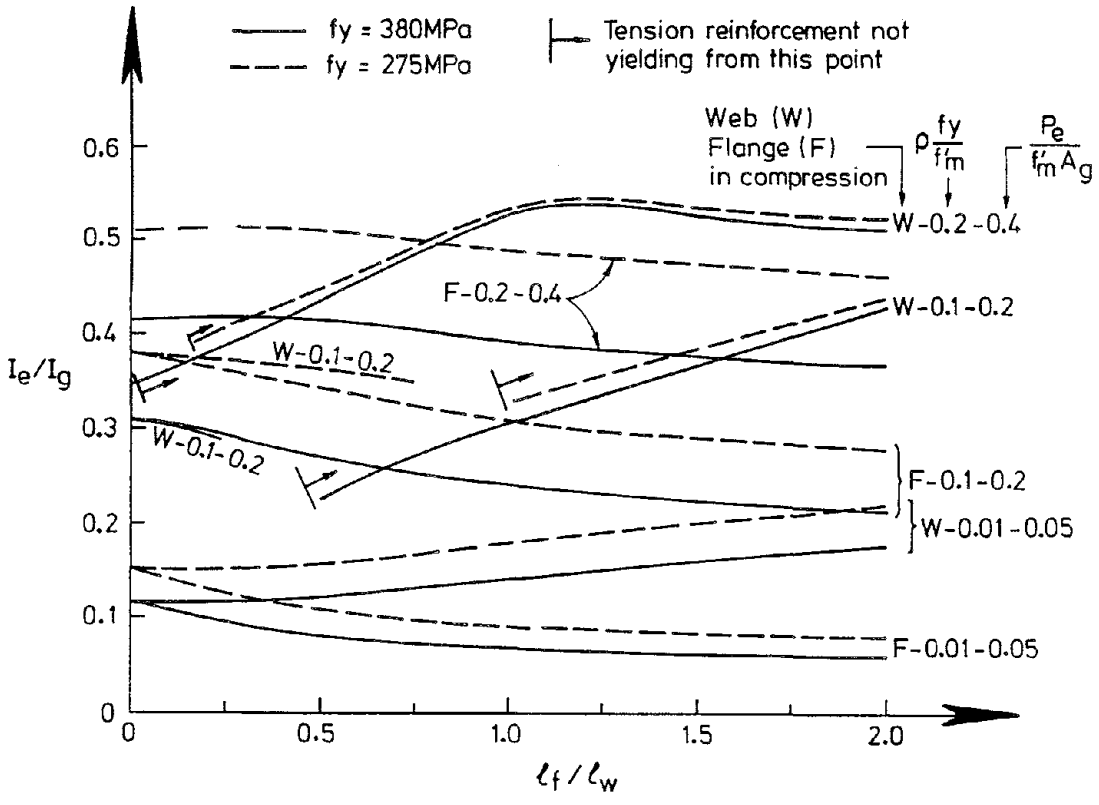

FIG. 2-18 INFLUENCE OF ℓ_f/ℓ_w, LOAD, AND REINFORCEMENT ON EFFECTIVE MOMENT OF INERTIA

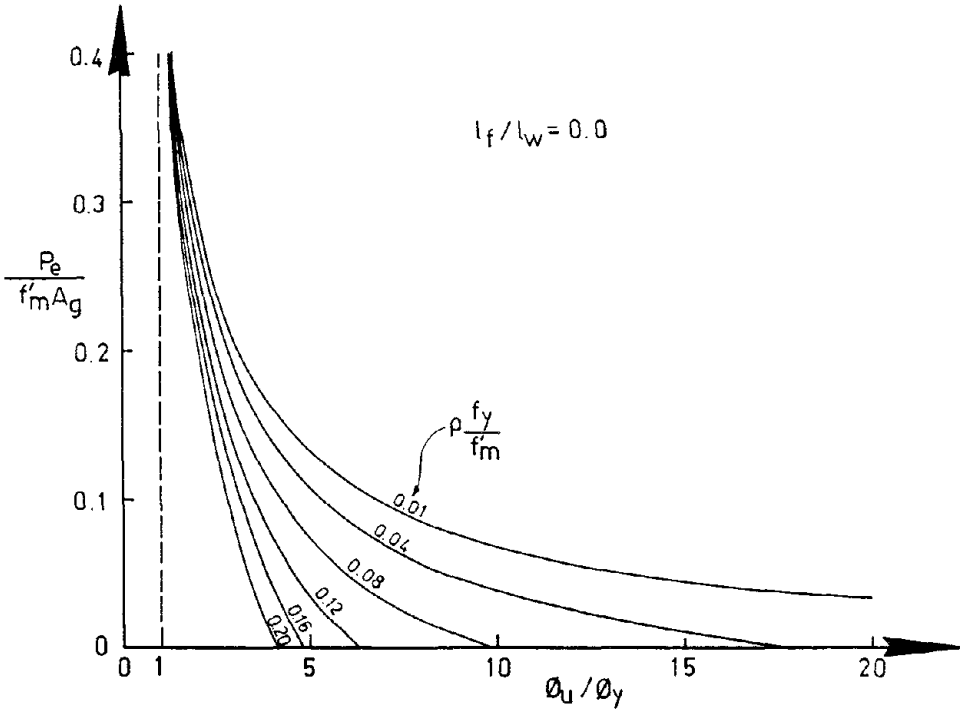

FIG. 2-19 CURVATURE DUCTILITY, ℓ_f/ℓ_w = 0 (RECTANGULAR SECTION)

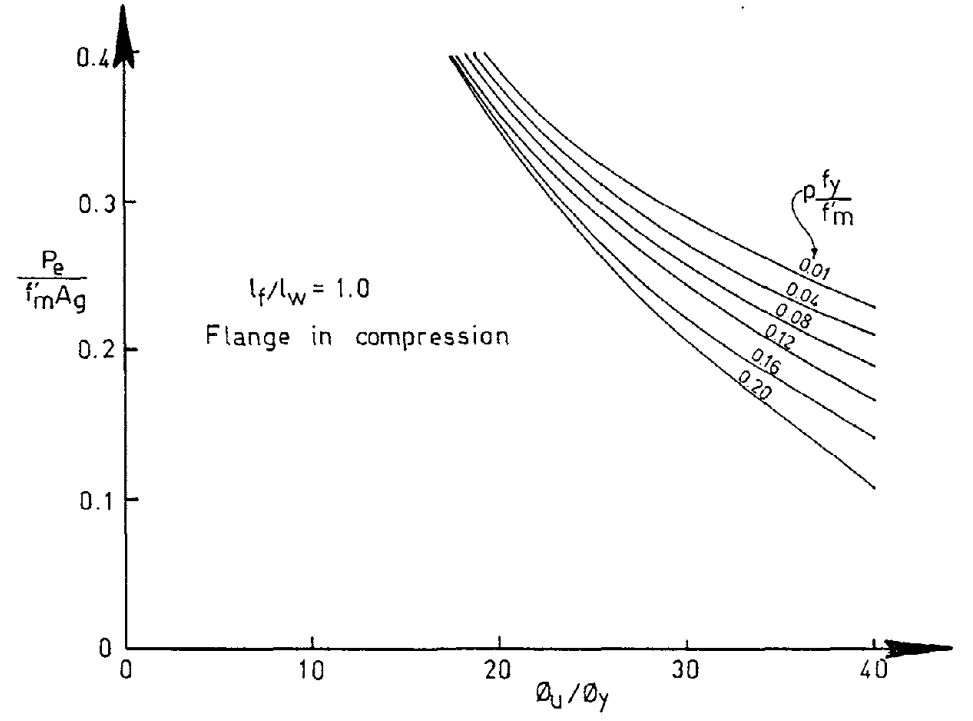

FIG. 2-20 CURVATURE DUCILITY, ℓ_f/ℓ_w = 1.0, FLANGE IN COMPRESSION

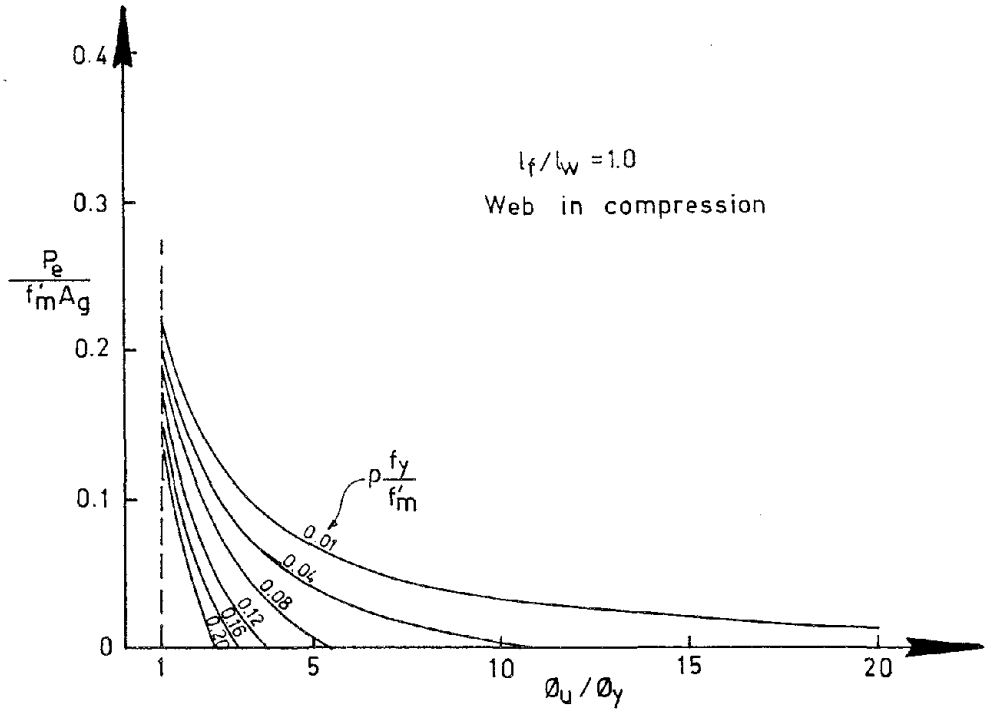

FIG. 2-21 CURVATURE DUCTILITY $\ell_f/\ell_w = 1.0$ WEB IN COMPRESSION

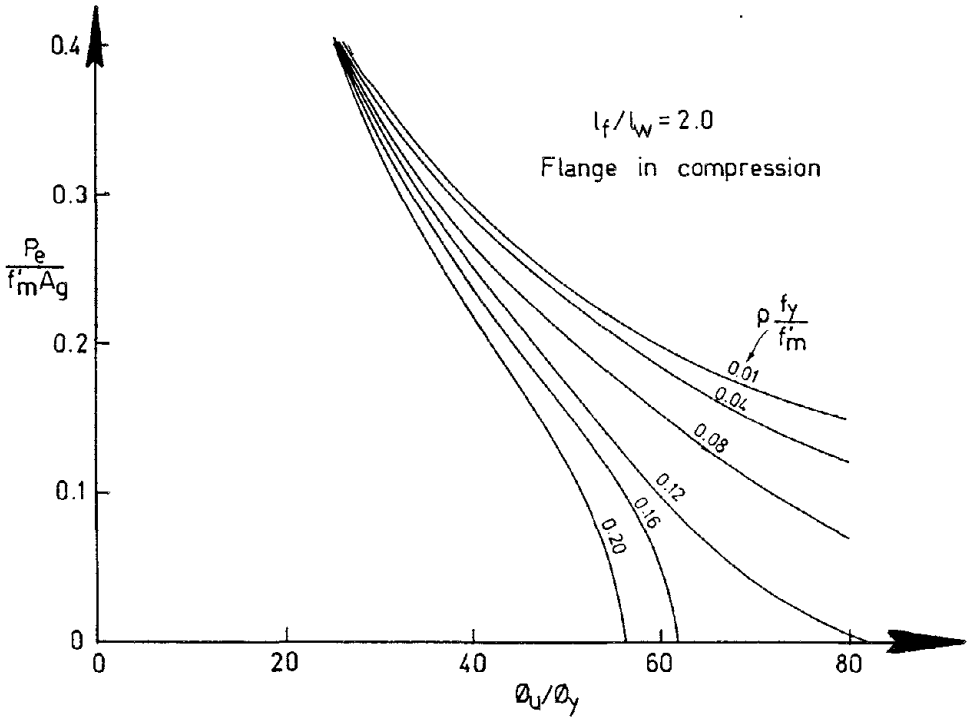

FIG. 2-22 CURVATURE DUCTILITY $\ell_f/\ell_w = 2.0$ FLANGE IN COMPRESSION

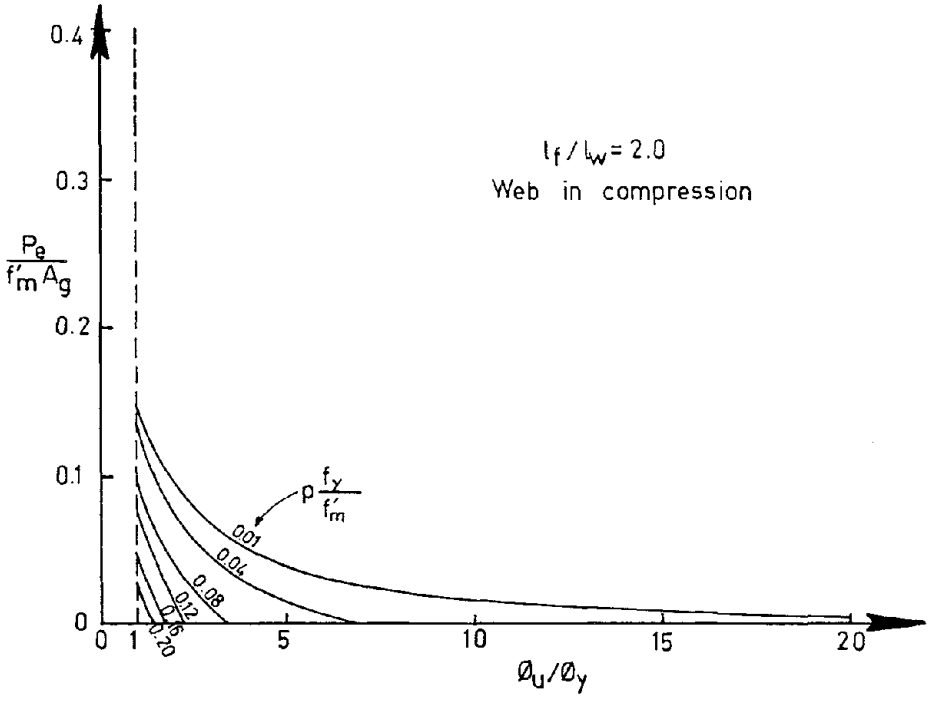

FIG. 2-23 CURVATURE DUCTILITY, ℓ_f/ℓ_w = 2.0 WEB IN COMPRESSION

higher axial loads had been considered, the flexural capacity with the flange in compression would have been higher than with the web in compression.

Interaction curves for flanged walls with $\ell_f/\ell_w = 2$ are shown in Figs. 2-10 and 2-11 for flange in compression and web in compression respectively. Similar trends to those noted for $\ell_f/\ell_w = 1$ are apparent, though the discrepancy in moment capacity is rather larger at low to moderate axial loads. Note that a different moment scale has been used in the two diagrams.

The influence of section aspect ratio (ℓ_f/ℓ_w) on moment capacity is further emphasized in Fig. 2-12, which plots flexural strength against aspect ratio for both directions of loading for a lightly reinforced wall with low axial load ($\rho = 0.01$, $P_e/f'_m A_g = 0.05$), a moderately reinforcement wall with moderate axial load ($\rho = 0.10$, $P_e/f'_m A_g = 0.2$), and heavily reinforced wall with high axial load ($\rho = 0.20$, $P_\ell/f'_m A_g = 0.4$).

For the first case (0.01 - 0.05) the strength difference increases linearly with aspect ratio. Similar behavior is apparent for the second case (0.1 - 0.2), though the differences are not particularly significant until $\ell_f/\ell_w = 0.25$. In the third case (0.2 - 0.4), differences in flexural capacity between the two loading directions are rather small.

2.5.2 Effective Stiffness

The ratio of cracked-section to gross effective stiffness I_e/I_g is plotted against axial load and mechanical reinforcement ratio $\rho f_y/f'_m$ in Figs. 2-13 to 2-18. In many cases, particulary with the web in compression, the section was beyond balanced conditions. That is, ultimate moment conditions were reached without the extreme tension reinforcement attaining yield stress. Under these conditions, the definition of equivalent stiffness given by Eqn. 66 had no validity, and an approximate value based

on the stiffness corresponding to the ultimate moment and ultimate curvature was adopted. The change between definition of stiffness caused a small but significant step change. This is identified, and the compression failure condition represented by an arrow and the legend "tension reinforcement not yielding", in the stiffness plots.

Effective stiffness for rectangular section walls (ℓ_f/ℓ_w = 0) are shown in Fig. 2-13.

It will be noted that, though walls with different reinforcement yield strengths, but identical $\rho f_y/f'_m$ ratios have almost identical moment capacities, there is a significant influence of yield strength on stiffness, with grade 380 reinforcement resulting in lower stiffness (for equal yield force) than grade 275. This is because the higher yield curvature ϕ'_y resulting form the higher yield strain reduces I_e in Eqn. 66 for a constant value m_{yn}.

It will also be noted that for the typically low axial load and reinforcement ratios common for masonry walls, effective stiffness are about $0.25I_g$ or less.

Figs. 2-14 and 2-15 show effective stiffness ratios for flanged walls with ℓ_f/ℓ_w = 1.0. With the flange in compression, stiffnesses are significantly lower that for the rectangular wall (compare Figs. 2-14 and 2-13), and are typically about 50% of the stiffness with the web in compression (compare Figs. 2-14 and 2-15). Note that with the web in compression and axial loads higher than about $0.15f'_mA_g$, tension reinforcement is not yielding, and stiffness is based on ultimate conditions as above. As with the rectangular case, reinforcement yield stress has a significant influence on stiffness.

Effective stiffnesses for walls with aspect ratio ℓ_f/ℓ_w = 2 are shown in Figs. 2-16 and 2-17. Similar trends are observed as

with Figs. 2-14 and 2-15. It should be noted that for high axial loads with the web in compression, maximum stiffnesses do not exceed about $0.5I_g$. The reason for this is softening of the compression zone due to the non-linear compression stress-strain curve and the use in Eqn. 66 of the initial modulus of elasticity for assessment purposes. At high axial loads, these figures reflect reduction in effective modulus of elasticity as much as reduction in cracked-section moment of inertia.

Fig. 2-18 plots effective stiffness against section aspect ratio ℓ_f/ℓ_w for the light, medium and heavy reinforcement/axial load combination of Fig. 2-12. General trends indicate an increase of stiffness with axial load and reinforcement ratio. With the flange in compression, (F curves), the effective stiffness tends to decrease with increasing aspect ratio. An opposite trend is apparent with the web in compression (W curves).

Figs. 2-13 to 2-18 do not include the influence of tension stiffening between cracks. Consequently the curves must be considered as lower bounds to the total stiffness. Also, since the curves relate to the critical section, they will tend to underestimate stiffnesses at sections higher up the wall, where the moment will be lower. However, these effects are compensated to some extent by the reduction in effective stiffness resulting from tensile strain penetration into the wall base, which adds finite rotation at the base of the wall. Calibration of the stiffness charts for rectangular walls with experimental data indicates that use of the I_e/I_g curves results in predictions of yield displacements within ±25% of measured values. At this stage, the curves have not been compared with data for flanged walls.

2.5.3 Curvature Ductility

Charts giving curvature ductility ratios are included in

Figs. 2-19 to 2-23. As with the moment and stiffness charts, ductility ratios are plotted against axial load ratio for a number of mechanical reinforcement ratios $\rho f_y/f'_m$. Charts are only included for f_y = 275 NPa (40 ksi). Curvature ductility ratios for f_y = 380 MPa (55 ksi) are typically about 25% lower.

Fig. 2.19 for rectangular walls indicates that ductility reduces with reinforcement ratio and axial load ratio, as has been noted elsewhere[5].

Fig. 2.20 and 2.21 compare ductilities for flanged walls with ℓ_f/ℓ_w = 1.0 with flange in compression and web in compression respectively. The enormous difference in ductility capacity dependent on the loading direction is immediately apparent. With the flange in compression, very large ductilities are available for all practical combinations of reinforcement ratios and axial load. With the web in compression, very low ductilities result in almost all cases, and for $P_\ell/f'_m A_g \geq 0$, non-ductile response ($\phi_n/\phi_y < 1$) is indicated, implying that tension reinforcement does not yield, as noted in stiffness charts discussed in the previous section.

Similar, though even more highly accentuated behavior occurs with ℓ_f/ℓ_w = 2.0 (see Figs. 2.22 and 2.23). Note the different scales for curvature ductility indicated by these two diagrams.

2.5.4 Example On Use Of Charts

To illustrate the use of the charts, and the significance of directional characteristics of T-section walls, a specific example is worked in the following.

Problem:

Calculate the flexural strength, yield and ultimate displacement and displacement ductility factors for a T-Section cantilever wall of web length 3.6 m (11.8 ft.), flange length 3.8

m (12.5 ft.), thickness = 190 mm (7.48 m) uniformly reinforced with 1 D20 (diameter = 0.787 in., f_y = 275 ksi) bar every 400 mm (16 in.). Masonry compression strength may be taken as 12 MPa (1740 psi). Height to center of seismic lateral forces = 18 m (59 ft.), and total axial load at the wall base is 2460 kN (553 Kips).

Solution:

- Dimensions: $\ell_w = 3.6$m, $\ell_f = 3.8 - 0.19 \approx 3.6$ $\quad t_f = 0.19$.
  $g = (3.6 - 2x0.1)/3.6 = 0.95$

  Axial Load Ratio: $\dfrac{P_e}{f'_m A_g} = \dfrac{2.460}{12 \bullet 2 \bullet 3.6 \bullet .19} = 0.150$

  Reinforcement Ratio: $\dfrac{\rho f_y}{f'_m} = \dfrac{\pi \bullet 10^2 \bullet 275}{400 \bullet 190 \bullet 12} = 0.095$

- Moment Capacity:

With the flange in compression, from Fig. 2.8, with axial load and reinforcement ratios as above, and interpolating between curves,

$$M_{if} = 0.125 f'_m \ell_w^2 t$$
$$= 0.125 \bullet 12 \bullet 3.6^2 \bullet 0.19$$
$$= 3.69 \text{ MNm } (32{,}700 \text{ K"})$$

With the web in compression, from Fig. 2.9,

$$M_{iw} = 0.247 f'_m \ell_w^2 t$$
$$= 7.30 \text{ MNm } (64{,}600 \text{ K"})$$

- Stiffnesses:

With flange in compression, interpolating between curves in Fig. 2.14,

$$I_e/I_g = 0.265$$

The gross section moment of inertia is

$$I_g = 1.73 m^4$$

hence

$$I_{ef} = 0.458 m^4 \quad (53.0 \text{ ft}^4)$$

With web in compression, from Fig. 2-15, the wall is in the transition region between tension yield and ultimate assessment of stiffness. An average of approximately

$I_e/I_g = 0.32$ is taken

Hence $I_{ew} = 0.32 \bullet 1.73 = 0.553 m^4$ (64.0 ft^4)

- Curvature Ductility

With flange in compression, extrapolating in Fig. 2.20, $(\phi_u/\phi_y)_f \approx 44.5$.

With web in compression, from Fig. 2.21, $(\phi_u/\phi_y)_w \approx 1.3$.

- Yield Displacement

Yield displacement can be expressed as $\Delta_y = Mh^2/3EI$

Priestley has recommended a value of $E_m = 1500f'_m$ for deflection calculation to ensure adequately high estimates of stiffness[14], thus

Flange in Compression

$$\Delta_y = \frac{3.69 \times 18^2}{3 \bullet 1500 \bullet 12 \bullet 0.458} = 48.3 \text{ mm } (1.90 \text{ in.})$$

Web in Compression

$$\Delta_y = \frac{7.30 \times 18^2}{3 \bullet 1500 \bullet 12 \bullet 0.553} = 79.2 \text{ mm } (3.11 \text{ in.})$$

- Displacement Ductility

Eqn. 63 gives the displacement ductility as

$$\mu = 1 + 3\left(\frac{\phi_u}{\phi_y} - 1\right)\frac{L_p}{h}\left(1 - \frac{L_p}{2h}\right)$$

Take $L_p = 0.5\ell_w = 1.8$ m. Hence $L_p/h = 1.8/18 = 0.1$.

Flange in Compression:

$$\mu = 1 + 3(44.5 - 1)0.1(1 - 0.05) = 13.4$$

Web in Compression:

$$\mu = 1 + 3(1.3 - 1)0.1 \bullet 0.95 = 1.09$$

- Ultimate Displacement

$$\Delta_u = \mu\Delta_y$$

Flange in compression: $\Delta_u = 13.4 \bullet 48.3 = 647$ mm (25.5 in.)

Web in compression: $\Delta_u = 1.09 \bullet 79.2 = 86.3$ mm (3.40 in.)

The results are summarized in the table below.

SUMMARY OF WORKED EXAMPLE

	Flange in Compression	Web in Compression
Flexural Strength	3.69 MNm (32700K")	7.30 MNm (64,600K")
Effective Stiffness	0.458 m^4 (53.0 ft^4)	0.553 m^4 (64.0 ft^4)
Curvature Ductility	44.5	1.3
Yield Displacement	48.3 mm (1.90 in.)	79.2 mm (3.11 in.)
Displacement Ductility	13.4	1.09
Ultimate Displacement	647 mm (25.5 in.)	86.3 mm (3.40 in.)

CHAPTER 3: SHAKE-TABLE TESTS OF A T-SECTION MASONRY WALL

3.1 INTRODUCTION

In order to provide some preliminary experimental confirmation of the theoretical difference in strength and stiffness characteristics of T-Section walls when loaded in the two opposite directions parallel to the web, a wide-flanged T-Section masonry wall was constructed and subjected to shake-table inertial loading. The tests were carried out in the Civil Engineering laboratories of the University of Canterbury and consisted of three stages.

Stage 1: Free vibration tests to enable elastic stiffness and damping to be measured.

Stage 2: Sinusoidal excitation at gradually increasing levels of table acceleration amplitude to enable the different performance in the opposite directions to be observed.

Stage 3: Simulated seismic excitation applying a scaled earthquake accelerogram to the shake table, at sufficient intensity to develop the full strength and ductility of the wall.
Of particular interest in the test program was the influence of shear lag in the flange on the strength and stiffness of the wall.

3.2 DESIGN AND CONSTRUCTION OF TEST WALL

3.2.1 Construction

The size and weight of the test wall were limited by the load capacity of the available 4m x 2m (13' x 6'6") single-axis shake table. Maximum driving force was 200kN (45 kips), with a maximum velocity of approximately 1m/s (39.4 in/sec), and a maximum stroke of ±150mm (±6 in.).

These limits indicated that a 2m (6'- 6") high wall of

flange by web dimensions 2.2m x 1.0m (7'2" x 3'3") supporting an inertia mass of 5 tons would represent the largest element that would be tested to destruction on the table.

Fig. 3.1 gives overall dimensions of the wall, and identifies the block types used for construction. The wall was constructed out of 190mm wide (7.48in.) fully grouted concrete masonry. Three styles of block were used. End closures were either half-lintel (20.11) or full-lintel (20.13) blocks on side. All other blocks were open-end bond beam units (20.16), allowing transverse reinforcement to be placed at each course.

The intersection of the web and flange is a natural plane of weakness and deserves special attention in design and construction. Continuity of grout, and hence relatively monolithic action was provided by removing the top half of the face shell on the flange block at the web interface, shown by the broken line in the sectional plan XX of Fig. 3.1. When a half-lintel unit (identified as "11" in Fig. 3.1) butted against the flange, half-depth saw cuts were made in the end of the block and the top half of the unit knocked out to allow continuity of grout and transverse reinforcement.

The wall was constructed on a 250mm (10in.) thick foundation slab. Full-height vertical reinforcement was welded to 50 x 50mm (2" x 2") angle sections at the base of the foundation slab to ensure adequate anchorage. The foundation slab was bolted to the shake table by M12 high strength bolts (0.5" dia.) at centers shown in Fig. 3.1.

A professional mason was employed to lay-up the wall to ensure that normal standards of workmanship were achieved. Transverse reinforcement was placed as the wall was constructed, and the entire masonry wall was high-lift grouted in one operation. A pencil insertion vibrator was used to compact the grout.

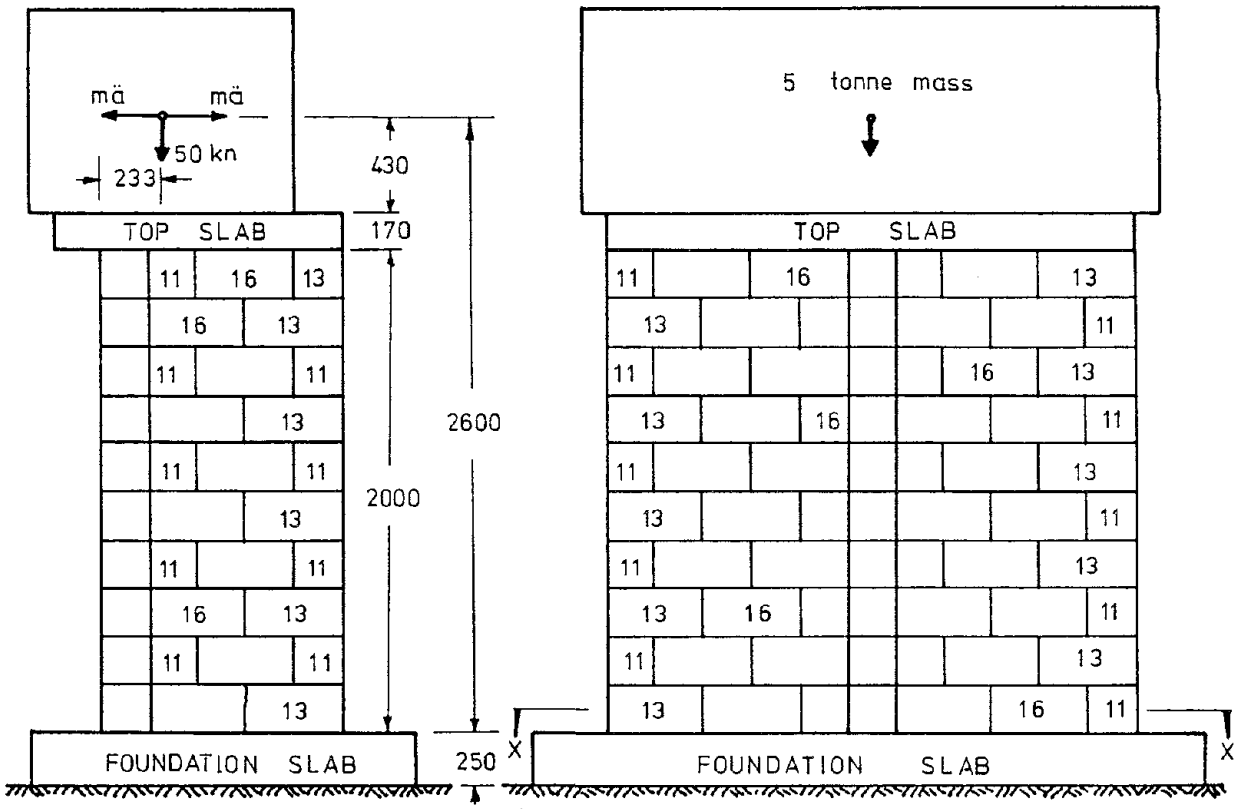

SIDE ELEVATION

FRONT ELEVATION

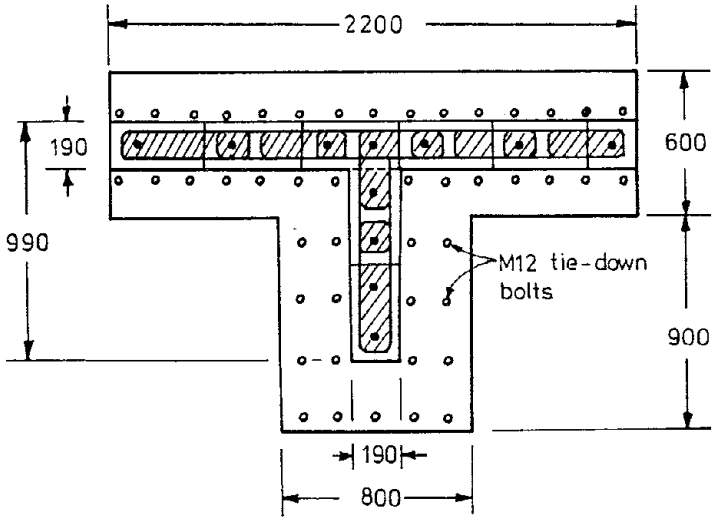

SECTIONAL PLAN XX

FIG. 3-1 TEST WALL DIMENSIONS (mm)

Following completion of the wall, boxing was placed for the top slab, which was 170mm (6.7 in.) thick. The purpose of this slab was to ensure that the inertia force was uniformly distributed to the wall top by the stiff slab diaphragm action.

The main inertia mass was provided by a 5 ton concrete mass which had been used in a previous shake table experiment program. The mass was carefully positioned above the wall so that the center lined up with the centroid of the uncracked section of the wall. This required the apparently eccentric positioning of the mass shown in Fig. 3.1.

3.2.2 Wall Reinforcement

Wall reinforcement positioning is shown in Fig. 3.2. Vertical reinforcement in the web consisted of 5D16 (0.63in.) deformed bars (i.e. one bar in each cell). In the flange, a reduced quantity of reinforcement was provided because of doubts about the capacity of the table to induce inertia response at a sufficiently high level to develop the ultimate moment capacity with the flange in tension, if all cells had been reinforced. Consequently only six additional D16 bars were placed in the flange overhangs.

The resulting reinforcement ratios for the wall were

wall web: $\rho_w = 0.00529$
wall flange: $\rho_f = 0.00317$
average ratio: $\rho = 0.00388$

Transverse reinforcement consisted of D16 (0.63in.) at 200mm (8in.) centers vertically in both the web and the flange. Web horizontal reinforcement was based on capacity design principles to ensure web shear strength exceeded the maximum feasible flexural strength, assuming that all shear was carried by truss mechanisms involving the transverse web reinforcement, and 45°

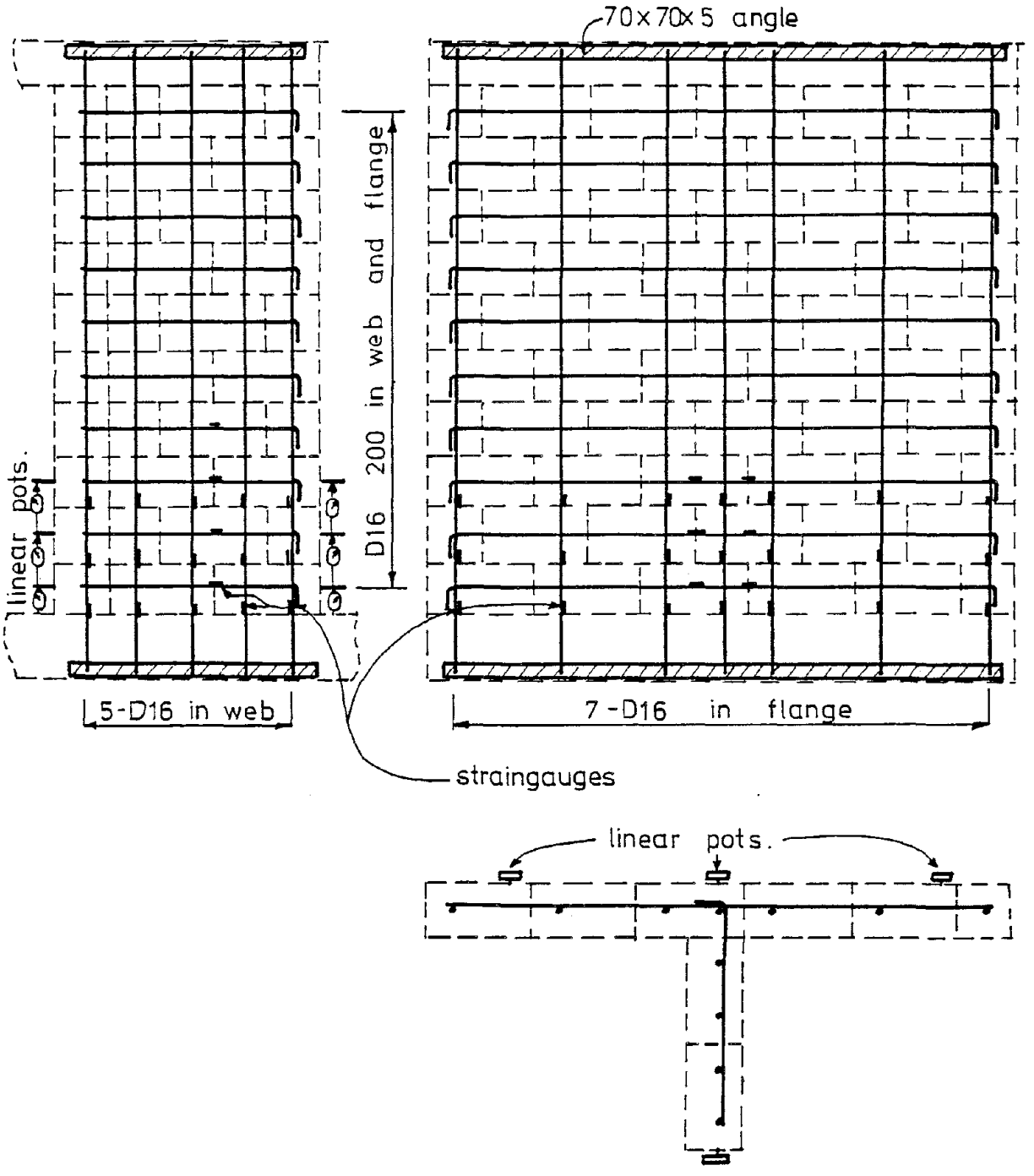

FIG. 3-2 TEST WALL REINFORCEMENT AND INSTRUMENTATION

diagonal masonry compression struts. The web reinforcement was anchored by bending into standard 90° hooks at each end, with the end at the web toe being bent vertically, and the end at the flange intersection being bent horizontally, as shown in Fig. 3-2.

No rational design procedure was available for the flange horizontal reinforcement, which was arbitrarily set equal to the web reinforcement, and anchored in the end cells by standard 90° hooks. In practice, this reinforcement would probably be governed by response requirements under excitation parallel to the flange.

3.2.3 Material Properties

Masonry unit compression strength was provided by the masonry supplier. Grout and mortar compression strengths were assessed by compression tests of standard cylinders at the time of testing the wall. Samples of the D16 reinforcement were tested in an Avery Universal Testing Machine to establish yield and ultimate strength. The following average values were obtained.

Masonry unit compression strength	34.5 MPa = 5000 psi
Mortar compression strength	17.0 MPa = 2470 psi
Grout compression strength	17.7 MPa = 2570 psi
D16 reinforcement yield strength	f_y = 332 MPa = 48100 psi
D16 reinforcement ultimate strength	f_u = 477 MPa = 69200 psi

Masonry prism tests were not carried out. However, an estimate of the probable compression strength can be obtained from the constituent properties, using equations developed by Priestley and Chai[14], namely

$$f'_m = \frac{\chi f'_{cb}}{1.5} \cdot \left\{ \frac{f'_{tb} + \alpha f'_j}{f'_{tb} + \alpha f'_{cb}} \right\} + 0.9375(1-\chi) f'_g \qquad [71]$$

where χ is the ratio of net shell area to gross prism area

(=0.55)

f'_{cb} is the masonry unit compression strength (34.5 MPa).

f'_{tb} is the masonry unit biaxial tension strength ($\approx 0.1 f'_{cb} = 3.45$).

α = j/4.1h where j = mortar bed thickness, h is the masonry unit height. (j = 10mm, h = 190mm, hence α = 0.01284).

f'_j = mortar compression strength = 17 MPa.

f'_g = grout compression strength = 17.7 MPa.

Substituting the values in Eqn. 71, yields $\underline{f'_m = 19.4 \text{ MPa}}$. This value is adopted in the following computation for strength, stiffness and ductility of the test wall.

3.3 THEORETICAL BEHAVIOR OF TEST WALL

3.3.1 Strength and Ductility from Design Charts

Theoretical strengths and ductilities may be found from the design charts of appendix A, with some adjustment necessary to account for the different reinforcement ratios in the web and flange. The approximate equivalent flange width is

$$\begin{aligned} \ell_f &= \ell(\rho_f/\rho_w) \\ &= 2.0 \bullet (0.00317/0.00529) \\ &= 1.12\text{m} \end{aligned}$$

This value should be used when calculating flexural strengths and stiffnesses with the flange in tension. The axial load ratio must be adjusted to ensure that the total load on the equivalent section is the same as the real section, and a small error in moment capacity will result from the incorrect point of application of the resultant axial load.

With the flange in compression, more accurate results should be obtained, particularly for ultimate curvature, but using the full width of the section, and again basing the reinforcement

content on the web ratio of $\rho_w = 0.00529$.

In order to assess the errors resulting from the above approximations, theoretical values for moments, curvatures and displacements at first yield and at ultimate were also calculated from first principals. The results of the comparison are shown in Table 3.1. Only these values obtained directly from the tables are included. The value of axial load at the wall base was taken as:

$P = 49.9kN$ [inertia mass]
$+ 10.8kN$ [top slab: 2.2m x 1.2m x 0.17m]
$+ 22.8kN$ [wall weight at $20kN/m^3$]
$= 83.5kN$

The parameters for use in the design tables were thus:

Flange in Compression: $\ell_f/\ell_w = 2.0$, $\rho = 0.00529$,
$\rho f_y/f'_m = 0.00529 \times 332/19.4 = 0.0905$
$P/f'_m A_g = 0.0835/19.4(3 \times 0.19)$
$= 0.00755$

Web in Compression: $\ell_f/\ell_w = 1.19$
$\rho f_y/f'_m = 0.0905$
$P/f'_m A_g = 0.0835/19.4(2.19 \times 0.19)$
$= 0.0103$

It will be seen from Table 3.1 that the agreement between the hand calculations and the approximate values using the tables is within about 5%, except for the curvature ductility factor with the flange in compression. Here the approximate value from the tables is low by 39%. The error occurs because use of the tables results in an incorrectly high quantity of flange reinforcement, which actually yields in tension when the flange is in compression, since the neutral axis depth is only about 30-40mm. The extra tensile reinforcement implied increases the depth of compression, hence reducing the ultimate curvature and

curvature ductility factor.

TABLE 3.1 THEORETICAL LIMIT STATES

Parameter	Web in Compression		Flange in Compression	
	Exact	Tables	Exact	Tables
Yield moment M_y (kNm)	434	•	131	•
Yield curvature ϕ_y/mm	2.98×10^{-6}	•	2.02×10^{-6}	•
Elastic stiffness $[M_y/\phi'_y]$ (Nm^2)	146	•	65x10	•
Ultimate moment M_i (kNm)	494	479	213	225
Ultimate curv. ϕ_u/mm	10.3×10^{-6}	•	94.3×10^{-6}	•
Curv. ductility $[M_y/M_u,\ \phi_u/\phi'_y]$	3.09	2.92	28.5	17.5
Yield displacement Δy(mm)	7.50	8.0	7.45	7.61
Ult. displacement Δy(mm)	15.7	•	114.3	•
Displacement duct. μ	2.09	•	15.3	•

The small discrepancies between the "exact" and "table" values with the web in compression result from a more accurate shape of the compression stress-strain curve adopted in preparing the tables, and from the effect of shifting the center of application of the axial load, as noted above.

It is apparent that the tables can give a useful estimate of behavior for sections with different rebar ratios in web and flange. However, caution is advised when axial load levels are high, as significant errors in moment capacity could occur with the web in compression. Errors in curvature ductility for the flange in compression case are not likely to be significant, as the ductility capacity for this case will normally be more adequate.

3.3.2 Theoretical Shear Strength:

Assuming no contribution from masonry shear resisting mechanisms in the plastic hinge region

$$V_i = A_v f_y d/s = 202 \times 332 \times 0.89N/0.2$$
$$= 297.8kN$$

At ideal flexural capacity, with the flange in tension,

$$V_u = M_i/2.6 = 494/2.6 = 190kN$$

therefore $V_i/V_u = 1.56 > 1.25$ required for capacity design. Note, at expected over strength of 1.25 x 190 = 238kN, shear stress is

$$v_o = 238/(0.99 \times 0.19)\ kN/m^2 = 1.27\ MPa$$

At this level of shear stress, diagonal cracking is expected.

3.4 INSTRUMENTATION

Vertical and horizontal reinforcement within the plastic hinge region was straingauged with 51 - 5mm gauge-length Showa straingauges. Position of the gauges are identified in Fig. 3.2.

Sakae Linear potentiometers were attached to the end of the web and to three locations on the outer face of the flange, using 10mm dia rods epoxied into holes drilled into the wall. Potentiometer locations are also identified in Fig. 3.2.

Showa straingauge accelerometers were attached to the table and to mid-height of the inertia mass to enable table and response accelerations to be monitored.

Table displacements were controlled by the DARTEC servohydraulic operating system, and response acceleration relative to the table datum were measured by a straingauged

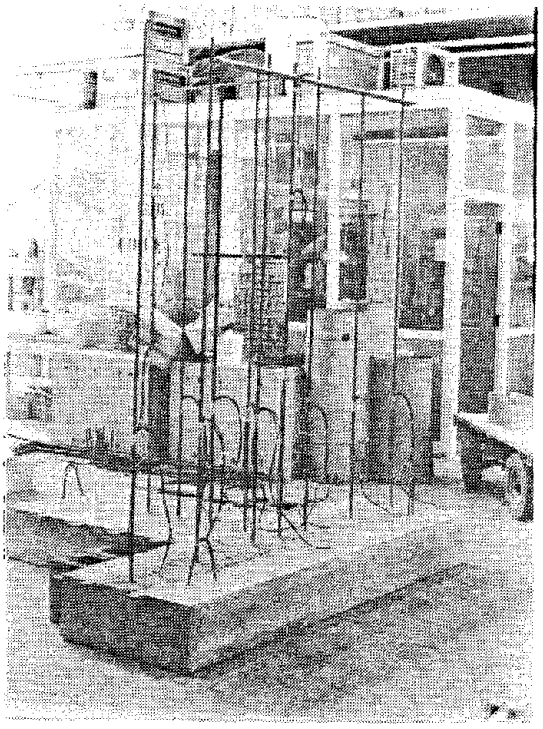

(a) Wall Base and Straingauged Vertical Rebars

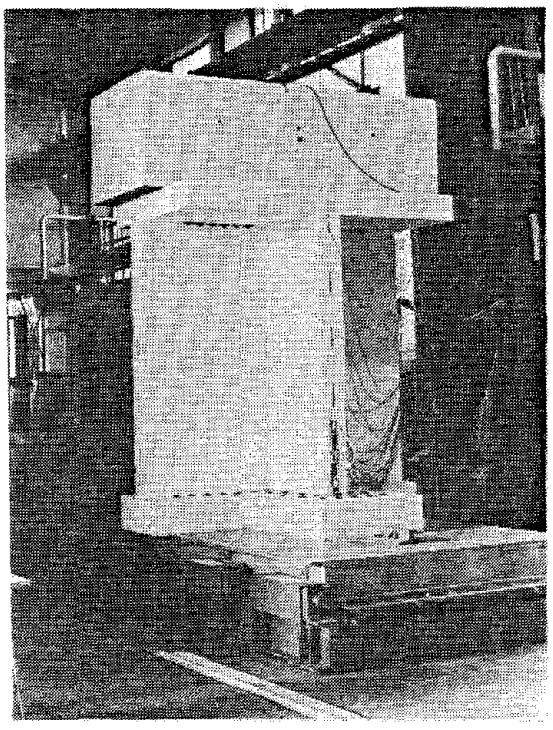

(b) Wall Ready for Test

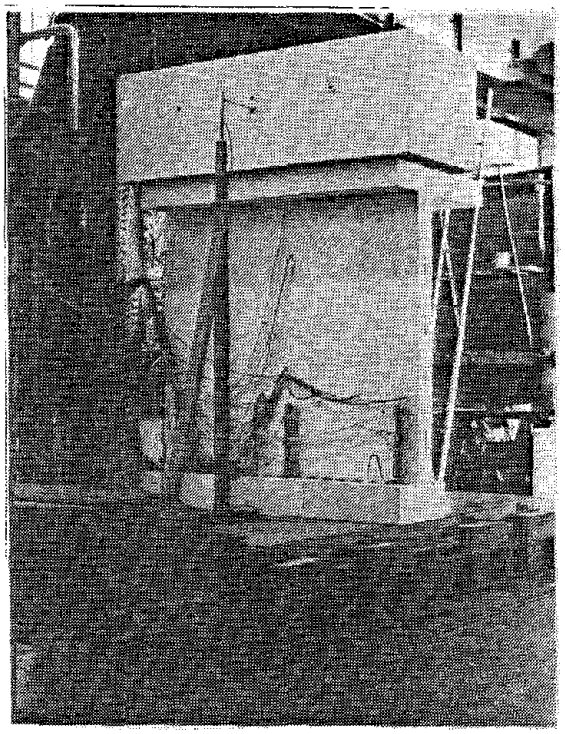

(c) Wall ready for test

FIG. 3-3 WALL CONSTRUCTION

cantilever displacement gauge constructed specially for the test. This gauge had a nominal range of ±30mm, and was mounted on a steel support frame, bolted to the table.

All data was recorded by a high speed data acquisition system capable of reading 64 channels at 100Hz. The data was recorded by computer and stored for subsequent analysis and manipulation.

Fig. 3.3 shows the wall base and reinforcement ready for blocklaying, and the completed wall with instrumentation and inertia block attached.

3.5 TEST PROGRAM

Testing of the wall was carried out in three stages: free vibration, sinusoidal excitation, and simulated seismic excitation.

3.5.1 Free Vibration Tests

Prior to forced vibration testing, a small amplitude excitation was applied to the table, and abruptly stopped, causing the table to vibrate in its natural frequency. By monitoring the center of mass displacement, the frequency and damping of the decay curve could be calculated. In this initial test it was expected that the wall would be essentially uncracked.

The modification of stiffness and damping during the forced vibration sinusoidal testing was monitored by measuring the frequency and damping of the free decay after sinusoidal input was completed.

3.5.2 Sinusoidal Testing

The second stage of testing involved application of a series of 10-cycle bursts of sinusoidal excitation at gradually increasing acceleration amplitude. The schedule of tests is

defined in Table 3.2. Test S8-2 was carried out between tests E3 and E4 in order to measure stiffness degradation of the model induced by high-amplitude seismic response.

3.5.3 Seismic Excitation

The El Centro 1940 N-S component was used as input acceleration to investigate response under real earthquake conditions. Because the excitation mass of the model was low compared with the flexural strength and stiffness, a time scale of 1/3 was adopted. This resulted in higher acceleration inputs, and more seismic energy in the frequency range of the wall model.

The very large increase in intensity between tests E7 and E8 was unintentional, due to human error, and resulted in the ultimate capacity of the wall being achieved in test E8.

TABLE 3.2 DYNAMIC TESTS OF WALL

Test #	Excitation	Time Scale Tm/Tp	Max Table Acc (xg)	Test Duration (sec)
S1	Free Vibration	1		1
S2	Free Vibration	1		1
S3	5Hz	1	0.3	2
S4	5Hz	1	0.4	2
S5	5Hz	1	0.5	2
S6	5Hz	1	0.6	2
S7	5Hz	1	0.7	2
S8	5Hz	1	0.8	2
S9	5Hz	1	0.9	2
S8-2	5Hz	1	0.8	2
E1	El Centro x 0.5	0.333	0.16	9
E2	El Centro x 0.75	0.333	0.24	9
E3	El Centro x 1.0	0.333	0.32	9
E4	El Centro x 1.5	0.333	0.48	9
E5	El Centro x 2.0	0.333	0.64	9
E6	El Centro x 2.5	0.333	0.80	9
E7	El Centro x 3.0	0.333	0.96	9
E8	El Centro x 6.0	0.333	1.92	9

3.6 RESULTS OF TEST PROGRAM

3.6.1 Observed Behavior

During early stages of sinusoidal excitation, the test unit appeared to behave as a homogeneous unit, with no visible cracking developing at any location. After test S4 (maximum table acceleration = 0.4g nominal) flexural cracking developed at the end of the web/base interface. In subsequent tests to higher accelerations, the extent of cracking along the base progressed, until by test S9 the crack was visible virtually to the inside edge of the flange.

Cracking at the outside edge of the flange (resulting from acceleration pulses putting the flange in tension) was not observed until test S8 (nominal table acceleration of 0.8g). At this stage, the visible crack covered the central 2/3 of the flange interface, but did not extend to the corners, indicating shear lag effects. After test S9 (nominal table acceleration of 0.9g), the length of flange cracking extended to one corner of the flange, and about 300mm from the other corner.

Fig. 3.4 shows the condition of the lower region of the test unit after S9. The markings S5, S6, S7, etc., indicate the extent of cracking at the end of the corresponding test. It will be noted that at this stage cracking was confined to the wall/base interface. Mortar beds at levels above the base apparently remained uncracked.

During simulated earthquake excitation tests, flexural cracks gradually developed at courses 2 and 3 above the base in the web, but no cracking was noted above the wall/base interface in the flange. Cracking over the lower 400mm of the flange/web interface was noted after test E7.

As noted earlier, test E8 involved table excitations of approximately twice those of test E7 due to operator error.

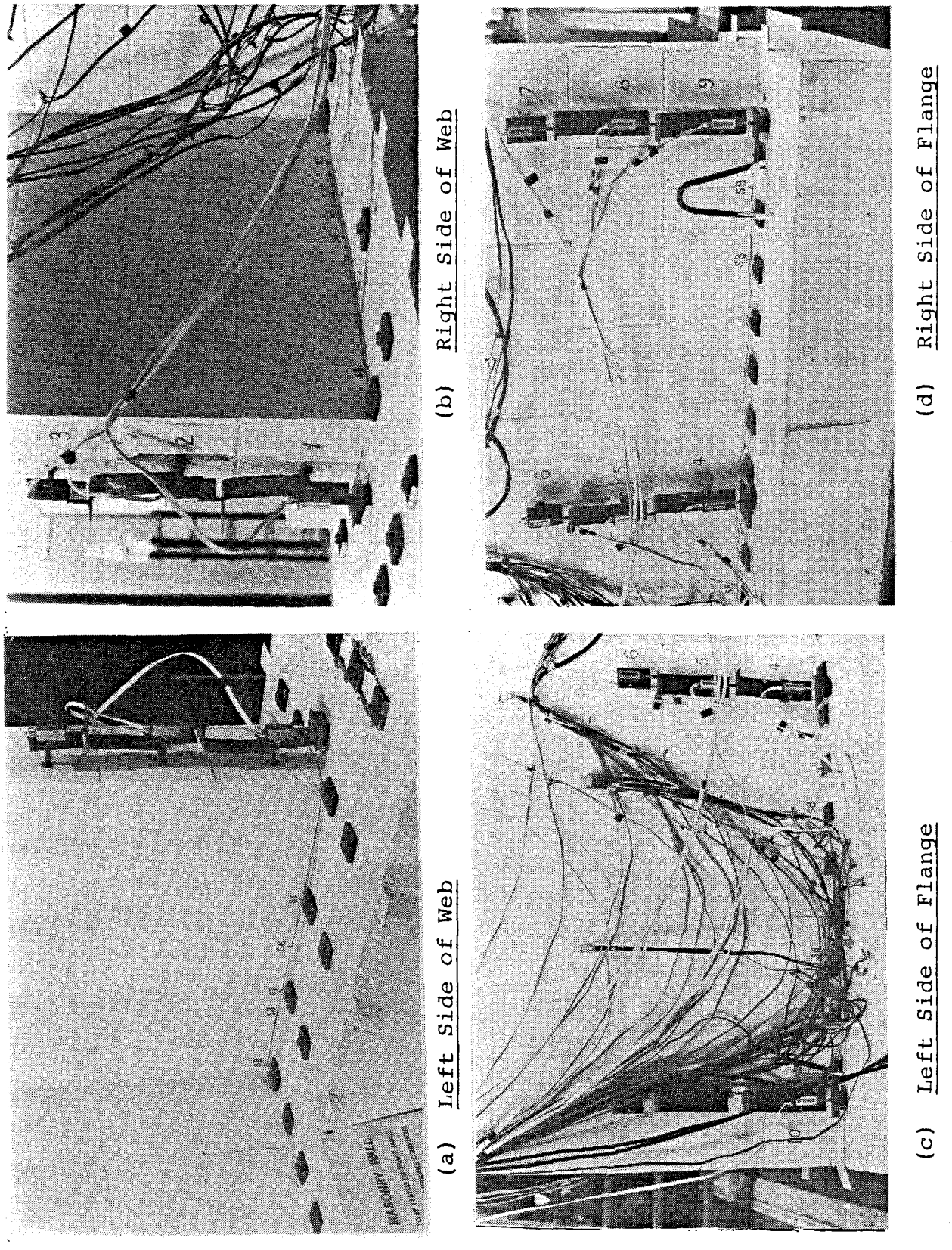

(a) Left Side of Web

(b) Right Side of Web

(c) Left Side of Flange

(d) Right Side of Flange

FIG. 3-4 CRACK PATTERN AFTER SINUSOIDAL-EXCITATION TESTS

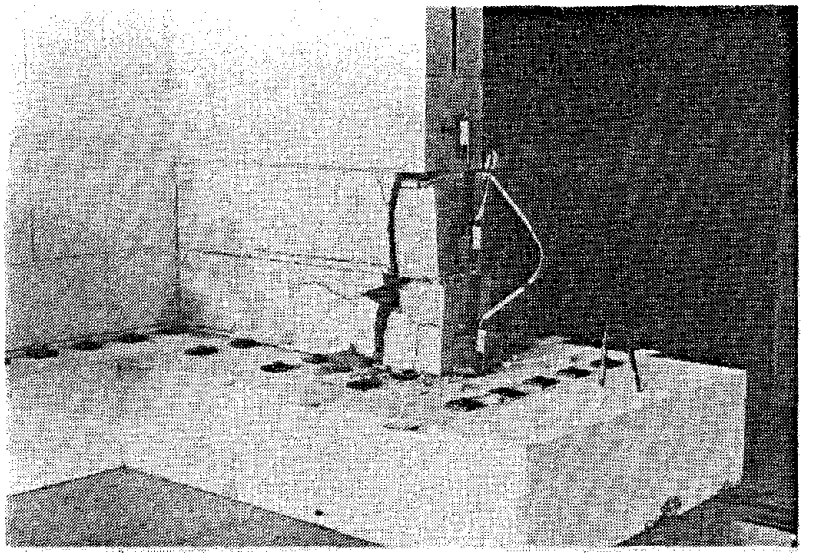

(a) Compression Failure of Web Toe

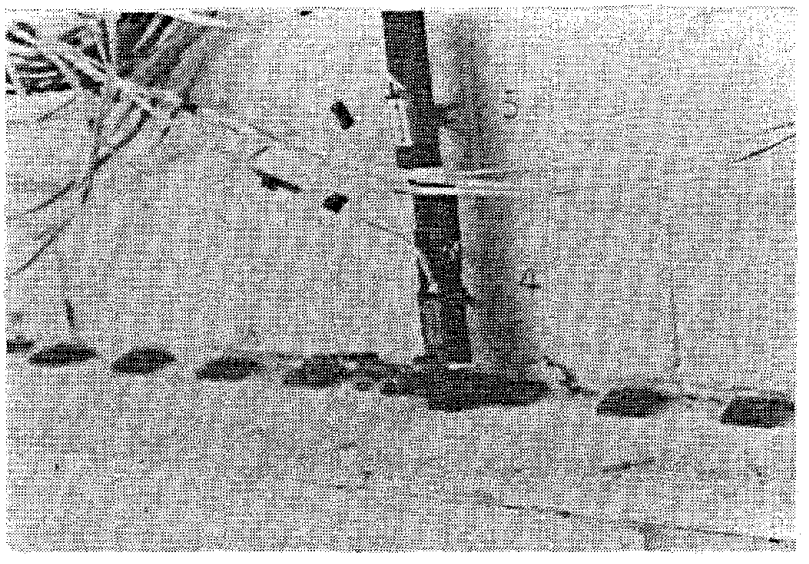

(b) Evidence of Wall Sliding on Base (Flange Base)

FIG. 3-5 CONDITION OF WALL AFTER EARTHQUAKE EXCITATION (TEST E8)

During test E8, crushing and vertical splitting of the lower two courses of blocks at the end of the web occurred, indicating that the limits to available ductility had been achieved. Incipient diagonal cracking of the web due to shear was also noted.

The condition of the web at the end of test E8 is shown in Fig. 3-5a. Fig. 3-5b shows a detail of the flange at the same stage of testing. Cracking was still confined to the wall base, but there is clear indication of several mm sliding displacement of the wall of the base. At this stage, testing of the wall was terminated.

3.6.2 Acceleration and Displacement Response of Wall

Typical time-history plots of displacement and acceleration response of the wall to sinusoidal excitation are shown in Figs. 3-6 and 3-7, which depict response to tests S7 and S9 respectively. In these figures, W.I.C. and F.I.C. mean web in compression, and flange in compression respectively, and define the direction of response. The displacement plotted is the displacement of the center of mass relative to the table, and the acceleration is the absolute center-of-mass acceleration. Examination of the figures indicates the following.

- The displacement traces have a high frequency (approx. 40Hz) of significant amplitude superimposed on the basic 5Hz response. As this frequency is not apparent in the acceleration response, it is clear that it does not represent a true displacement of the model, but must result from natural frequency response of the support system for the displacement transducer. The effect is less noticeable in test S9 then in S7, perhaps due to the larger amplitude of true center-of-mass displacement.

- With the effects of spurious support frame displacements removed by curve smoothing, displacements with the flange in compression are about 50% to 100% larger than with the flange in tension.

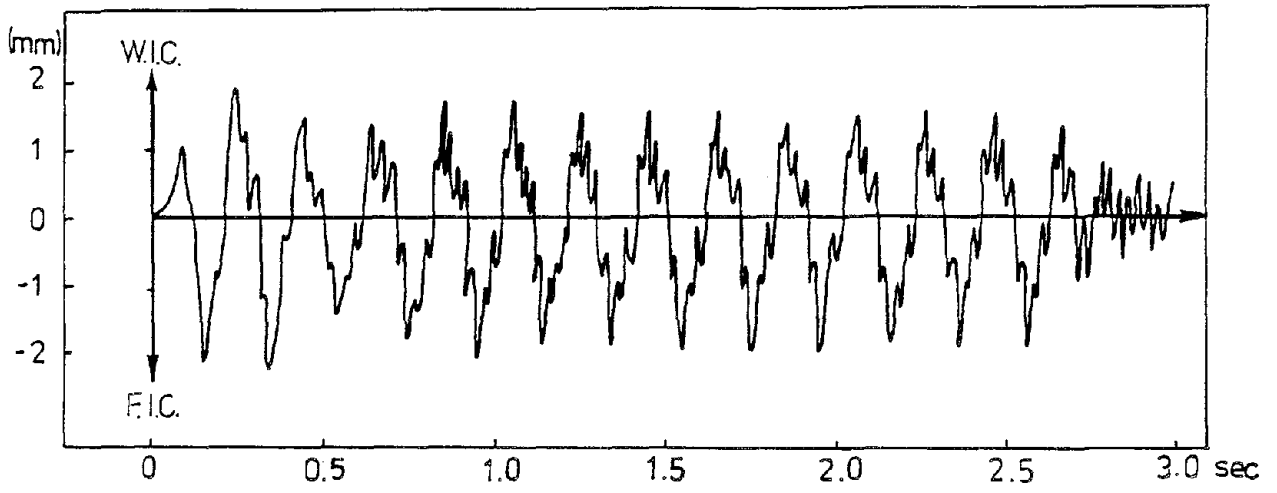

(a) Displacement

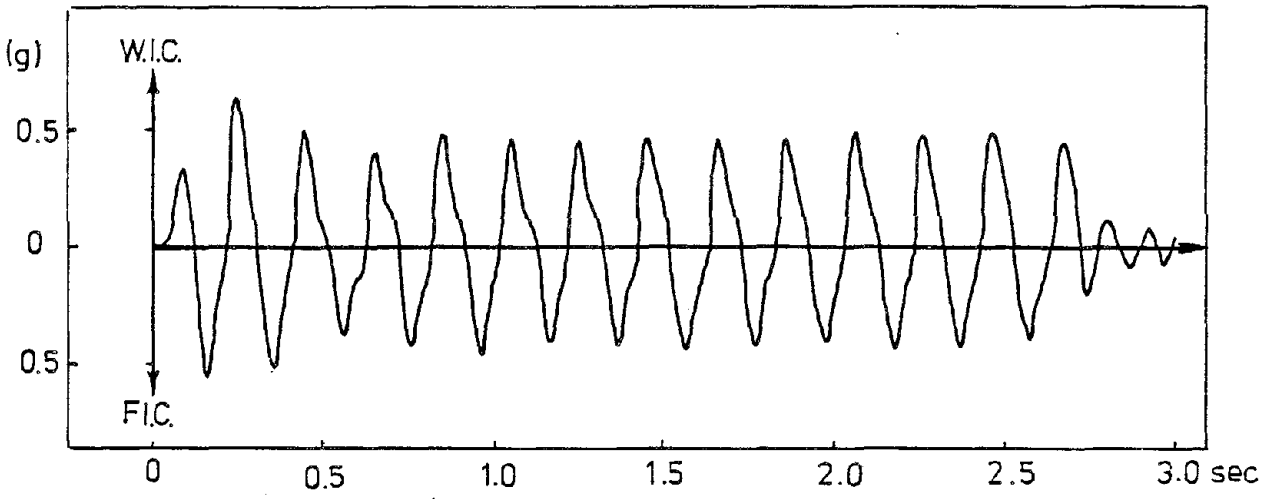

(b) Acceleration

FIG. 3-6 CENTER-OF-MASS RESPONSE DURING TEST S-7

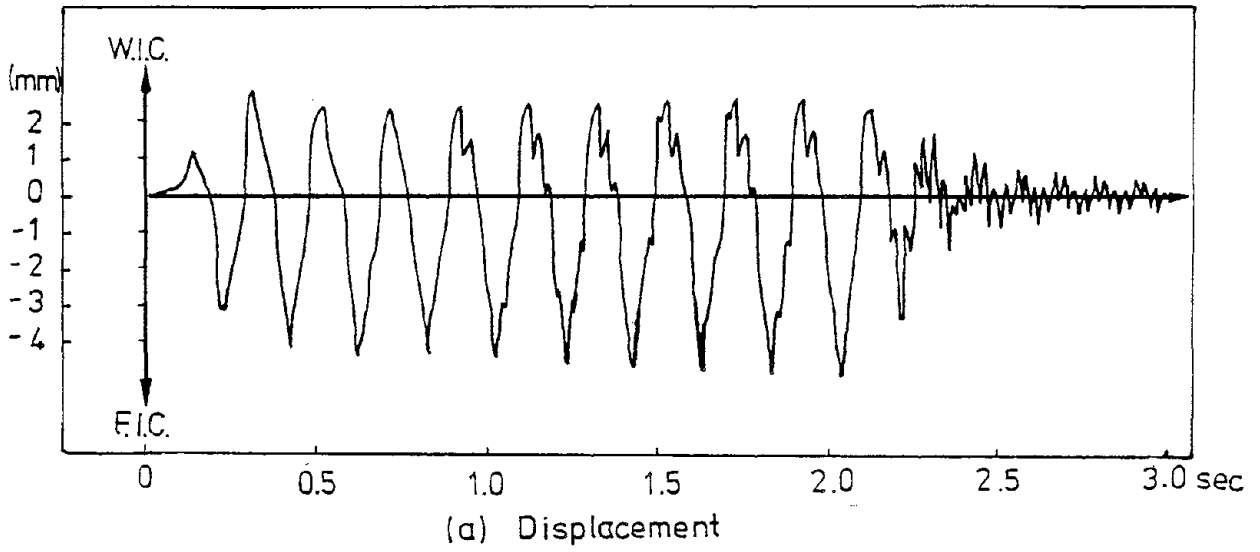

(a) Displacement

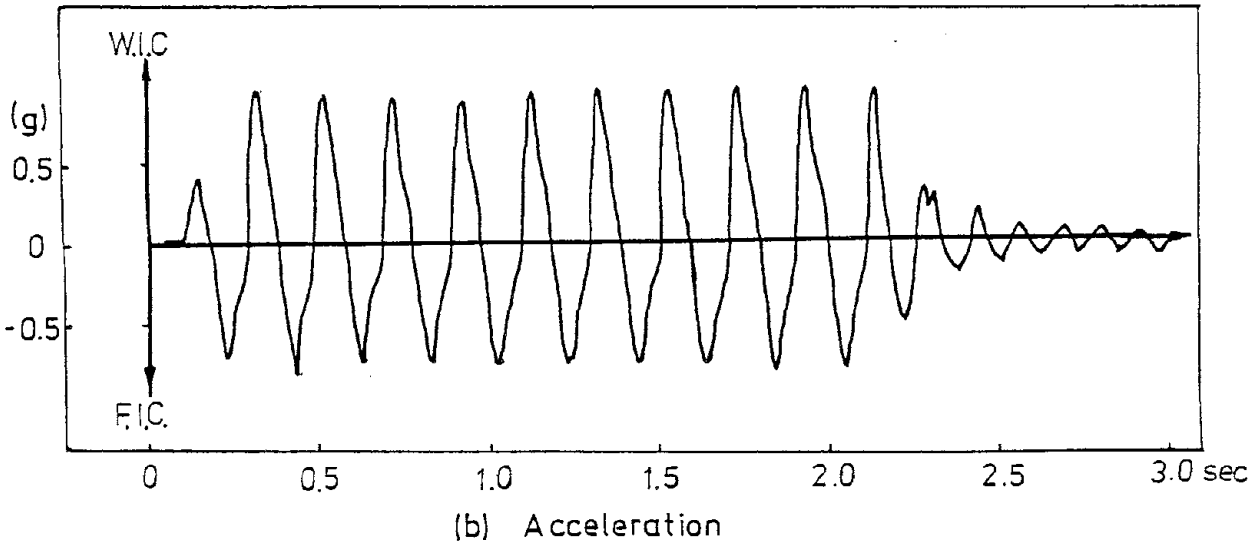

(b) Acceleration

FIG. 3-7 CENTER-OF-MASS RESPONSE DURING TEST S-9

• Acceleration response is reasonably stable, but the wave form differs significantly from sinusoidal, and peak accelerations with the flange in compression are significantly less than with the flange in tension.

• An approximate estimate of the relative stiffness of the wall in the opposite directions of loading may be found from the ratio of peak acceleration/displacement calculated for the two directions. From the test S9 data, the ratio is

$$(EI)_w/(EI)_F \approx 2.21$$

where $(EI)_w$ and $(EI)_F$ are the effective stiffness with the web and flange in compression respectively. This is in excellent agreement with the calculated stiffness ratio of 2.25 based on the hand calculations summarized in Table 3-1.

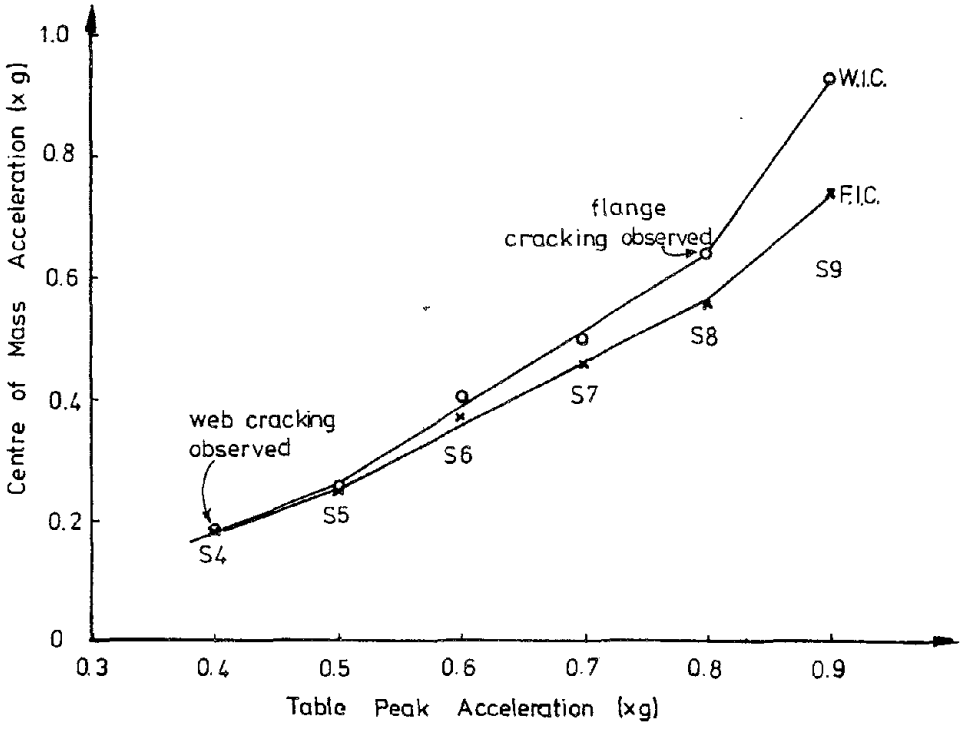

FIG. 3-8 ACCELERATION RESPONSE OF WALL VS. TABLE ACCELERATION

Fig. 3-8 shows the relationship between stabilized

acceleration response of the center of mass, and table peak single-amplitude acceleration. As is apparent from Figs. 3-6 and 3-7, wall response took 2-3 cycles to stabilized, and response in Fig. 3-8 represents average behavior for the later cycles in each of tests S4 to S9. For earlier tests (S1 - S3), the level of noise/signal was too great for accurate determination of peak acceleration.

Two trends are apparent in Fig. 3-8. Initially, peak response in the two opposite directions (web in compression and flange in compression) was essentially the same. After test S4, when web cracking was first observed, response in the two directions diverged, with higher acceleration being recorded in the W.I.C. direction, as expected. After flange cracking was noted at test S8, the divergence increased further.

The second trend is the apparent tri-linear nature of the response curves. There are pronounced changes in the slope of the curves at S5 and S8. It is felt that these correspond to significant changes in effective natural frequency of the wall, with the corresponding period drop bringing response closer to the excitation frequency, and hence resulting in greater amplification of the excitation.

Figs. 3-9 to 3-11 show displacement and acceleration time-histories for three simulated earthquake tests. Response is essentially elastic for tests E5 and E7, but the response to test E8 is markedly different. A significant lengthening of the period of response to about T = 0.3 sec. which occurred after a large inelastic pulse at 1.2 sec. is apparent, and large residual displacements (about 28 mm) with the flange in compression occurred. The peak displacement of 19.1mm with web in compression was sufficient to cause the web toe crushing noted earlier in this section, but the much larger displacement of 57mm with the flange in compression caused no apparent distress to the flange. Peak accelerations during test E8 were 2.55g with the

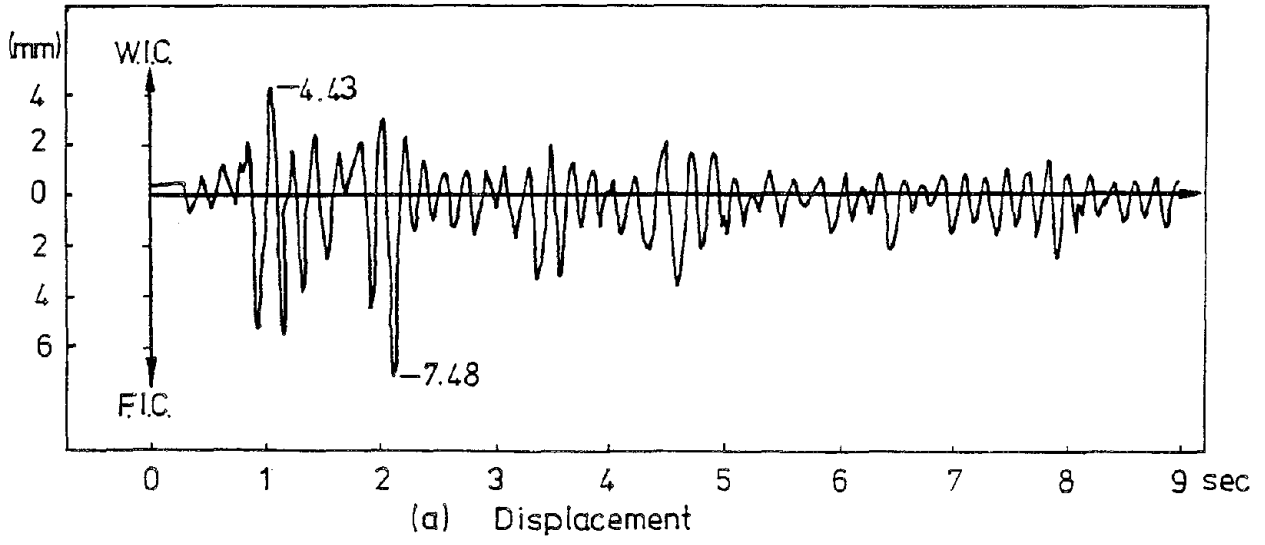

(a) Displacement

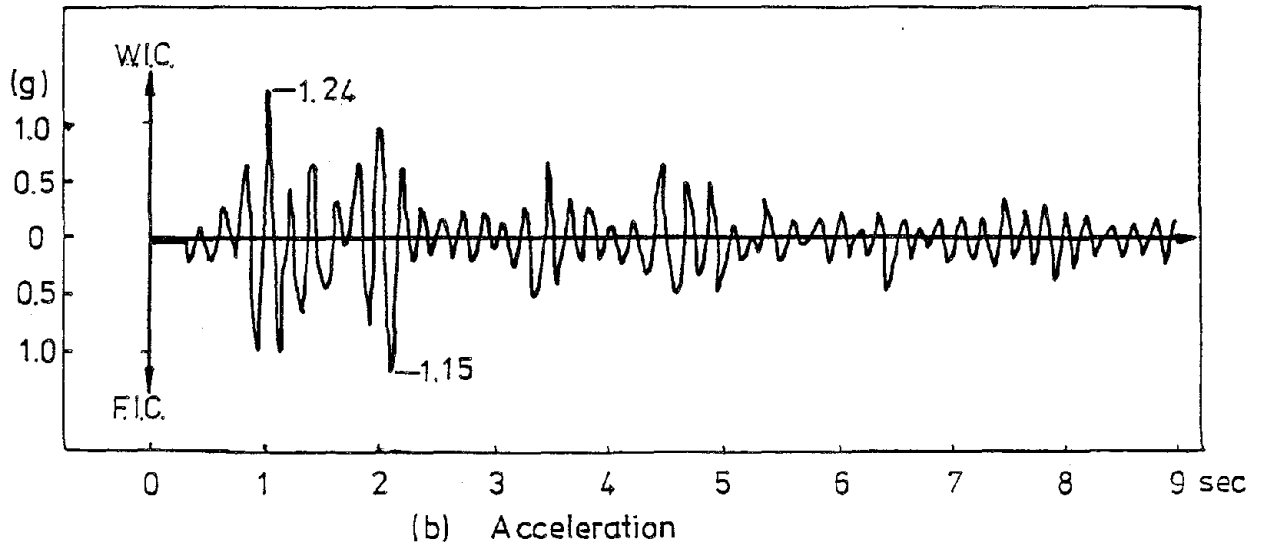

(b) Acceleration

FIG. 3-9 CENTER-OF-MASS RESPONSE TO TEST E-5

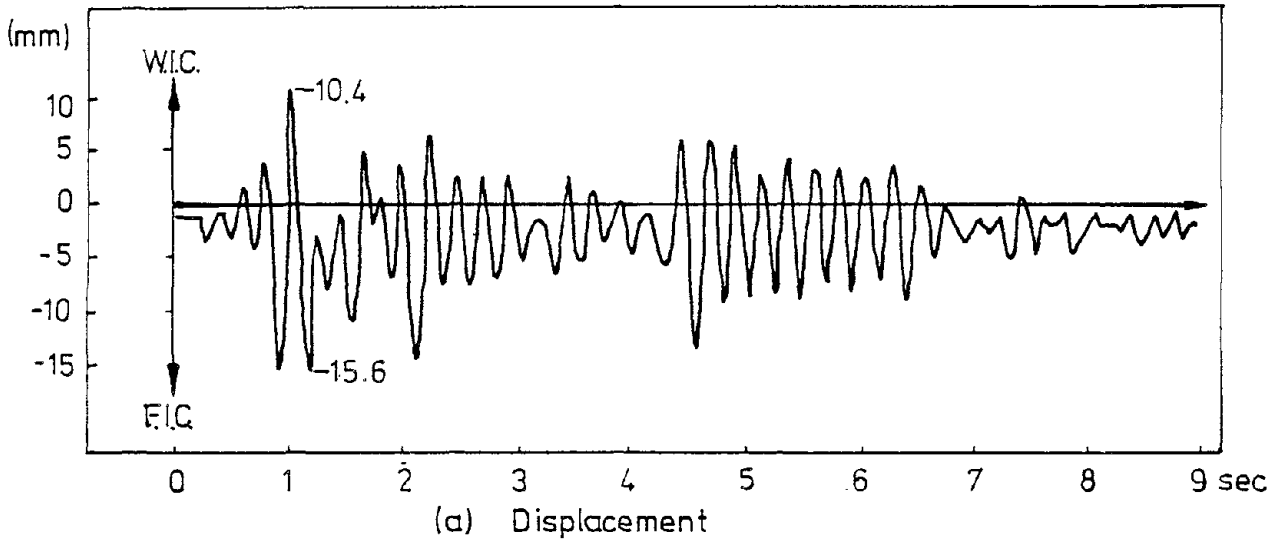

(a) Displacement

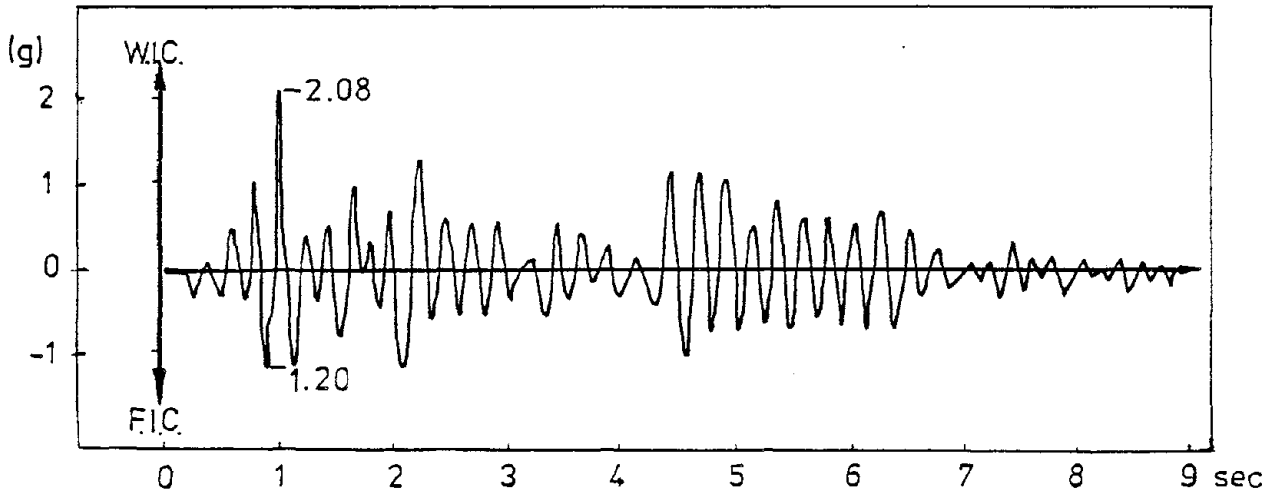

(b) Acceleration

FIG. 3-10 CENTER OF MASS RESPONSE TO TEST E-7

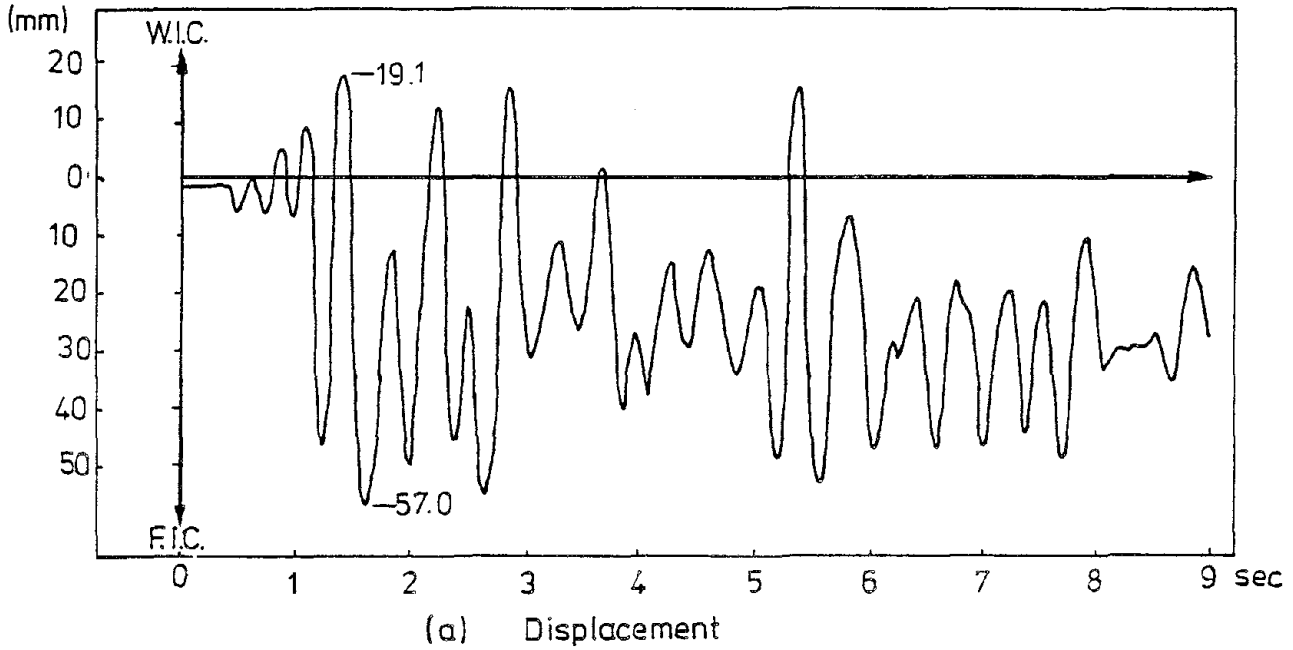

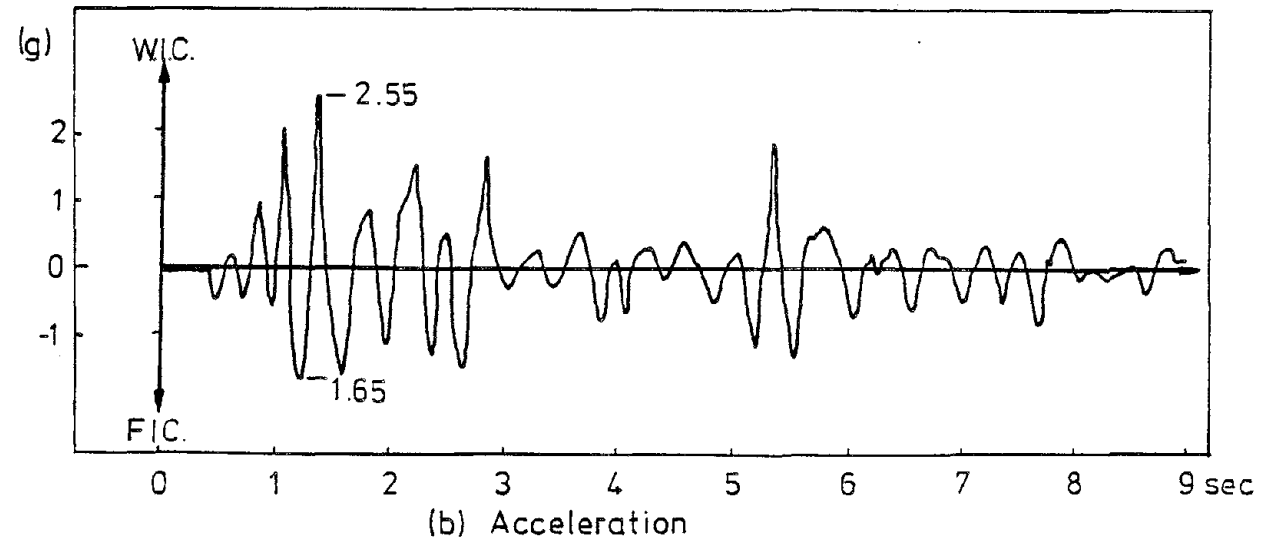

FIG. 3-11 CENTER-OF-MASS RESPONSE TO TEST E-8

web in compression, and 1.65g with the flange in compression.

In Fig. 3-12, selected hysteresis loops from tests E4, E7 and E8 are plotted. The behavior during test E4 is essentially linear-elastic, but the difference in stiffness in the two directions of response is clearly visible. In test E7, the stiffness in the direction with the flange in compression has decreased significantly, but in the opposite directions, the stiffness degradation is comparatively minor. Although the E7 trace is irregular, the area within the loop indicates significant hysteretic energy absorption, resulting from the initiation of steel yield at the web toe. The E8 loop plotted corresponds to the period from 1.1 sec. to 1.4 sec. (see Fig. 3-11) and indicates considerable inelasticity of response as indicated by the large area within the hysteresis loop.

Only short portions of each trace have been plotted in Fig. 3-12 to enable the character of the different records to be identified without a large number of low intensity cycles "muddying" the picture.

3.6.3 Strength and Ductility

It is of interest to compare the peak response during test E8 with predicted maxima based on the analysis reported earlier in section 3. Results are summarized in Table 3.3 below.

With the web in compression, the maximum moment recorded experimentally was approximately 5% below the predicted ultimate moment. At 19.1mm, the maximum displacement in the W.I.C. direction, crushing had occurred. During test E7, the maximum displacement with W.I.C. was 10.4mm, with no crushing visible. Thus the actual displacement at crushing must have been in the range 10.4 - 19.1mm, which is in good agreement with the predicted value of 15.7mm.

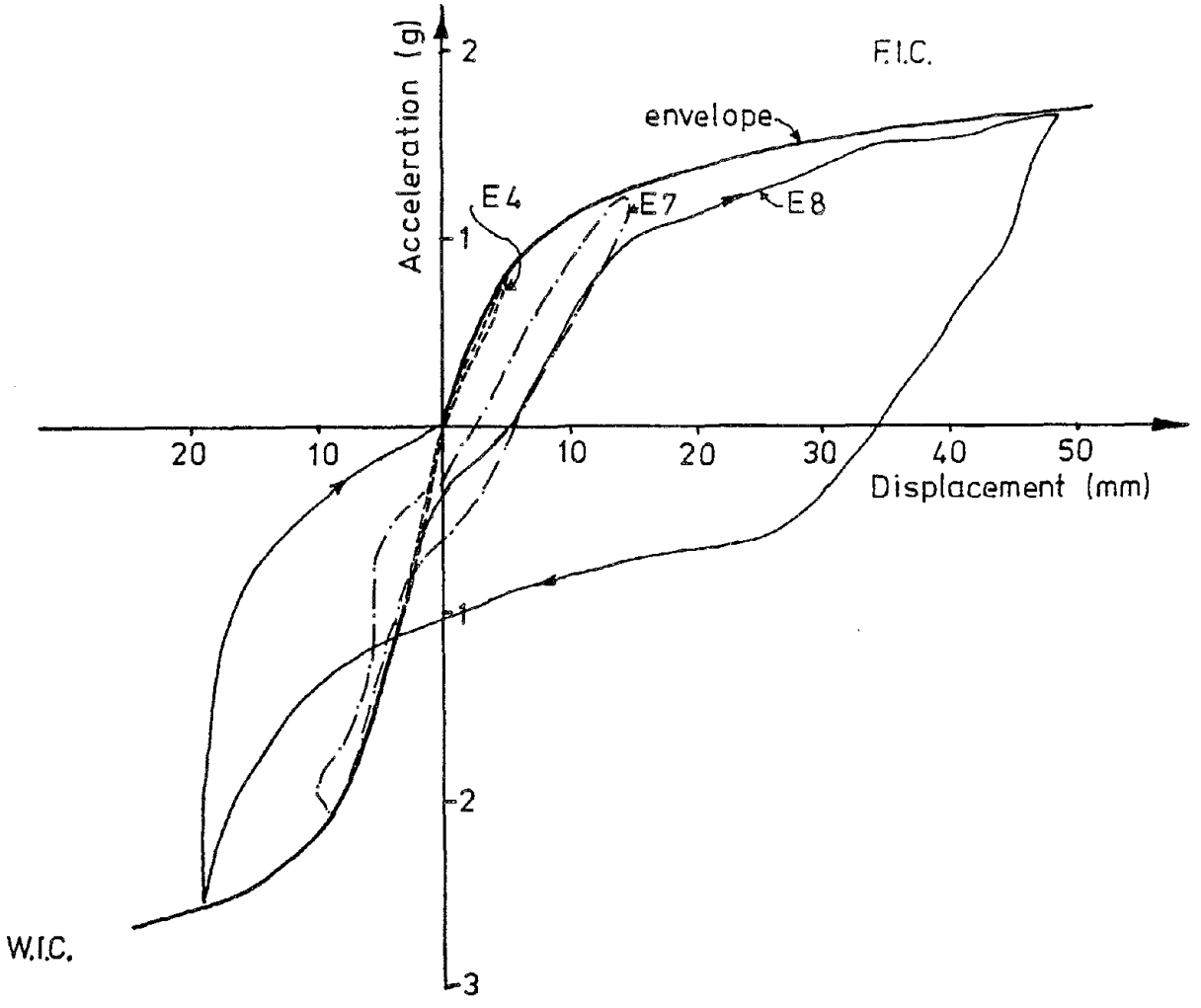

FIG. 3-12 MAXIMUM-RESPONSE HYSTERESIS LOOPS FOR TESTS E-4, E-7, E-8

TABLE 3.3 COMPARISON OF PREDICTED AND MEASURED PEAK RESPONSE

Parameter	Web in Compression	Flange in Compression
Theor. Ult. Moment M_T	494kNm	213kNm
Maximum Exp Moment M_E	470kNm	297kNM
M_E/M_T	0.951	1.39
Theor. Ult. Displ. Δ_T	15.7mm	114mm
Maximum Exp Moment Δ_E	19.1mm	57mm
Δ_E/Δ_T	1.22	0.50

With the flange in compression, the maximum displacement recorded was only 50% of the expected displacement at first crushing. However, in light of the lack of damage during response in this direction, it is clear that the wall could have displaced further. The peak recorded moment was substantially higher than predicted. A number of reasons can be advanced to explain this. First, at peak measured response, the tensile strain in the extreme tension rebar is estimated to be about 4%. (Experimental measurements result in higher values.) At this strain, substantial strain hardening (at least 10 - 15%) can be expected, thus enhancing the ultimate moment capacity. Second, the tensile strain rate for the extreme tension rebar was approximately 0.5/s. At this rate, the yield stress of the reinforcement is typically increased by 20-30%. The combined effects can thus explain the flexural strength enhancement noted.

It is of interest, however, that the same enhancement did not occur in the other direction. It should be noted that with the web in compression, peak steel strains are predicted to be less than 0.7%, and hence strain hardening is not expected. The lower strain rate (approximately 0.1/s) results in a less significant strain-rate effect. Also, the eccentric nature of

the response means that the Baushinger Effect for inelastic cyclic response of steel may have reduced steel stresses below equivalent static yield. Finally, the theoretical ultimate moment was based on the assumption of the Navier-Bernoulli "plane-sections" hypothesis and at the comparatively low steel strains, the tension reinforcement at the edges of the flange may not have contributed fully to the flexural capacity.

3.6.4 Natural Frequency and Damping

The initial natural frequency of the wall was 10.5Hz. This was much lower than the predicted value of the 20.9Hz based on the uncracked section properties, ignoring shear lag effects, and assuming $E_m = 1000f'_m$ (i.e. 19.4GPa). The initial measured value was closer to the predicted cracked-section frequencies listed in Table 3-4. It should be emphasized that because of the different stiffnesses in the two opposite directions of response, the concept of natural frequency is not strictly applicable, and the data in Table 3-4 are included to represent the expected range of possible values.

TABLE 3-4 PREDICTED NATURAL FREQUENCIES

MODEL	UNCRACKED GROSS-SECTION	CRACKED, W.I.C.*	CRACKED, F.I.C.*	UNCRACKED, NO FLANGE	MEASURED INITIAL	MEASURED AFTER CRACKING
Section Stiffness	$I_g = 0.0372m^4$	$0.22\ I_g$	$0.0767\ I_g$	$0.426\ I_g$		
Predicted Frequency (Hz)	20.9	9.8	5.8	13.6	10.5	6.9 - 9.0
Natural Period (sec.)	0.048	0.102	0.173	0.074	0.095	.145 - .111

* W.I.C. = Web in Compression; F.I.C. = Flange in Compression

There are a number of possible explanations for this behavior: The Modulus of Elasticity could have been lower than expected. However, for this to be the cause of a 50% drop in

frequency, E_m would need to be 1/4 of the predicted value.

The effects of shear lag could have made the flange less than fully effective in contributing to stiffness. In the extreme case, where the flange is totally ineffective, the wall would behave as a rectangular wall of length 990mm. This case is considered in column 4 of Table 3-4, and results in a predicted frequency of 13.6Hz, still substantially higher than measured.

Although care was taken to ensure the wall was not subjected to unintentional loading it is possible that it was cracked during construction or during installation on the shake-table. There was, however, no visible evidence of this, and it is not felt to be the probable cause.

The most likely cause of the unexpectedly low natural frequency appears to have been due to flexibility of the shake table in the passive configuration. As the table itself is not infinitely rigid, it will have acted as a flexible foundation to the wall, decreasing the natural frequency by foundation rotation. More importantly, the axial flexibility of the table and model on the column of oil inside the hydraulic drive actuator is significant. Assuming a bulk modulus of 3450 MPa (500,000 psi) for the oil results in an equivalent spring stiffness of the oil of 110×10^6N/m. With a total load of table and mass of about 10 tons, the resulting natural frequency of movement on the oil column is about 16.7Hz. As the behavior of the wall on the table/actuator system is a multi degree of freedom system, the lowest frequency may have been lower than this. More detailed calculations should be carried out to determine the natural frequency in more detail.

It should be noted that this behavior depends on the actuator being in a passive state. Under active control, the oil-column flexibility should not influence response.

During sinusoidal tests S7, S8, S9, S8-2, under active control, natural frequencies measured during the free decay stage of response were in the range 6.9 - 9.0Hz, with the frequency dropping as the intensity of response increased. These agree well with the predicted range of 5.8Hz to 9.8Hz which are the values for web in compression and flange in compression respectively.

Damping values from free decay were in the range 6% - 9% of equivalent viscous damping.

3.6.5 Longitudinal Reinforcement Strains

Longitudinal reinforcement strains were monitored on all eleven vertical bars at three different sections: wall base level, 200mm above base, and 400mm above base, as shown in Fig. 3-2. It was expected that these strains would help to determine the extent of shear lag in the flange, and the degree to which the "plane-section-remain-plane" hypothesis was applicable.

Figs. 3-13 and 3-14 show typical strain profiles recorded during tests S8 and E8 respectively. In each case the profiles on the left side of the page refer to peak displacements with the flange in compression, and those on the right to peak displacements with the web in compression.

Examination of Fig. 3-13 reveals that, with the flange in compression peak tensile strains at the extreme tension rebar at the base were just below the expected yield strain of 1650$\mu\epsilon$. Although the flange strain profiles for this case are somewhat erratic, compressive steel strains at the edges of the flange average 59% of the strain at the flange rebar in line with the web, indicating a significant shear lag effect.

With the web in compression, all steel strains at the base are significantly lower than with the web in compression. The maximum tensile strain of 195$\mu\epsilon$ on the flange rebar in line with

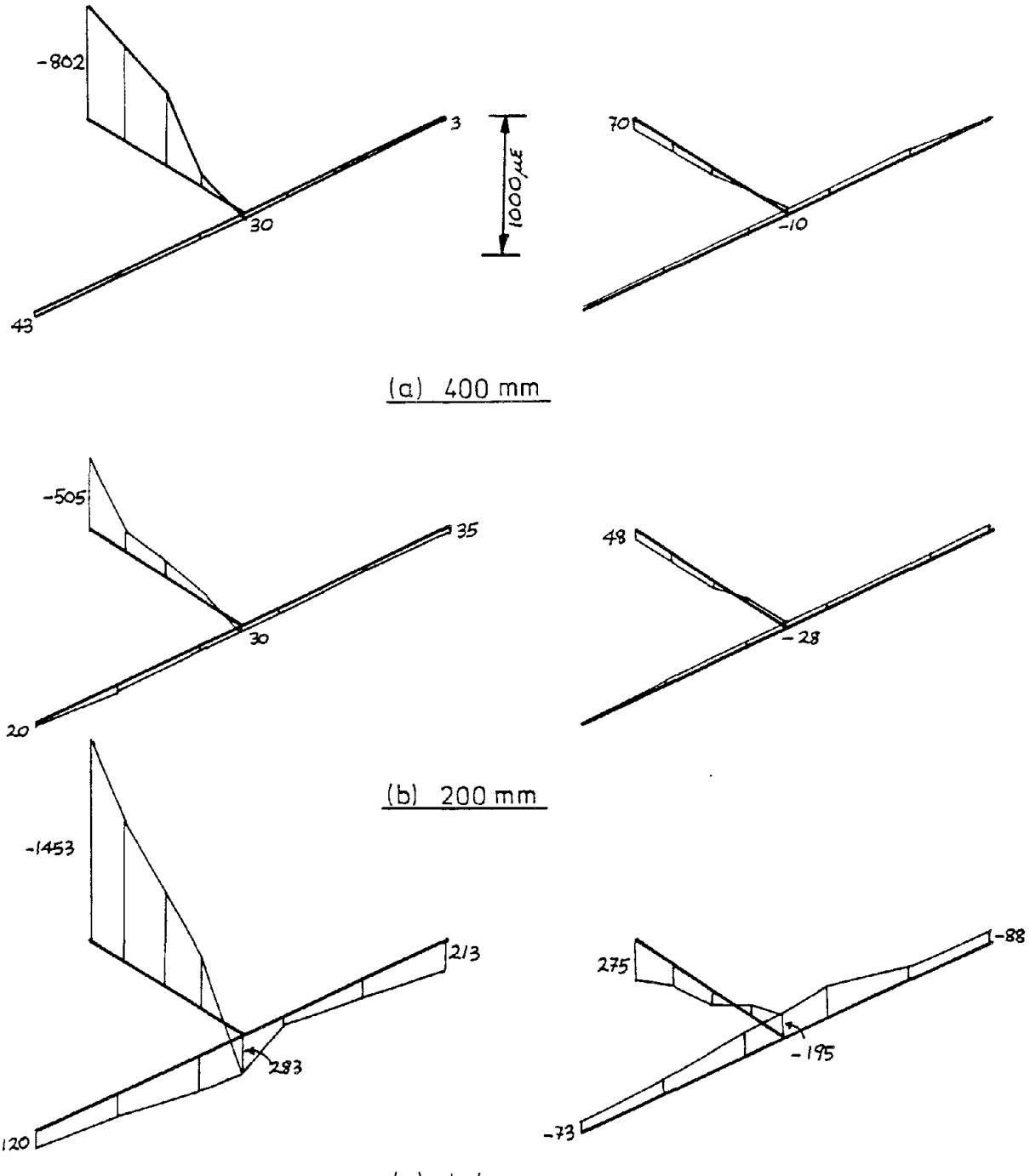

FIG. 3-13 TEST S-9 LONGITUDINAL REBAR STRAIN PROFILES AT DIFFERENT HEIGHTS ABOVE WALL BASE

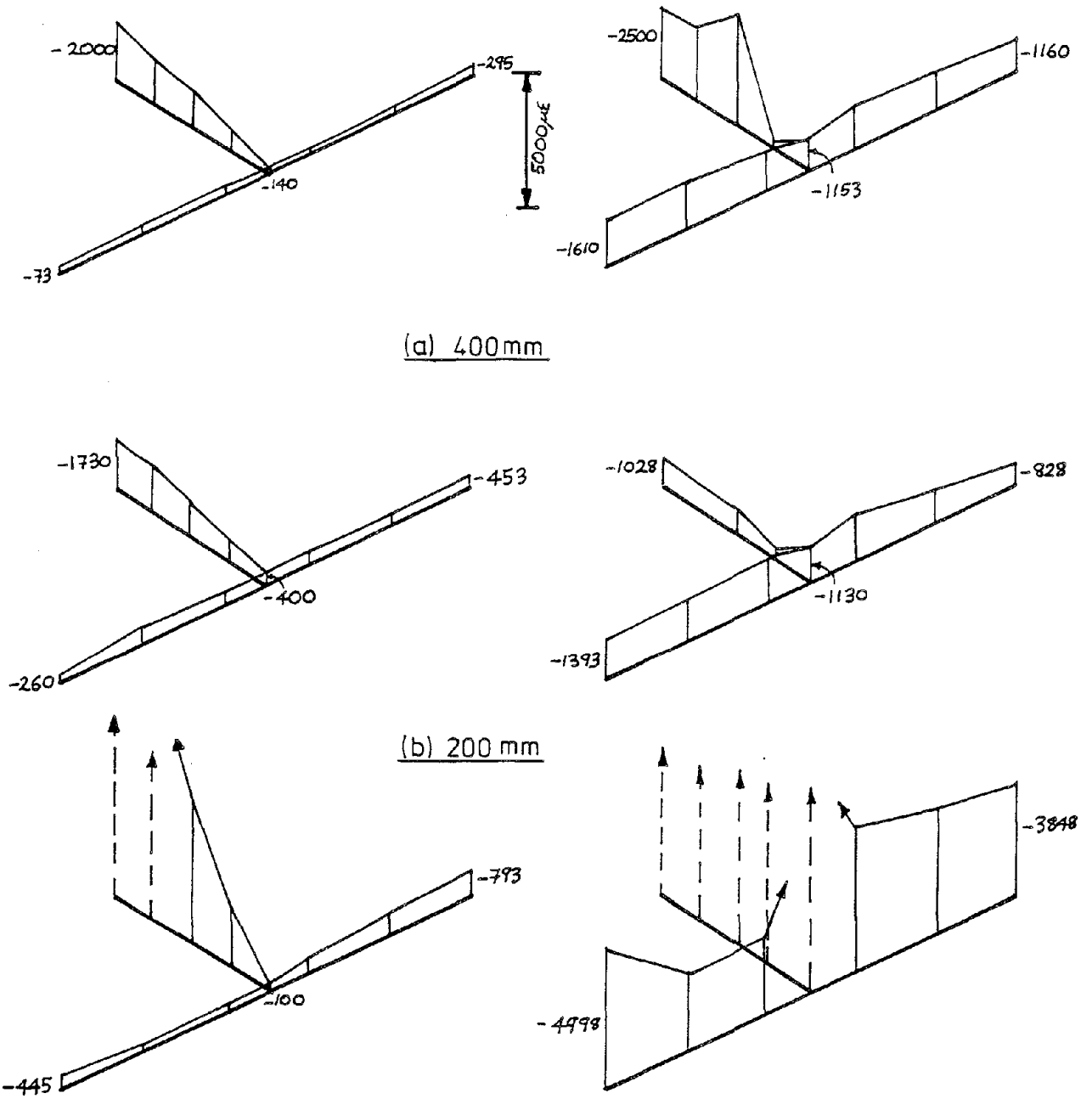

FIG. 3-14 TEST E-8 LONGITUDINAL REBAR STRAINS PROFILES AT DIFFERENT HEIGHTS ABOVE WALL BASE

the web reduces to an average of 80$\mu\epsilon$ (41%) at the rebar at the flange edges.

At levels above the base, steel strains reduce significantly. With the flange in compression, steel strains at the section 400mm above the base are significantly higher than at the section 200mm above the base, despite the lower moment. It is apparent that a crack had formed at the top of the second course of blocks by this stage, although visual examination of the wall had not revealed it.

With the web in compression, steel strains at both sections at 200mm and 400mm above the base were very low (maximum of 70$\mu\epsilon$) indicating that these sections had not cracked.

During test E8 longitudinal rebar strains were much higher than during test S8. As discussed earlier, the intensity of excitation during this test was roughly twice the intended value. This, coupled with a strain limit of 5000$\mu\epsilon$ set by the selected strain sensitivity of 2.5$\mu\epsilon$ and the data logger recording range (2048 digits) meant that peak strains at many locations were out of range, and only tentative conclusions may be drawn from Fig. 3-14.

Profiles in Fig. 3-14 for flange in compression relate to a stage comparatively early in the test E8 record, and strain profiles are reasonably regular. At the base, peak tensile strains in the web are many times yield strain. Peak steel strains at sections 200mm and 400mm above the base are just above yield strain.

With the web in compression, at a later stage of the response record, steel strain profiles are much more irregular. At the base section, only strains in the rebar in the outer portions of the flange are still within the data logger range.

The most striking thing apparent in the profiles of Fig. 3-14 is that no gauges were indicating compressive strains. It is clear that most gauges had been subjected to inelastic tensile strains, and that under moment reversal, compressive forces were acting to reduce inelastic (residual) tensile strains rather than putting the bars into compressive strains. Thus the strains do not necessarily indicate tensile stress at all locations. A complete Bauschinger stress-strain time-history analysis would be necessary to predict stress levels in the reinforced from the measured strains. This was beyond the scope of this preliminary investigation, but will be carried out for the subsequent detailed investigation planned.

It is probable that shear displacements along cracks in the lower region of the wall caused compression stress in the masonry to be developed despite apparent dilation stresses indicated by the rebar straingauges. Thus the lack of compression strain in the profiles of Fig. 3-14 should not be taken as indicating a lack of masonry compressive stress in the flexural compression zones.

3.6.6 Transverse (Shear) Reinforcement Strains

The extent of strain gauging to monitor strains in transverse reinforcement was very limited, as a result of the limitation of the data acquisition system. As shown in Fig. 3-3, each of the lower four horizontal bars in the web were gauged approximately 400mm (16in.) from the web end, in order to investigate shear transfer in the web. Gauges were also placed on the lower three flange horizontal bars, 100mm (4in.) either side of the flange centerline, in order to monitor any strains developed as a result of shear lag effects.

Strains in all horizontal bars during all tests except E8 were low, and indicated essentially elastic uncracked response. Strains developed in the four lower web bars during test E8 are shown as time histories in Figs. 3-14(a) to 3-14(d). Strains in

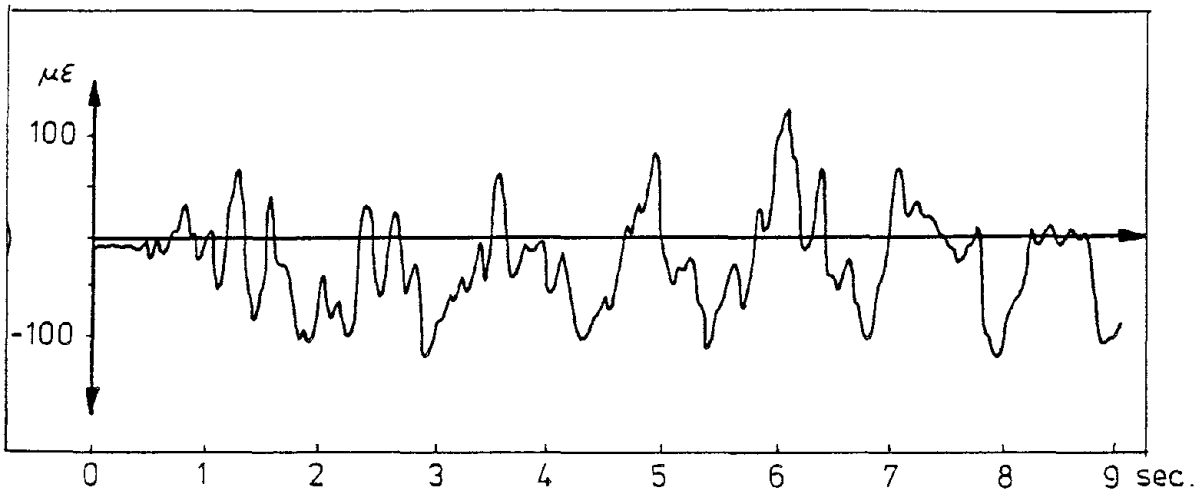

(a) 700mm. above base

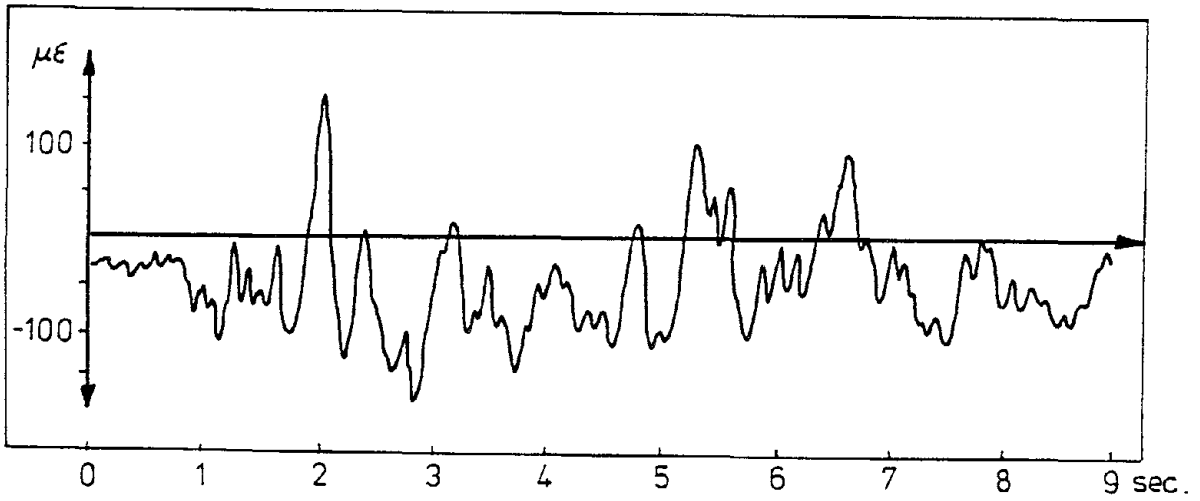

(b) 500 mm. above base

FIG. 3-15 TEST E-8 WEB SHEAR REBAR STRAIN HISTORIES

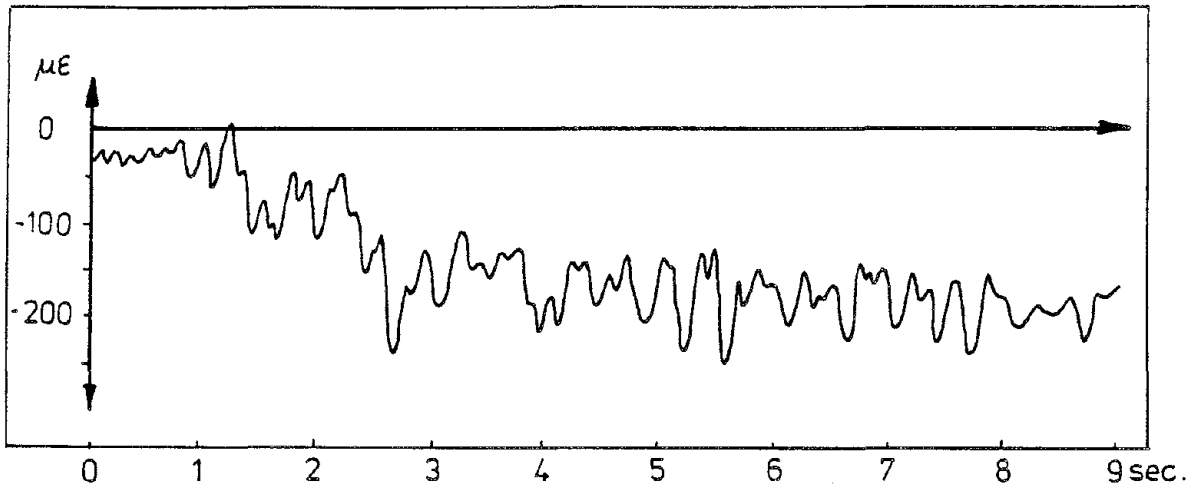

(c) 300 mm above base

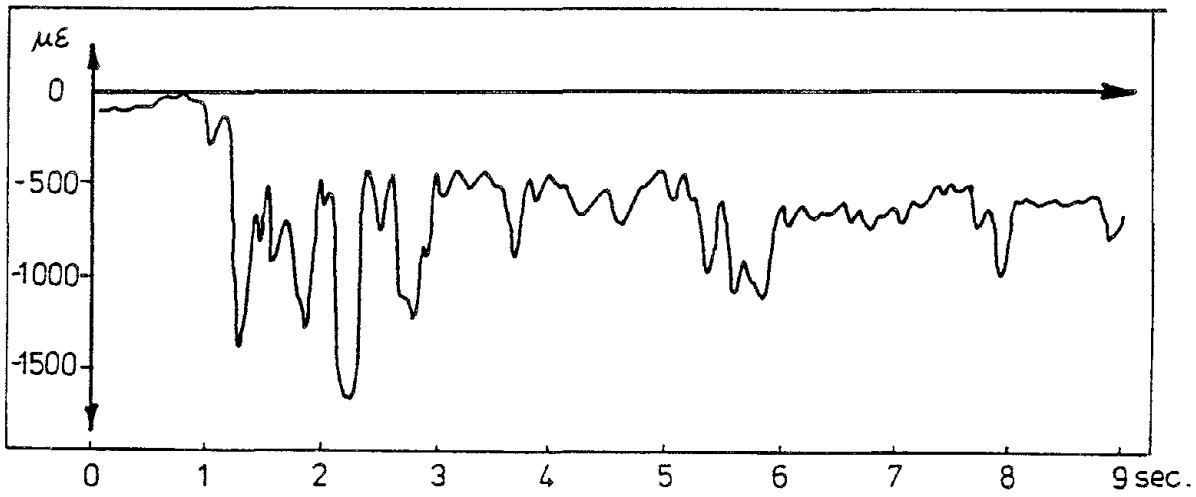

(d) 100 mm. above base

FIG. 3-15 (cont.) TEST E-8 WEB SHEAR REBAR STRAIN HISTORIES

the bars 500mm and 700mm above the base indicate uncracked response, since the magnitude of strain is low, and peak compressive strains are of similar magnitude to peak tensile strains. The strains developed in the lower two bars (Figs. 3-14(c) and (d)) have a different character, being offset to the tension side of the strain axis, and of higher magnitude than the other gauged bars. Maximum strain recorded in the bottom bar, at 1690$\mu\epsilon$, just exceeds yield. This would appear to indicate the presence of a diagonal tension crack in the lower region of the wall.

Examination of the web crack pattern for test E8 (see Fig. 3-4) does not however indicate visible diagonal cracking. It is probable that the recorded tensile strains were in fact related to the forces developed in the lower two bars by the vertical splitting at the web toe tending to separate the toe from the body of the wall.

The maximum shear force sustained by the wall occurred with the web in compression, and corresponded to a maximum recorded base moment of 470kNm. The corresponding shear force was thus

$$V_{max} = 470/2.6 = 181kN$$

The corresponding nominal shear stress was thus

$$v = \frac{V_{max}}{bd} = \frac{0.181 \quad MPa}{0.19 \times 0.895} = 1.06MPa$$

Earlier statically loaded shear walls with low axial load have generally developed diagonal cracking at nominal shear stress levels between 0.7 - 1.0 MPa, and hence diagonal cracking would have been expected in this case. It is not clear whether the lack of diagonal cracking should be attributed to the flanged section shape, or to the influence of dynamic loading. Further testing is needed to clarify the shear response.

3.6.7 Curvatures

Curvatures in the lower regions of the wall were monitored by linear potentiometers attached to the face shells of the wall on the axis of the web (see Fig. 3-2). These potentiometers recorded strain over vertical gauge lengths of either 100mm (lowest gauge pair) or 200mm (second and third gauge pair). Differencing the strains recorded by the two gauges at opposite ends of the web and dividing by the horizontal distance between the gauges yielded the average curvature over the gauge length.

The lateral displacement could be estimated from the curvature distribution, by assuming linear reduction with height from the top of the third gauge length, and integrating the curvature distribution thus:

$$\Delta = \int_0^H \psi_{(y)}(H-y)dy \qquad [71]$$

where $\psi_{(y)}$ is the curvature distribution, y is the height above the base, and H is the height at which lateral displacement is predicted.

This approach produced predicted displacements that were in reasonable agreement with the measured values for the earlier tests, but for tests E7 and E8 significant errors resulted. For tests E7, deflections predicted by integrating the curvature distribution were 89.9% and 43.8% of measured displacements (15.6mm, 10.4mm respectively) with the flange in compression, and the web in compression respectively. For test E8, the corresponding values were 55.9% and 56.6% of measured displacements (57.0mm and 19.05mm).

There are a number of reasons for the discrepancies.

1. Displacements predicted by integrating curvatures ignore shear displacements and sliding of the wall along the base.

At the latter stages of the stage program, the base sliding was noted to be particularly significant, but measurements were not taken. Since diagonal cracking did not develop, shear deformations are not expected to be particularly severe. Calculations based on an effective area of about 25% of the web area indicate expected shear deformations in the range 1-2mm.

2. The lateral deflectometer was deflected considerably beyond its design limit in test E8, and the recorded displacements are subject to some uncertainty.

3. The damage to the wall toe during test E8 will have made curvature measurements at peak displacements unreliable.

In future tests planned as a development of this program, shear and base-slip deformations will be monitored.

CHAPTER 4: CONCLUSIONS AND FUTURE RESEARCH PLANS

This report presents results of an initial investigation into the seismic response of flanged masonry shear walls. Theoretical studies were carried out to identify key parameters affecting the non-symmetrical strength, stiffness and ductility characteristics of flanged T-Section Walls. These were reported in the form of dimensionless design charts.

The predicted non-symmetrical response was investigated experimentally by testing a single T-Section wall on a shake table. Although the results were necessarily limited in general applicability, they confirmed the expected non-symmetrical strength, stiffness and ductility characteristics, and measured values agreed well with predicted values. There was only limited evidence of shear lag in the wide flange, which effectively contributed fully to the flexural capacity of the wall, both when in tension and in compression.

Additional analytical studies are needed in the following areas:

Design Charts

The work described in Chapter 2 should be extended to

- Develop design charts for strength, stiffness and ductility of confined masonry T-Section walls.
- Develop analyses for T-Section walls loaded parallel to the flange.
- Develop envelope moment-curvature analyses for T-Section walls.
- Investigate biaxial seismic attack on T-Section walls.

Analytical Techniques

In addition to the above, analytical models need to be developed to

- Predict the influence of shear lag on the effective

contribution of tension flanges to seismic response.

- Develop lumped-parameter, structural-component, and finite element models for dynamic analysis of flanged walls. This should be done by extending the LPM, SCM and FEM models for rectangular wall sections currently being developed as part of TCCMAR Task 2.1.

Experimental Studies

The single T-Section wall tested produced general confirmation of predicted behavior. However, as an initial, pilot wall, there were inevitable problems with experimental technique, and the range of parameters investigated was limited. An accidental excessive increase in excitation intensity between tests E7 and E8 meant that much of the most useful data was lost. Further tests are planned as part of TCCMAR Task 4.1. These tests will include both static cyclic tests of T-Section wall to investigate strength and ductility under more controlled conditions than is possible with shake table testing, and dynamic shake table tests of duplicates of the static test units to investigate the influence of dynamic loading, and to provide experimental data to compare with analytical predictions of dynamic response, using the various degrees of analytical complexity represented by the CPM, SCM and FEM analytical models.

Current plans call for four static test units and an equivalent four dynamic test units, all loaded parallel to the T-Section web. A fifth dynamic test will be carried out on a T-Section model mounted at a 45° skew to the shake table axis.

The pilot wall test indicated the importance of monitoring base slip, shear deformation, and vertical deflections at the wall top in addition to lateral deflections and wall curvatures. Also, the extent of instrumentation for the pilot wall, which was limited by the 64 channel data logger was insufficient to clearly define structural response. In particular, a larger number of strain gauges on horizontal reinforcement should be provided.

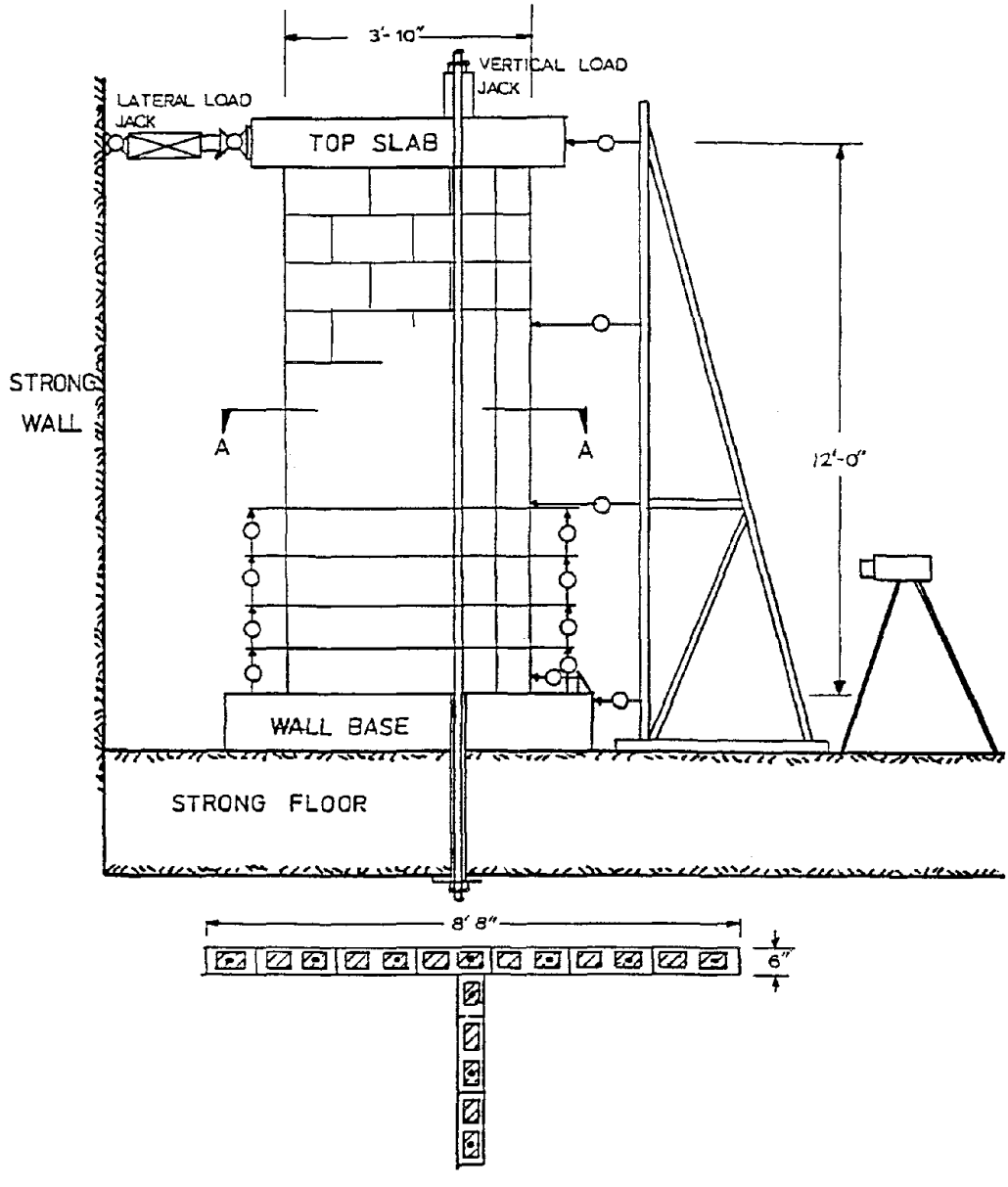

FIG. 4-1 PROPOSED STATIC WALL TESTS

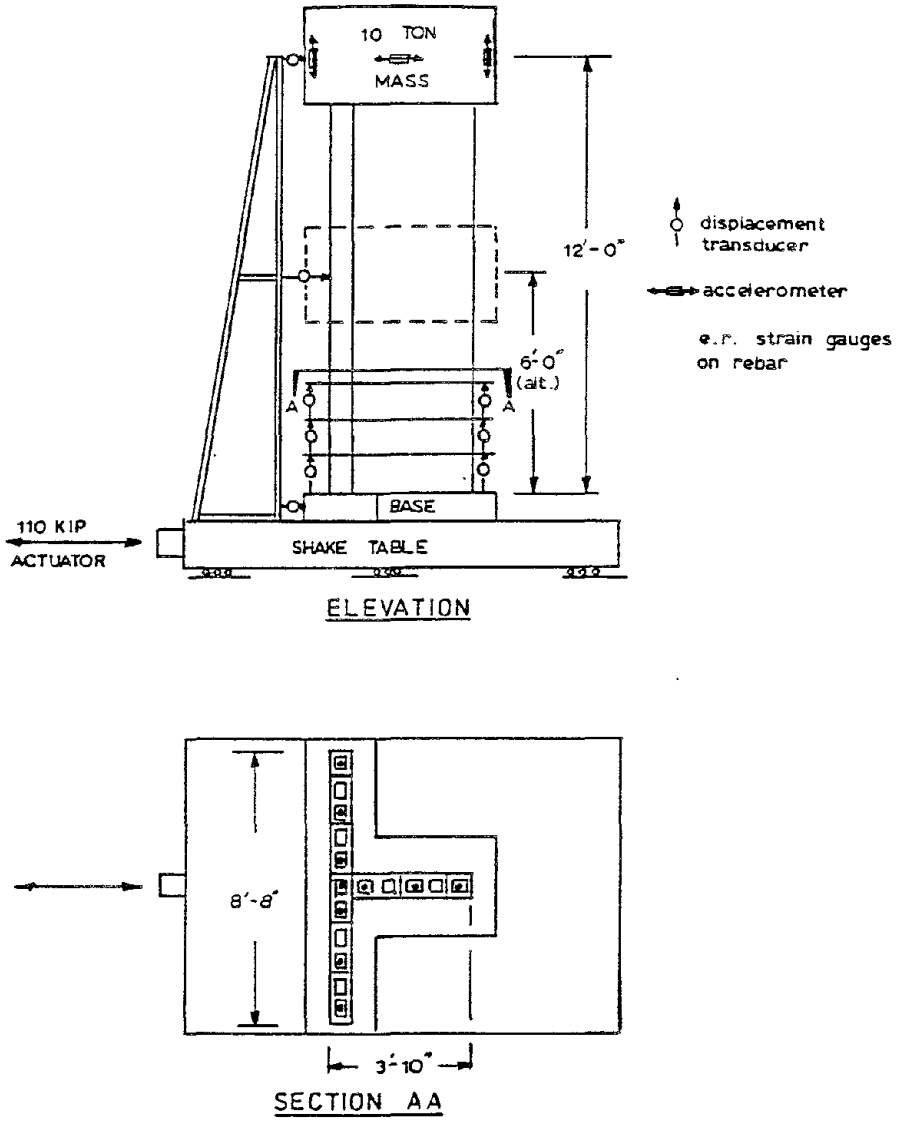

FIG. 4-2 PROPOSED DYNAMIC WALL TESTS

These short-comings in the pilot test will be rectified in the main study.

Figs. 4.1 and 4.2 represent the planned static and dynamic test configuration under TCCMAR task 4.1.

The proposed test matrix is summarized in Table 4.1.

TABLE 4.1 TEST MATRIX FOR TCCMAR TASK 4.1

WALL	TEST REGIME	WALL DIMENSIONS H x Lf x Lw	AXIAL LOAD	VERTICAL REINFORCEMENT	ADDITIONAL DATA
F1	Static	12'x8'-8"x3'-10"	100 psi	#6 @ 16" crs	
F2	Static	12'x8'-8"x3'-10"	100 psi	#4 @ 16" crs	
F3	Static	12'x16'-8"x3'-10"	100 psi	#4 @ 16" crs	
F4	Static	12'x8'-8"x3'-10"	100 psi	#6 @ 16" crs	Confined toe
F5	Dynamic	12'x8'-8"x3'-10"	100 psi	#6 @ 16" crs	
F6	Dynamic	12'x8'-8"x3'-10"	100 psi	#4 @ 16" crs	
F7	Dynamic	6'x8'-8"x3'-10"	100 psi	#4 @ 16" crs	
F8	Dynamic	12'x8'-8"x3'-10"	100 psi	#6 @ 16" crs	Confined toe
F9	Dynamic	12'x8'-8"x3'-10	100 psi	#6 @ 16" crs	Skewed 45° Table Axis

H = wall height, L_f = flange length, L_w = web length

REFERENCES

1. PRIESTLEY, M.J.N., "Seismic Resistance of Reinforced Concrete Masonry Shear Walls with High Steel Percentages", Bulletin, New Zealand National Society for Earthquake Engineering (Wellington), Vol. 10, No. 1, March 1977, pp. 1-16.

2. PRIESTLEY, MJN and D.M. ELDER, "Seismic Behavior of Slender Concrete Masonry Shear Walls". Dept. of Civil Engineering Research Report 82-4. University of Canterbury, March 1982, 116 pp.

3. MAYES, R.L., Y. OMOTO, and R.W. CLOUGH, "Cyclic Shear Tests of Masonry Piers", University of California, Berkeley, Report EERC 76-8, May 1976, 84 pp.

4. PRIESTLEY, M.J.N. and D.M. ELDER., "Cyclic Loading Tests of Slender Concrete Masonry Shear Walls", Bulletin, New Zealand National Society for Earthquake Engineering (Wellington), Vol. 15, No. 1, March 1982, pp. 3-21.

5. PRIESTLEY, M.J.N., "Ductility of Unconfined and Confined Concrete Masonry Shear Walls", Masonry Society Journal, Vol. 1, No. 2, July/Dec. 1981, pp. T-28 to T-39.

6. PRIESTLEY, M.J.N., "Flexural Strength of Rectangular Unconfined Masonry Shear Walls with Distributed Reinforcement", The Masonry Society Journal, Vol. 5, No. 2, July/Dec. 1986, pp. T-1 to T-15.

7. SHING, B., et al, "Response of Reinforced Masonry Story-Height Walls to Fully Reversed In-Plane Lateral Loads", TCCMAR Task 3-16. Report in Preparation, University of Colorado, Boulder.

8. NOLAND, J.L., "U.S. Research Plan", U.S.-Japan Coordinated Program for Masonry Building Research, Atkinson-Noland Assoc., Boulder, 1984, 22 pp.

9. ABRAMS, D.P., "Dynamic Response of Building Models", TCCMAR Task 7.1, Status Report, Jan 1988, (Unpublished) 8 pp.

10. "Code of Practice for Masonry Design", NZS 4203P, Standards Association of New Zealand, Wellington, 1984.

11. ACI COMMITTEE 531, "Building Code Requirements for Concrete Masonry Structures (ACI 531-79) (Revised 1981) and Commentary", American Concrete Institute, Detroit, 1981, 60 pp.

12. PAULAY, T., M.J.N. PRIESTLEY and A.J. SYNGE, "Ductility of Earthquake Resisting Squat Shear Walls", ACI Journal, Proceedings, Vol. 79, No. 4, July/Aug. 1982, pp. T-28 to T-39.

13. PRIESTLEY, M.J.N. and D.M. ELDER, "Stress-Strain Curves for Unconfined and Confined Concrete Masonry", ACI Journal, Proceedings, Vol. 80, No. 3, May/June 1983, pp. 192 - 201.

14. PRIESTLEY, M.J.N. and CHAI YUK HON, "Seismic Design of Reinforced Concrete Masonry Moment Resisting Frames", The Masonry Society Journal, Vol. 5, No. 1, Jan./June 1985.

APPENDIX (a)

DIMENSIONLESS DESIGN CHARTS FOR

- EFFECTIVE MOMENT OF INERTIA (I_{cr}/I_{gross})
- MOMENT ($M_i/f'_m t \ell_w^2$)
- CURVATURE DUCTILITY (ϕ_u/ϕ_y) (Elasto-plastic)

Refer to Fig. 2-3 for Nomenclature

Note: A tabulated curvature ductility factor of 1.000 indicates that ultimate curvature is reached before the extreme tension reinforcement yields. Thus ϕ_y does not exist in these cases.

CASE 1 g = 0.95, ℓ_f/ℓ_w = 0 (RECTANGULAR)

Icr/Igross
1f/lw=0.00 g=0.95 fy=275.0 Mpa

Axial Load Ratio Nu/f'm.Ag

fy/f'm	0.0000	0.0500	0.1000	0.1500	0.2000	0.2500	0.3000	0.3500	0.4000
0.0100	0.0226	0.1407	0.2202	0.2785	0.3211	0.3519	0.3731	0.3801	0.3683
0.0200	0.0423	0.1532	0.2298	0.2864	0.3284	0.3589	0.3792	0.3863	0.3747
0.0400	0.0775	0.1774	0.2492	0.3028	0.3422	0.3713	0.3915	0.3983	0.3877
0.0600	0.1090	0.2004	0.2677	0.3183	0.3567	0.3846	0.4031	0.4104	0.4003
0.0800	0.1379	0.2222	0.2854	0.3337	0.3704	0.3970	0.4154	0.4227	0.4128
0.1000	0.1648	0.2432	0.3032	0.3489	0.3841	0.4102	0.4277	0.4348	0.4257
0.1200	0.1902	0.2637	0.3203	0.3641	0.3977	0.4226	0.4400	0.4468	0.4382
0.1400	0.2143	0.2832	0.3372	0.3791	0.4112	0.4358	0.4523	0.4591	0.4508
0.1600	0.2373	0.3024	0.3534	0.3940	0.4248	0.4482	0.4646	0.4711	0.4633
0.1800	0.2594	0.3210	0.3698	0.4082	0.4383	0.4613	0.4769	0.4834	0.4758
0.2000	0.2807	0.3391	0.3857	0.4229	0.4517	0.4737	0.4892	0.4954	0.4883

Mi/f'm.t.lw**2
1f/lw=0.00 g=0.95 fy=275.0 Mpa

Axial Load Ratio Nu/f'm.Ag

fy/f'm	0.0000	0.0500	0.1000	0.1500	0.2000	0.2500	0.3000	0.3500	0.4000
0.0100	0.0049	0.0280	0.0484	0.0660	0.0809	0.0930	0.1025	0.1092	0.1133
0.0200	0.0098	0.0323	0.0522	0.0694	0.0839	0.0957	0.1049	0.1115	0.1153
0.0400	0.0191	0.0407	0.0596	0.0760	0.0898	0.1010	0.1097	0.1157	0.1192
0.0600	0.0280	0.0487	0.0668	0.0824	0.0956	0.1063	0.1144	0.1201	0.1233
0.0800	0.0366	0.0564	0.0737	0.0887	0.1012	0.1114	0.1191	0.1245	0.1274
0.1000	0.0449	0.0639	0.0805	0.0948	0.1067	0.1164	0.1237	0.1287	0.1314
0.1200	0.0529	0.0711	0.0870	0.1008	0.1122	0.1214	0.1283	0.1331	0.1355
0.1400	0.0606	0.0781	0.0934	0.1066	0.1176	0.1263	0.1329	0.1373	0.1396
0.1600	0.0681	0.0850	0.0997	0.1123	0.1228	0.1312	0.1374	0.1416	0.1437
0.1800	0.0754	0.0916	0.1058	0.1179	0.1280	0.1360	0.1420	0.1459	0.1478
0.2000	0.0825	0.0981	0.1118	0.1234	0.1331	0.1408	0.1465	0.1502	0.1519

ϕu.My/ϕy.Mi
1f/lw=0.00 g=0.95 fy=275.0 Mpa

Axial Load Ratio Nu/f'm.Ag

fy/f'm	0.0000	0.0500	0.1000	0.1500	0.2000	0.2500	0.3000	0.3500	0.4000
0.0100	75.8975	13.8575	6.9223	4.3955	3.1622	2.4391	1.9636	1.6197	1.3261
0.0200	35.0610	11.5183	6.2925	4.1474	3.0491	2.3848	1.9437	1.6076	1.3302
0.0400	17.7173	8.5525	5.3272	3.7627	2.8589	2.2871	1.8977	1.5967	1.3384
0.0600	11.8687	6.9233	4.6884	3.4639	2.7147	2.2035	1.8517	1.5801	1.3402
0.0800	8.9843	5.8641	4.2165	3.2124	2.5823	2.1339	1.8203	1.5654	1.3421
0.1000	7.2917	5.1296	3.8387	3.0352	2.4777	2.0838	1.7909	1.5567	1.3449
0.1200	6.2702	4.6038	3.5719	2.8623	2.3834	2.0244	1.7634	1.5426	1.3469
0.1400	5.4905	4.2073	3.3429	2.7257	2.2977	1.9819	1.7376	1.5359	1.3489
0.1600	4.9274	3.8781	3.1406	2.6183	2.2305	1.9391	1.7202	1.5287	1.3509
0.1800	4.5074	3.6231	2.9849	2.5177	2.1791	1.9104	1.6969	1.5172	1.3482
0.2000	4.1518	3.3995	2.8431	2.4420	2.1211	1.8724	1.6815	1.5108	1.3504

CASE 2 g = 0.95, ℓ_f/ℓ_w = 0.25 WEB IN COMPRESSION

Icr/Igross
lf/lw=0.25 g=0.95 fy=275.0 Mpa

Axial Load Ratio Nu/f'm.Ag

fy/f'm	0.0000	0.0500	0.1000	0.1500	0.2000	0.2500	0.3000	0.3500	0.4000
0.0100	0.0251	0.1352	0.2079	0.2596	0.2961	0.3197	0.3248	0.2735	0.3199
0.0200	0.0469	0.1493	0.2187	0.2686	0.3037	0.3266	0.3311	0.2797	0.3245
0.0400	0.0855	0.1762	0.2401	0.2863	0.3192	0.3404	0.3432	0.2913	0.3327
0.0600	0.1196	0.2015	0.2605	0.3036	0.3345	0.3539	0.3547	0.3019	0.3418
0.0800	0.1508	0.2254	0.2801	0.3206	0.3494	0.3673	0.3666	0.3135	0.3509
0.1000	0.1796	0.2482	0.2992	0.3371	0.3642	0.3805	0.3790	0.3242	0.3600
0.1200	0.2067	0.2701	0.3178	0.3533	0.3788	0.3937	0.3908	0.3359	0.3701
0.1400	0.2322	0.2911	0.3358	0.3693	0.3933	0.4065	0.4025	0.3465	0.3802
0.1600	0.2565	0.3115	0.3534	0.3850	0.4076	0.4195	0.4141	0.3583	0.3893
0.1800	0.2798	0.3312	0.3707	0.4005	0.4218	0.4321	0.4256	0.3690	0.3993
0.2000	0.3021	0.3503	0.3876	0.4157	0.4360	0.4448	0.4379	0.3796	0.4094

Mi/f'm.t.lw**2
lf/lw=0.25 g=0.95 fy=275.0 Mpa

Axial Load Ratio Nu/f'm.Ag

fy/f'm	0.0000	0.0500	0.1000	0.1500	0.2000	0.2500	0.3000	0.3500	0.4000
0.0100	0.0073	0.0415	0.0714	0.0971	0.1185	0.1357	0.1486	0.1572	0.1615
0.0200	0.0145	0.0479	0.0771	0.1021	0.1229	0.1396	0.1520	0.1604	0.1642
0.0400	0.0284	0.0602	0.0880	0.1117	0.1315	0.1472	0.1589	0.1666	0.1695
0.0600	0.0416	0.0720	0.0985	0.1211	0.1399	0.1547	0.1656	0.1726	0.1750
0.0800	0.0543	0.0834	0.1087	0.1302	0.1480	0.1620	0.1722	0.1788	0.1805
0.1000	0.0666	0.0944	0.1185	0.1391	0.1560	0.1693	0.1789	0.1849	0.1860
0.1200	0.0783	0.1050	0.1281	0.1478	0.1638	0.1764	0.1855	0.1911	0.1917
0.1400	0.0897	0.1153	0.1375	0.1562	0.1716	0.1834	0.1920	0.1971	0.1974
0.1600	0.1008	0.1253	0.1466	0.1645	0.1792	0.1905	0.1985	0.2033	0.2030
0.1800	0.1115	0.1350	0.1554	0.1726	0.1866	0.1974	0.2050	0.2094	0.2088
0.2000	0.1219	0.1446	0.1641	0.1806	0.1940	0.2042	0.2114	0.2154	0.2145

ϕu.My/ϕy.Mi
lf/lw=0.25 g=0.95 fy=275.0 Mpa

Axial Load Ratio Nu/f'm.Ag

fy/f'm	0.0000	0.0500	0.1000	0.1500	0.2000	0.2500	0.3000	0.3500	0.4000
0.0100	71.0203	11.2368	5.4766	3.4592	2.4622	1.8760	1.4598	1.0000	1.0000
0.0200	32.8619	9.4283	4.9978	3.2685	2.3822	1.8360	1.4453	1.0000	1.0000
0.0400	16.2861	7.1684	4.3197	2.9963	2.2511	1.7760	1.4160	1.0000	1.0000
0.0600	10.7628	5.8698	3.8268	2.7838	2.1454	1.7275	1.3916	1.0000	1.0000
0.0800	8.2772	4.9997	3.4782	2.6153	2.0584	1.6824	1.3749	1.0000	1.0000
0.1000	6.6845	4.4198	3.2093	2.4662	1.9884	1.6401	1.3564	1.0000	1.0000
0.1200	5.6982	3.9872	2.9805	2.3461	1.9242	1.6068	1.3413	1.0000	1.0000
0.1400	4.9992	3.6306	2.7975	2.2489	1.8651	1.5805	1.3268	1.0000	1.0000
0.1600	4.4832	3.3753	2.6509	2.1705	1.8176	1.5505	1.3128	1.0000	1.0000
0.1800	4.0913	3.1536	2.5328	2.0983	1.7802	1.5264	1.2993	1.0000	1.0000
0.2000	3.7602	2.9769	2.4251	2.0310	1.7448	1.5043	1.2885	1.0000	1.0000

CASE 3 $g = 0.95$, $\ell_f/\ell_w = 0.25$ FLANGE IN COMPRESSION

Icr/Igross
lf/lw=0.25 g=0.95 fy=275.0 Mpa

Axial Load Ratio Nu/f'm.Ag

fy/f'm	0.0000	0.0500	0.1000	0.1500	0.2000	0.2500	0.3000	0.3500	0.4000
0.0100	0.0161	0.1166	0.1939	0.2545	0.3022	0.3393	0.3682	0.3879	0.3993
0.0200	0.0314	0.1283	0.2036	0.2626	0.3098	0.3467	0.3735	0.3934	0.4060
0.0400	0.0604	0.1510	0.2226	0.2795	0.3242	0.3596	0.3863	0.4064	0.4185
0.0600	0.0878	0.1732	0.2409	0.2955	0.3393	0.3735	0.3991	0.4183	0.4300
0.0800	0.1139	0.1947	0.2594	0.3115	0.3536	0.3864	0.4119	0.4302	0.4423
0.1000	0.1388	0.2154	0.2772	0.3273	0.3678	0.4002	0.4246	0.4432	0.4547
0.1200	0.1628	0.2355	0.2947	0.3430	0.3820	0.4131	0.4374	0.4550	0.4670
0.1400	0.1860	0.2553	0.3121	0.3586	0.3962	0.4269	0.4502	0.4680	0.4792
0.1600	0.2084	0.2746	0.3288	0.3741	0.4103	0.4398	0.4630	0.4798	0.4914
0.1800	0.2301	0.2933	0.3457	0.3889	0.4244	0.4527	0.4757	0.4927	0.5036
0.2000	0.2512	0.3118	0.3621	0.4042	0.4385	0.4665	0.4885	0.5045	0.5168

Mi/f m.t.lw**2
lf/lw=0.25 g=0.95 fy=275.0 Mpa

Axial Load Ratio Nu/f'm.Ag

fy/f'm	0.0000	0.0500	0.1000	0.1500	0.2000	0.2500	0.3000	0.3500	0.4000
0.0100	0.0050	0.0298	0.0539	0.0774	0.1002	0.1215	0.1378	0.1498	0.1575
0.0200	0.0101	0.0347	0.0587	0.0820	0.1047	0.1257	0.1416	0.1533	0.1608
0.0400	0.0200	0.0443	0.0681	0.0913	0.1139	0.1339	0.1491	0.1602	0.1673
0.0600	0.0298	0.0539	0.0776	0.1006	0.1229	0.1419	0.1565	0.1671	0.1738
0.0800	0.0395	0.0634	0.0869	0.1098	0.1318	0.1499	0.1638	0.1740	0.1803
0.1000	0.0491	0.0729	0.0963	0.1190	0.1405	0.1577	0.1711	0.1808	0.1869
0.1200	0.0586	0.0823	0.1055	0.1282	0.1490	0.1654	0.1783	0.1876	0.1934
0.1400	0.0682	0.0918	0.1148	0.1372	0.1573	0.1731	0.1855	0.1944	0.1999
0.1600	0.0777	0.1011	0.1241	0.1462	0.1654	0.1806	0.1926	0.2011	0.2064
0.1800	0.0871	0.1104	0.1333	0.1551	0.1734	0.1881	0.1996	0.2079	0.2129
0.2000	0.0965	0.1198	0.1424	0.1637	0.1813	0.1956	0.2067	0.2146	0.2195

ϕu.My/ϕy.Mi
lf/lw=0.25 g=0.95 fy=275.0 Mpa

Axial Load Ratio Nu/f'm.Ag

fy/f'm	0.0000	0.0500	0.1000	0.1500	0.2000	0.2500	0.3000	0.3500	0.4000
0.0100	449.591	81.1487	40.3078	25.2629	16.7279	8.4424	4.4206	3.0291	2.2923
0.0200	192.045	64.5302	37.0117	23.7605	16.0021	7.8023	4.2687	2.9698	2.2839
0.0400	87.4744	51.3247	31.7837	21.2759	13.7063	6.6527	4.0151	2.8894	2.2624
0.0600	61.1041	40.1145	26.6588	19.2085	11.9798	5.9771	3.8170	2.8226	2.2370
0.0800	50.3625	34.4197	23.7530	17.4992	10.2241	5.4077	3.6386	2.7455	2.2181
0.1000	42.6140	30.0658	21.3662	15.6445	8.8964	5.0349	3.4999	2.6942	2.2004
0.1200	36.7813	26.6254	20.0507	13.7901	7.7521	4.6587	3.3726	2.6394	2.1836
0.1400	32.2419	23.8813	18.3128	12.3079	6.8595	4.4145	3.2553	2.5939	2.1677
0.1600	28.6204	21.6053	16.8175	10.8829	6.2147	4.1864	3.1661	2.5578	2.1527
0.1800	25.6677	20.3945	15.5625	9.7258	5.7377	3.9812	3.0827	2.5166	2.1384
0.2000	24.2270	18.6856	14.0924	8.6551	5.3271	3.8312	3.0044	2.4843	2.1295

CASE 4 g = 0.95, ℓ_f/ℓ_w = 0.50 WEB IN COMPRESSION

Icr/Igross
1f/lw=0.50 g=0.95 fy=275.0 Mpa

Axial Load Ratio Nu/f'm.Ag

fy/f'm	0.0000	0.0500	0.1000	0.1500	0.2000	0.2500	0.3000	0.3500	0.4000
0.0100	0.0286	0.1424	0.2150	0.2644	0.2967	0.3068	0.2741	0.3312	0.3809
0.0200	0.0530	0.1579	0.2268	0.2739	0.3046	0.3127	0.2816	0.3357	0.3829
0.0400	0.0957	0.1872	0.2495	0.2925	0.3201	0.3246	0.2967	0.3447	0.3898
0.0600	0.1331	0.2144	0.2711	0.3104	0.3349	0.3361	0.3109	0.3547	0.3965
0.0800	0.1668	0.2400	0.2918	0.3278	0.3493	0.3471	0.3248	0.3647	0.4030
0.1000	0.1978	0.2641	0.3116	0.3447	0.3630	0.3578	0.3379	0.3747	0.4115
0.1200	0.2265	0.2871	0.3308	0.3611	0.3766	0.3681	0.3509	0.3857	0.4189
0.1400	0.2535	0.3090	0.3493	0.3772	0.3897	0.3790	0.3638	0.3957	0.4272
0.1600	0.2789	0.3300	0.3672	0.3929	0.4018	0.3886	0.3759	0.4057	0.4355
0.1800	0.3031	0.3503	0.3847	0.4082	0.4146	0.3989	0.3887	0.4167	0.4447
0.2000	0.3262	0.3698	0.4017	0.4229	0.4265	0.3611	0.4007	0.4267	0.4529

Mi/f'm.t.lw**2
1f/lw=0.50 g=0.95 fy=275.0 Mpa

Axial Load Ratio Nu/f'm.Ag

fy/f'm	0.0000	0.0500	0.1000	0.1500	0.2000	0.2500	0.3000	0.3500	0.4000
0.0100	0.0098	0.0548	0.0937	0.1265	0.1532	0.1738	0.1881	0.1960	0.1981
0.0200	0.0192	0.0631	0.1010	0.1329	0.1587	0.1785	0.1923	0.1991	0.2007
0.0400	0.0375	0.0792	0.1151	0.1452	0.1695	0.1879	0.2006	0.2054	0.2063
0.0600	0.0550	0.0946	0.1286	0.1570	0.1799	0.1971	0.2086	0.2118	0.2119
0.0800	0.0716	0.1094	0.1417	0.1685	0.1900	0.2062	0.2163	0.2182	0.2176
0.1000	0.0876	0.1236	0.1542	0.1797	0.2000	0.2150	0.2239	0.2247	0.2235
0.1200	0.1030	0.1372	0.1665	0.1906	0.2097	0.2238	0.2314	0.2313	0.2293
0.1400	0.1178	0.1505	0.1783	0.2012	0.2192	0.2324	0.2388	0.2378	0.2353
0.1600	0.1321	0.1633	0.1899	0.2116	0.2286	0.2409	0.2461	0.2444	0.2414
0.1800	0.1459	0.1758	0.2010	0.2218	0.2379	0.2493	0.2533	0.2510	0.2475
0.2000	0.1593	0.1879	0.2121	0.2317	0.2469	0.2576	0.2605	0.2576	0.2536

ϕu.My/ϕy.Mi
1f/lw=0.50 g=0.95 fy=275.0 Mpa

Axial Load Ratio Nu/f'm.Ag

fy/f'm	0.0000	0.0500	0.1000	0.1500	0.2000	0.2500	0.3000	0.3500	0.4000
0.0100	58.4684	9.1911	4.4191	2.7806	1.9599	1.4420	1.0000	1.0000	1.0000
0.0200	29.1744	7.7345	4.0646	2.6388	1.8996	1.4181	1.0000	1.0000	1.0000
0.0400	14.2192	5.9494	3.5471	2.4301	1.8036	1.3698	1.0000	1.0000	1.0000
0.0600	9.4255	4.8872	3.1614	2.2628	1.7231	1.3244	1.0000	1.0000	1.0000
0.0800	7.1202	4.1972	2.8667	2.1273	1.6563	1.2859	1.0000	1.0000	1.0000
0.1000	5.7910	3.6970	2.6485	2.0162	1.5931	1.2533	1.0000	1.0000	1.0000
0.1200	4.9411	3.3404	2.4615	1.9248	1.5409	1.2218	1.0000	1.0000	1.0000
0.1400	4.2992	3.0628	2.3207	1.8418	1.4969	1.1983	1.0000	1.0000	1.0000
0.1600	3.8500	2.8269	2.1954	1.7795	1.4530	1.1725	1.0000	1.0000	1.0000
0.1800	3.5041	2.6512	2.1012	1.7154	1.4152	1.1505	1.0000	1.0000	1.0000
0.2000	3.2128	2.4957	2.0070	1.6665	1.3815	1.0000	1.0000	1.0000	1.0000

CASE 5 $g = 0.95$, $\ell_f/\ell_w = 0.50$ FLANGE IN COMPRESSION

Icr/Igross
lf/lw=0.50 g=0.95 fy=275.0 Mpa

Axial Load Ratio Nu/f'm.Ag

fy/f'm	0.0000	0.0500	0.1000	0.1500	0.2000	0.2500	0.3000	0.3500	0.4000
0.0100	0.0133	0.0999	0.1709	0.2303	0.2789	0.3190	0.3518	0.3774	0.3956
0.0200	0.0260	0.1103	0.1803	0.2384	0.2867	0.3267	0.3583	0.3841	0.4025
0.0400	0.0506	0.1310	0.1984	0.2545	0.3012	0.3397	0.3712	0.3959	0.4148
0.0600	0.0743	0.1515	0.2162	0.2706	0.3157	0.3527	0.3842	0.4076	0.4256
0.0800	0.0973	0.1714	0.2334	0.2857	0.3301	0.3669	0.3958	0.4208	0.4378
0.1000	0.1197	0.1906	0.2509	0.3016	0.3445	0.3799	0.4087	0.4326	0.4499
0.1200	0.1415	0.2098	0.2677	0.3166	0.3589	0.3928	0.4217	0.4443	0.4620
0.1400	0.1627	0.2285	0.2844	0.3324	0.3723	0.4070	0.4346	0.4575	0.4741
0.1600	0.1835	0.2469	0.3014	0.3473	0.3866	0.4200	0.4476	0.4692	0.4861
0.1800	0.2038	0.2650	0.3178	0.3629	0.4009	0.4330	0.4605	0.4823	0.4997
0.2000	0.2238	0.2830	0.3341	0.3777	0.4152	0.4460	0.4721	0.4940	0.5116

Mi/f m.t.lw**2
lf/lw=0.50 g=0.95 fy=275.0 Mpa

Axial Load Ratio Nu/f'm.Ag

fy/f'm	0.0000	0.0500	0.1000	0.1500	0.2000	0.2500	0.3000	0.3500	0.4000
0.0100	0.0051	0.0304	0.0550	0.0791	0.1027	0.1258	0.1483	0.1703	0.1860
0.0200	0.0102	0.0353	0.0598	0.0839	0.1074	0.1304	0.1529	0.1748	0.1902
0.0400	0.0203	0.0452	0.0695	0.0934	0.1168	0.1398	0.1622	0.1839	0.1985
0.0600	0.0304	0.0549	0.0790	0.1028	0.1262	0.1491	0.1716	0.1928	0.2068
0.0800	0.0403	0.0645	0.0886	0.1123	0.1356	0.1584	0.1808	0.2017	0.2151
0.1000	0.0500	0.0741	0.0981	0.1217	0.1450	0.1677	0.1901	0.2104	0.2234
0.1200	0.0596	0.0837	0.1076	0.1312	0.1543	0.1771	0.1993	0.2190	0.2317
0.1400	0.0693	0.0933	0.1171	0.1405	0.1637	0.1865	0.2085	0.2276	0.2399
0.1600	0.0789	0.1028	0.1266	0.1500	0.1731	0.1957	0.2177	0.2362	0.2482
0.1800	0.0884	0.1123	0.1361	0.1594	0.1825	0.2050	0.2269	0.2447	0.2565
0.2000	0.0980	0.1219	0.1454	0.1689	0.1917	0.2143	0.2360	0.2532	0.2647

$\phi u.My/\phi y.Mi$
lf/lw=0.50 g=0.95 fy=275.0 Mpa

Axial Load Ratio Nu/f'm.Ag

fy/f'm	0.0000	0.0500	0.1000	0.1500	0.2000	0.2500	0.3000	0.3500	0.4000
0.0100	451.381	117.857	67.0238	42.4763	29.9464	22.4731	17.0978	10.8034	4.5153
0.0200	270.021	98.8230	60.1954	39.3431	29.4451	22.1996	16.8899	10.3343	4.4239
0.0400	148.015	74.3340	49.6996	35.9052	27.3288	20.8530	16.0709	9.4697	4.3016
0.0600	87.7320	59.5061	44.7481	33.0472	25.5081	19.6667	14.9479	8.7325	4.1723
0.0800	68.4659	53.0324	40.6397	30.5426	23.9231	19.2656	14.2613	8.0087	4.0653
0.1000	56.0892	47.8211	37.3252	28.4743	22.5294	18.2718	13.3636	7.3679	3.9937
0.1200	51.1414	43.6255	34.4513	26.6093	22.0600	17.3782	12.8566	6.8180	3.8974
0.1400	46.9210	40.0621	31.9923	26.0799	20.8366	16.6187	12.1205	6.3609	3.8336
0.1600	43.2768	37.0329	29.9137	24.5343	19.7927	16.3419	11.4622	6.0064	3.7730
0.1800	42.8813	34.4209	28.0403	23.2102	18.8492	15.6420	10.6568	5.7049	3.7269
0.2000	39.7543	32.1426	27.5815	21.9761	18.5808	15.0018	10.1120	5.4711	3.6712

CASE 6 $g = 0.95$, $\ell_f/\ell_w = 0.75$ WEB IN COMPRESSION

Icr/Igross
1f/lw=0.75 g=0.95 fy=275.0 Mpa

Axial Load Ratio Nu/f'm.Ag

fy/f'm	0.0000	0.0500	0.1000	0.1500	0.2000	0.2500	0.3000	0.3500	0.4000
0.0100	0.0321	0.1521	0.2258	0.2732	0.2974	0.2604	0.3285	0.3904	0.4395
0.0200	0.0593	0.1689	0.2382	0.2829	0.3042	0.2700	0.3339	0.3931	0.4416
0.0400	0.1061	0.2002	0.2618	0.3016	0.3169	0.2892	0.3458	0.3996	0.4452
0.0600	0.1466	0.2290	0.2841	0.3193	0.3286	0.3075	0.3577	0.4069	0.4504
0.0800	0.1827	0.2557	0.3051	0.3362	0.3398	0.3236	0.3695	0.4141	0.4551
0.1000	0.2154	0.2807	0.3251	0.3518	0.3502	0.3386	0.3804	0.4223	0.4605
0.1200	0.2456	0.3043	0.3443	0.3667	0.3597	0.3535	0.3913	0.4305	0.4666
0.1400	0.2735	0.3266	0.3626	0.3800	0.3683	0.3675	0.4032	0.4385	0.4737
0.1600	0.2998	0.3478	0.3804	0.3936	0.3365	0.3814	0.4141	0.4476	0.4804
0.1800	0.3245	0.3681	0.3973	0.4056	0.3549	0.3945	0.4250	0.4566	0.4870
0.2000	0.3479	0.3876	0.4134	0.4167	0.3735	0.4074	0.4368	0.4657	0.4945

Mi/f'm.t.lw**2
1f/lw=0.75 g=0.95 fy=275.0 Mpa

Axial Load Ratio Nu/f'm.Ag

fy/f'm	0.0000	0.0500	0.1000	0.1500	0.2000	0.2500	0.3000	0.3500	0.4000
0.0100	0.0121	0.0678	0.1152	0.1541	0.1849	0.2072	0.2203	0.2259	0.2236
0.0200	0.0239	0.0780	0.1240	0.1617	0.1912	0.2126	0.2240	0.2287	0.2265
0.0400	0.0466	0.0977	0.1409	0.1762	0.2037	0.2232	0.2314	0.2347	0.2323
0.0600	0.0681	0.1164	0.1571	0.1902	0.2157	0.2332	0.2388	0.2409	0.2382
0.0800	0.0886	0.1343	0.1727	0.2037	0.2274	0.2424	0.2462	0.2470	0.2440
0.1000	0.1081	0.1514	0.1876	0.2168	0.2388	0.2512	0.2535	0.2534	0.2500
0.1200	0.1268	0.1679	0.2021	0.2294	0.2498	0.2598	0.2608	0.2598	0.2560
0.1400	0.1447	0.1837	0.2160	0.2417	0.2606	0.2681	0.2681	0.2662	0.2622
0.1600	0.1620	0.1990	0.2296	0.2537	0.2713	0.2763	0.2753	0.2728	0.2684
0.1800	0.1786	0.2138	0.2427	0.2653	0.2816	0.2844	0.2826	0.2794	0.2745
0.2000	0.1947	0.2281	0.2554	0.2767	0.2919	0.2924	0.2898	0.2861	0.2808

ϕu.My/ϕy.Mi
1f/lw=0.75 g=0.95 fy=275.0 Mpa

Axial Load Ratio Nu/f'm.Ag

fy/f'm	0.0000	0.0500	0.1000	0.1500	0.2000	0.2500	0.3000	0.3500	0.4000
0.0100	52.3098	7.7021	3.6868	2.2947	1.5825	1.0000	1.0000	1.0000	1.0000
0.0200	25.7683	6.5535	3.3846	2.1821	1.5355	1.0000	1.0000	1.0000	1.0000
0.0400	12.3848	5.0601	2.9517	2.0120	1.4476	1.0000	1.0000	1.0000	1.0000
0.0600	8.2184	4.1558	2.6404	1.8734	1.3757	1.0000	1.0000	1.0000	1.0000
0.0800	6.1848	3.5583	2.3980	1.7589	1.3112	1.0000	1.0000	1.0000	1.0000
0.1000	5.0001	3.1403	2.2152	1.6605	1.2546	1.0000	1.0000	1.0000	1.0000
0.1200	4.2379	2.8217	2.0670	1.5830	1.2047	1.0000	1.0000	1.0000	1.0000
0.1400	3.6886	2.5843	1.9441	1.5085	1.1604	1.0000	1.0000	1.0000	1.0000
0.1600	3.2980	2.3936	1.8359	1.4479	1.0000	1.0000	1.0000	1.0000	1.0000
0.1800	2.9945	2.2385	1.7506	1.3929	1.0000	1.0000	1.0000	1.0000	1.0000
0.2000	2.7537	2.1023	1.6783	1.3402	1.0000	1.0000	1.0000	1.0000	1.0000

CASE 7 $g = 0.95$, $\ell_f/\ell_w = 0.75$ FLANGE IN COMPRESSION

Icr/Igross
1f/1w=0.75 g=0.95 fy=275.0 Mpa

Axial Load Ratio Nu/f'm.Ag

fy/f'm	0.0000	0.0500	0.1000	0.1500	0.2000	0.2500	0.3000	0.3500	0.4000
0.0100	0.0118	0.0900	0.1566	0.2130	0.2621	0.3035	0.3366	0.3644	0.3869
0.0200	0.0232	0.0998	0.1651	0.2210	0.2688	0.3100	0.3432	0.3712	0.3940
0.0400	0.0453	0.1189	0.1821	0.2371	0.2834	0.3230	0.3563	0.3829	0.4044
0.0600	0.0668	0.1378	0.1990	0.2521	0.2979	0.3361	0.3678	0.3946	0.4165
0.0800	0.0878	0.1564	0.2157	0.2671	0.3112	0.3491	0.3808	0.4080	0.4287
0.1000	0.1083	0.1748	0.2323	0.2830	0.3257	0.3621	0.3939	0.4196	0.4407
0.1200	0.1285	0.1930	0.2488	0.2979	0.3402	0.3751	0.4070	0.4313	0.4527
0.1400	0.1483	0.2106	0.2651	0.3127	0.3534	0.3896	0.4185	0.4446	0.4647
0.1600	0.1678	0.2284	0.2814	0.3276	0.3679	0.4026	0.4315	0.4562	0.4766
0.1800	0.1869	0.2456	0.2970	0.3423	0.3812	0.4156	0.4446	0.4696	0.4885
0.2000	0.2058	0.2631	0.3131	0.3571	0.3956	0.4286	0.4577	0.4811	0.5003

Mi/f'm.t.lw**2
1f/1w=0.75 g=0.95 fy=275.0 Mpa

Axial Load Ratio Nu/f'm.Ag

fy/f'm	0.0000	0.0500	0.1000	0.1500	0.2000	0.2500	0.3000	0.3500	0.4000
0.0100	0.0052	0.0307	0.0558	0.0802	0.1043	0.1278	0.1507	0.1733	0.1955
0.0200	0.0103	0.0358	0.0607	0.0851	0.1090	0.1325	0.1554	0.1779	0.2001
0.0400	0.0206	0.0458	0.0704	0.0946	0.1185	0.1419	0.1649	0.1875	0.2096
0.0600	0.0307	0.0558	0.0801	0.1042	0.1280	0.1514	0.1743	0.1968	0.2189
0.0800	0.0408	0.0655	0.0897	0.1137	0.1374	0.1607	0.1836	0.2062	0.2284
0.1000	0.0508	0.0751	0.0993	0.1232	0.1469	0.1703	0.1932	0.2156	0.2377
0.1200	0.0606	0.0848	0.1088	0.1328	0.1563	0.1796	0.2025	0.2252	0.2471
0.1400	0.0703	0.0944	0.1184	0.1422	0.1659	0.1890	0.2119	0.2345	0.2564
0.1600	0.0799	0.1040	0.1280	0.1518	0.1752	0.1985	0.2215	0.2439	0.2658
0.1800	0.0895	0.1135	0.1374	0.1612	0.1848	0.2079	0.2308	0.2532	0.2752
0.2000	0.0991	0.1231	0.1470	0.1707	0.1942	0.2172	0.2401	0.2628	0.2846

$\phi u.My/\phi y.Mi$
1f/1w=0.75 g=0.95 fy=275.0 Mpa

Axial Load Ratio Nu/f'm.Ag

fy/f'm	0.0000	0.0500	0.1000	0.1500	0.2000	0.2500	0.3000	0.3500	0.4000
0.0100	*******	161.964	81.7818	56.0879	39.5315	29.7304	24.0490	19.2753	14.6484
0.0200	443.309	130.793	72.3950	51.3636	38.7879	29.2958	23.7793	19.1157	14.5684
0.0400	190.343	93.2700	63.3360	46.5201	35.7716	28.5126	22.4753	18.1729	13.9415
0.0600	120.209	71.9885	56.3581	42.3699	33.1908	26.7108	21.9556	17.8374	13.7497
0.0800	87.4858	63.5641	50.7921	41.1566	32.3065	26.1312	21.5792	17.6073	13.2525
0.1000	68.5861	56.9666	46.2337	38.0549	30.2145	24.6246	20.5226	17.3235	13.0915
0.1200	61.7224	51.6254	45.1856	35.2735	29.6643	24.1823	20.2254	16.5651	12.6443
0.1400	56.1620	50.6165	41.5944	34.5806	27.8148	23.8699	19.8775	16.3974	12.5075
0.1600	51.4406	46.4043	38.5173	32.2858	27.4038	22.6273	18.9891	16.1784	12.1018
0.1800	51.1360	42.7607	37.8517	31.7741	25.8247	22.3087	18.7719	16.0366	11.9841
0.2000	47.1121	42.2543	35.2940	29.8323	25.5096	22.0176	18.5716	15.4016	11.6135

CASE 8 $g = 0.95\ \ell_f/\ell_w = 1.00$ WEB IN COMPRESSION

Icr/Igross
lf/lw=1.00 g=0.95 fy=275.0 Mpa

Axial Load Ratio Nu/f'm.Ag

fy/f'm	0.0000	0.0500	0.1000	0.1500	0.2000	0.2500	0.3000	0.3500	0.4000
0.0100	0.0357	0.1624	0.2371	0.2817	0.2893	0.3084	0.3830	0.4473	0.4409
0.0200	0.0656	0.1803	0.2498	0.2911	0.2940	0.3168	0.3865	0.4478	0.4481
0.0400	0.1163	0.2132	0.2739	0.3079	0.2639	0.3327	0.3955	0.4516	0.4597
0.0600	0.1596	0.2432	0.2963	0.3235	0.2875	0.3476	0.4034	0.4559	0.4724
0.0800	0.1977	0.2707	0.3172	0.3369	0.3108	0.3614	0.4123	0.4610	0.4835
0.1000	0.2319	0.2962	0.3369	0.3491	0.3294	0.3744	0.4212	0.4668	0.4943
0.1200	0.2631	0.3199	0.3552	0.3589	0.3464	0.3881	0.4311	0.4735	0.5047
0.1400	0.2917	0.3421	0.3720	0.3690	0.3624	0.4009	0.4409	0.4799	0.5136
0.1600	0.3184	0.3631	0.3871	0.3766	0.3775	0.4129	0.4498	0.4873	0.5207
0.1800	0.3434	0.3829	0.4005	0.3490	0.3924	0.4256	0.4596	0.4946	0.5261
0.2000	0.3667	0.4019	0.4133	0.3706	0.4064	0.4375	0.4695	0.5017	0.5324

Mi/f'm.t.lw**2
lf/lw=1.00 g=0.95 fy=275.0 Mpa

Axial Load Ratio Nu/f'm.Ag

fy/f'm	0.0000	0.0500	0.1000	0.1500	0.2000	0.2500	0.3000	0.3500	0.4000
0.0100	0.0145	0.0806	0.1358	0.1801	0.2135	0.2351	0.2461	0.2475	0.2314
0.0200	0.0286	0.0926	0.1459	0.1886	0.2205	0.2399	0.2493	0.2503	0.2355
0.0400	0.0556	0.1157	0.1655	0.2050	0.2343	0.2491	0.2561	0.2563	0.2432
0.0600	0.0810	0.1375	0.1841	0.2207	0.2474	0.2580	0.2627	0.2623	0.2511
0.0800	0.1051	0.1583	0.2018	0.2357	0.2601	0.2665	0.2696	0.2684	0.2586
0.1000	0.1280	0.1780	0.2187	0.2502	0.2709	0.2748	0.2765	0.2747	0.2661
0.1200	0.1498	0.1969	0.2350	0.2641	0.2807	0.2830	0.2835	0.2811	0.2735
0.1400	0.1706	0.2150	0.2506	0.2776	0.2902	0.2911	0.2906	0.2874	0.2805
0.1600	0.1906	0.2324	0.2657	0.2906	0.2994	0.2992	0.2976	0.2940	0.2872
0.1800	0.2097	0.2491	0.2803	0.3033	0.3083	0.3071	0.3047	0.3005	0.2936
0.2000	0.2281	0.2652	0.2944	0.3156	0.3171	0.3150	0.3118	0.3071	0.3001

ϕu.My/ϕy.Mi
lf/lw=1.00 g=0.95 fy=275.0 Mpa

Axial Load Ratio Nu/f'm.Ag

fy/f'm	0.0000	0.0500	0.1000	0.1500	0.2000	0.2500	0.3000	0.3500	0.4000
0.0100	46.9513	6.5829	3.1371	1.9308	1.2737	1.0000	1.0000	1.0000	1.0000
0.0200	22.8819	5.5951	2.8894	1.8368	1.2288	1.0000	1.0000	1.0000	1.0000
0.0400	10.8708	4.3335	2.5145	1.6863	1.0000	1.0000	1.0000	1.0000	1.0000
0.0600	7.2132	3.5579	2.2422	1.5621	1.0000	1.0000	1.0000	1.0000	1.0000
0.0800	5.4091	3.0562	2.0374	1.4533	1.0000	1.0000	1.0000	1.0000	1.0000
0.1000	4.3504	2.6998	1.8803	1.3654	1.0000	1.0000	1.0000	1.0000	1.0000
0.1200	3.6898	2.4252	1.7494	1.2846	1.0000	1.0000	1.0000	1.0000	1.0000
0.1400	3.2096	2.2072	1.6383	1.2187	1.0000	1.0000	1.0000	1.0000	1.0000
0.1600	2.8484	2.0413	1.5473	1.1565	1.0000	1.0000	1.0000	1.0000	1.0000
0.1800	2.5817	1.9041	1.4621	1.0000	1.0000	1.0000	1.0000	1.0000	1.0000
0.2000	2.3674	1.7973	1.3895	1.0000	1.0000	1.0000	1.0000	1.0000	1.0000

CASE 9 $g = 0.95$, $\ell_f/\ell_w = 1.00$ FLANGE IN COMPRESSION

Icr/Igross
1f/lw=1.00 g=0.95 fy=275.0 Mpa

Axial Load Ratio Nu/f'm.Ag

fy/f'm	0.0000	0.0500	0.1000	0.1500	0.2000	0.2500	0.3000	0.3500	0.4000
0.0100	0.0109	0.0835	0.1466	0.2021	0.2487	0.2902	0.3255	0.3540	0.3796
0.0200	0.0214	0.0930	0.1549	0.2090	0.2567	0.2968	0.3321	0.3608	0.3847
0.0400	0.0420	0.1109	0.1715	0.2240	0.2699	0.3098	0.3435	0.3725	0.3969
0.0600	0.0620	0.1290	0.1880	0.2389	0.2845	0.3229	0.3567	0.3841	0.4091
0.0800	0.0817	0.1465	0.2037	0.2537	0.2978	0.3359	0.3681	0.3957	0.4190
0.1000	0.1010	0.1643	0.2200	0.2686	0.3123	0.3490	0.3813	0.4094	0.4310
0.1200	0.1200	0.1815	0.2355	0.2834	0.3255	0.3621	0.3945	0.4209	0.4430
0.1400	0.1388	0.1986	0.2517	0.2981	0.3387	0.3751	0.4058	0.4325	0.4550
0.1600	0.1573	0.2155	0.2670	0.3129	0.3533	0.3882	0.4190	0.4439	0.4668
0.1800	0.1755	0.2323	0.2824	0.3276	0.3665	0.4012	0.4304	0.4575	0.4787
0.2000	0.1936	0.2490	0.2983	0.3413	0.3797	0.4143	0.4436	0.4690	0.4904

Mi/f'm.t.lw**2
1f/lw=1.00 g=0.95 fy=275.0 Mpa

Axial Load Ratio Nu/f'm.Ag

fy/f'm	0.0000	0.0500	0.1000	0.1500	0.2000	0.2500	0.3000	0.3500	0.4000
0.0100	0.0052	0.0311	0.0565	0.0812	0.1055	0.1293	0.1526	0.1756	0.1979
0.0200	0.0105	0.0362	0.0615	0.0861	0.1104	0.1342	0.1575	0.1804	0.2027
0.0400	0.0208	0.0464	0.0713	0.0958	0.1198	0.1436	0.1669	0.1898	0.2121
0.0600	0.0311	0.0565	0.0811	0.1054	0.1294	0.1530	0.1763	0.1992	0.2216
0.0800	0.0413	0.0664	0.0907	0.1149	0.1388	0.1626	0.1857	0.2087	0.2311
0.1000	0.0515	0.0761	0.1004	0.1245	0.1484	0.1720	0.1951	0.2181	0.2406
0.1200	0.0615	0.0858	0.1100	0.1340	0.1579	0.1814	0.2048	0.2275	0.2501
0.1400	0.0713	0.0954	0.1195	0.1436	0.1675	0.1910	0.2142	0.2370	0.2596
0.1600	0.0809	0.1050	0.1292	0.1531	0.1769	0.2004	0.2236	0.2464	0.2690
0.1800	0.0906	0.1146	0.1387	0.1627	0.1863	0.2098	0.2330	0.2558	0.2785
0.2000	0.1001	0.1242	0.1483	0.1721	0.1960	0.2193	0.2424	0.2653	0.2880

Table $\phi u.My/\phi y.Mi$ Flange in compression
1f/lw=1.00 g=0.95 fy=275.0 Mpa

Axial Load Ratio Nu/f'm.Ag

fy/f'm	0.0000	0.0500	0.1000	0.1500	0.2000	0.2500	0.3000	0.3500	0.4000
0.0100	*******	197.457	90.9798	66.3950	47.7126	36.5839	29.0967	22.8500	19.1553
0.0200	441.253	154.729	88.4017	60.0071	44.3944	34.3800	27.6424	22.6839	18.9562
0.0400	189.890	105.963	69.7128	53.8372	42.9997	33.5412	26.9795	22.2533	18.6852
0.0600	146.641	80.0369	61.8821	48.8149	39.7045	32.8055	26.5241	21.8616	18.4345
0.0800	101.019	70.0410	59.9044	47.5600	38.7256	30.6942	25.9836	21.5035	18.1047
0.1000	76.8554	62.5875	54.1777	43.6506	36.0519	30.1439	25.6191	21.2825	17.8908
0.1200	68.4779	56.4673	49.2885	42.7968	35.3336	29.6506	24.3057	20.9752	17.6910
0.1400	61.7865	55.5245	48.4600	39.6232	32.9698	27.9314	23.9059	20.6911	17.5036
0.1600	56.3931	50.7094	44.5382	39.0128	32.5545	27.5479	23.6447	20.4277	17.3276
0.1800	56.1796	50.0845	43.8613	36.3603	32.0644	27.1988	23.3034	20.2753	17.1617
0.2000	51.5971	46.1334	40.7183	35.8003	30.1169	26.8796	23.0851	20.0433	17.0052

CASE 10 g = 0.95, ℓ_f/ℓ_w = 1.25 WEB IN COMPRESSION

Icr/Igross
1f/lw=1.25 g=0.95 fy=275.0 Mpa

Axial Load Ratio Nu/f'm.Ag

fy/f'm	0.0000	0.0500	0.1000	0.1500	0.2000	0.2500	0.3000	0.3500	0.4000
0.0100	0.0393	0.1727	0.2478	0.2865	0.2693	0.3561	0.4360	0.4517	0.4280
0.0200	0.0717	0.1914	0.2606	0.2943	0.2820	0.3624	0.4379	0.4582	0.4352
0.0400	0.1262	0.2257	0.2847	0.3073	0.3043	0.3742	0.4425	0.4699	0.4478
0.0600	0.1719	0.2564	0.3068	0.3180	0.3243	0.3859	0.4479	0.4801	0.4602
0.0800	0.2118	0.2843	0.3267	0.3271	0.3423	0.3976	0.4542	0.4912	0.4739
0.1000	0.2471	0.3099	0.3438	0.3018	0.3592	0.4093	0.4603	0.5009	0.4858
0.1200	0.2791	0.3334	0.3587	0.3294	0.3743	0.4210	0.4674	0.5103	0.4990
0.1400	0.3082	0.3552	0.3712	0.3503	0.3892	0.4318	0.4754	0.5169	0.5106
0.1600	0.3348	0.3751	0.3813	0.3675	0.4040	0.4435	0.4834	0.5230	0.5234
0.1800	0.3593	0.3935	0.3902	0.3837	0.4178	0.4543	0.4924	0.5288	0.5345
0.2000	0.3824	0.4090	0.3500	0.3996	0.4316	0.4651	0.5002	0.5355	0.5455

Mi/f'm.t.lw**2
1f/lw=1.25 g=0.95 fy=275.0 Mpa

Axial Load Ratio Nu/f'm.Ag

fy/f'm	0.0000	0.0500	0.1000	0.1500	0.2000	0.2500	0.3000	0.3500	0.4000
0.0100	0.0169	0.0931	0.1556	0.2042	0.2392	0.2583	0.2660	0.2543	0.2339
0.0200	0.0332	0.1069	0.1670	0.2136	0.2462	0.2624	0.2690	0.2583	0.2382
0.0400	0.0644	0.1332	0.1889	0.2315	0.2587	0.2704	0.2752	0.2662	0.2463
0.0600	0.0937	0.1578	0.2094	0.2484	0.2699	0.2783	0.2815	0.2737	0.2543
0.0800	0.1212	0.1812	0.2290	0.2646	0.2803	0.2862	0.2879	0.2814	0.2626
0.1000	0.1473	0.2033	0.2475	0.2799	0.2901	0.2940	0.2944	0.2888	0.2705
0.1200	0.1720	0.2243	0.2652	0.2947	0.2996	0.3018	0.3011	0.2961	0.2787
0.1400	0.1954	0.2443	0.2821	0.3065	0.3088	0.3095	0.3080	0.3029	0.2865
0.1600	0.2178	0.2634	0.2983	0.3169	0.3176	0.3172	0.3148	0.3095	0.2946
0.1800	0.2391	0.2817	0.3139	0.3269	0.3264	0.3250	0.3219	0.3161	0.3023
0.2000	0.2596	0.2992	0.3288	0.3364	0.3349	0.3327	0.3288	0.3228	0.3100

ϕu.My/ϕy.Mi
1f/lw=1.25 g=0.95 fy=275.0 Mpa

Axial Load Ratio Nu/f'm.Ag

fy/f'm	0.0000	0.0500	0.1000	0.1500	0.2000	0.2500	0.3000	0.3500	0.4000
0.0100	42.3931	5.7719	2.6971	1.6371	1.0000	1.0000	1.0000	1.0000	0.0000
0.0200	20.4704	4.8922	2.4898	1.5524	1.0000	1.0000	1.0000	1.0000	0.0000
0.0400	9.6260	3.7648	2.1627	1.4065	1.0000	1.0000	1.0000	1.0000	0.0000
0.0600	6.3826	3.1057	1.9308	1.2915	1.0000	1.0000	1.0000	1.0000	0.0000
0.0800	4.7716	2.6579	1.7516	1.1897	1.0000	1.0000	1.0000	1.0000	0.0000
0.1000	3.8208	2.3374	1.6057	1.0000	1.0000	1.0000	1.0000	1.0000	0.0000
0.1200	3.2222	2.0988	1.4818	1.0000	1.0000	1.0000	1.0000	1.0000	1.0000
0.1400	2.8038	1.9165	1.3781	1.0000	1.0000	1.0000	1.0000	1.0000	1.0000
0.1600	2.4855	1.7662	1.2859	1.0000	1.0000	1.0000	1.0000	1.0000	1.0000
0.1800	2.2463	1.6409	1.2064	1.0000	1.0000	1.0000	1.0000	1.0000	1.0000
0.2000	2.0557	1.5347	1.0000	1.0000	1.0000	1.0000	1.0000	1.0000	1.0000

CASE 11 g = 0.95, ℓ_f/ℓ_w = 1.25 FLANGE IN COMPRESSION

Icr/Igross
1f/1w=1.25 g=0.95 fy=275.0 Mpa

Axial Load Ratio Nu/f'm.Ag

fy/f'm	0.0000	0.0500	0.1000	0.1500	0.2000	0.2500	0.3000	0.3500	0.4000
0.0100	0.0103	0.0795	0.1403	0.1928	0.2400	0.2814	0.3164	0.3469	0.3703
0.0200	0.0203	0.0882	0.1477	0.2008	0.2466	0.2879	0.3211	0.3516	0.3777
0.0400	0.0398	0.1055	0.1640	0.2156	0.2598	0.2992	0.3345	0.3633	0.3875
0.0600	0.0588	0.1226	0.1794	0.2292	0.2745	0.3123	0.3458	0.3749	0.3997
0.0800	0.0775	0.1397	0.1948	0.2440	0.2876	0.3254	0.3591	0.3865	0.4119
0.1000	0.0960	0.1565	0.2109	0.2588	0.3008	0.3386	0.3704	0.4004	0.4239
0.1200	0.1141	0.1733	0.2262	0.2735	0.3139	0.3517	0.3838	0.4119	0.4359
0.1400	0.1321	0.1900	0.2414	0.2871	0.3286	0.3648	0.3950	0.4234	0.4479
0.1600	0.1499	0.2061	0.2566	0.3018	0.3418	0.3779	0.4084	0.4348	0.4598
0.1800	0.1675	0.2225	0.2717	0.3165	0.3549	0.3892	0.4196	0.4462	0.4716
0.2000	0.1849	0.2389	0.2867	0.3300	0.3681	0.4023	0.4329	0.4600	0.4834

Mi/f'm.t.1w**2
1f/1w=1.25 g=0.95 fy=275.0 Mpa

Axial Load Ratio Nu/f'm.Ag

fy/f'm	0.0000	0.0500	0.1000	0.1500	0.2000	0.2500	0.3000	0.3500	0.4000
0.0100	0.0053	0.0315	0.0572	0.0822	0.1068	0.1309	0.1544	0.1775	0.2001
0.0200	0.0106	0.0367	0.0622	0.0871	0.1115	0.1356	0.1591	0.1822	0.2049
0.0400	0.0211	0.0469	0.0722	0.0968	0.1211	0.1451	0.1685	0.1917	0.2141
0.0600	0.0315	0.0572	0.0820	0.1064	0.1306	0.1545	0.1782	0.2012	0.2236
0.0800	0.0418	0.0672	0.0918	0.1161	0.1403	0.1641	0.1876	0.2106	0.2332
0.1000	0.0520	0.0771	0.1014	0.1257	0.1497	0.1736	0.1970	0.2201	0.2427
0.1200	0.0622	0.0868	0.1111	0.1353	0.1592	0.1830	0.2065	0.2296	0.2522
0.1400	0.0722	0.0965	0.1207	0.1448	0.1688	0.1924	0.2159	0.2390	0.2617
0.1600	0.0820	0.1061	0.1303	0.1544	0.1783	0.2021	0.2254	0.2485	0.2713
0.1800	0.0915	0.1158	0.1399	0.1639	0.1877	0.2116	0.2348	0.2580	0.2808
0.2000	0.1013	0.1253	0.1495	0.1734	0.1974	0.2210	0.2446	0.2674	0.2903

ϕu.My/ϕy.Mi
1f/1w=1.25 g=0.95 fy=275.0 Mpa

Axial Load Ratio Nu/f'm.Ag

fy/f'm	0.0000	0.0500	0.1000	0.1500	0.2000	0.2500	0.3000	0.3500	0.4000
0.0100	*******	197.425	102.268	72.3829	51.5343	39.1889	32.4059	26.2467	21.5954
0.0200	438.275	154.252	88.5076	65.4556	50.6900	38.7074	31.9053	25.9101	21.5158
0.0400	263.090	122.224	76.6731	58.5622	46.1823	37.6108	31.3767	25.4469	21.8336
0.0600	146.135	89.4133	67.4825	56.6494	45.2475	36.8612	29.3750	25.0245	21.5626
0.0800	119.019	77.5155	60.2841	51.4929	41.6467	34.3933	28.9769	24.6375	21.3101
0.1000	86.9861	68.5486	59.0458	47.1736	40.8011	33.8350	28.4554	24.4250	21.0740
0.1200	68.4254	61.6160	53.5583	46.3535	40.0559	33.3342	28.1343	24.0905	20.8527
0.1400	61.8409	60.7071	52.6101	45.4554	37.4000	32.8825	27.6933	23.7806	20.6445
0.1600	61.7232	55.1556	48.2319	42.0974	36.8365	30.9243	27.4297	23.4925	20.4483
0.1800	56.4652	54.5771	47.5837	41.5912	36.3298	30.4293	27.0512	23.2240	20.2629
0.2000	56.3284	50.1293	43.9672	40.9953	33.9948	30.1120	25.7007	23.0927	20.0874

CASE 12 g = 0.95, ℓ_f/ℓ_w = 1.50 WEB IN COMPRESSION

Icr/Igross
lf/lw=1.50 g=0.95 fy=275.0 Mpa

Axial Load Ratio Nu/f'm.Ag

fy/f'm	0.0000	0.0500	0.1000	0.1500	0.2000	0.2500	0.3000	0.3500	0.4000
0.0100	0.0428	0.1826	0.2575	0.2855	0.3082	0.4034	0.4611	0.4435	0.4185
0.0200	0.0777	0.2021	0.2703	0.2912	0.3188	0.4068	0.4659	0.4486	0.4256
0.0400	0.1356	0.2373	0.2938	0.2988	0.3387	0.4156	0.4764	0.4614	0.4380
0.0600	0.1836	0.2685	0.3139	0.2879	0.3557	0.4243	0.4843	0.4741	0.4518
0.0800	0.2249	0.2964	0.3301	0.3144	0.3715	0.4331	0.4919	0.4865	0.4637
0.1000	0.2612	0.3216	0.3432	0.3353	0.3872	0.4418	0.4968	0.4974	0.4753
0.1200	0.2933	0.3444	0.3521	0.3543	0.4011	0.4515	0.5025	0.5095	0.4884
0.1400	0.3224	0.3644	0.3135	0.3716	0.4149	0.4612	0.5078	0.5215	0.5013
0.1600	0.3489	0.3809	0.3446	0.3884	0.4285	0.4709	0.5141	0.5319	0.5139
0.1800	0.3730	0.3948	0.3703	0.4043	0.4413	0.4806	0.5213	0.5421	0.5248
0.2000	0.3951	0.4056	0.3875	0.4194	0.4540	0.4913	0.5284	0.5535	0.5371

Mi/f'm.t.lw**2
lf/lw=1.50 g=0.95 fy=275.0 Mpa

Axial Load Ratio Nu/f'm.Ag

fy/f'm	0.0000	0.0500	0.1000	0.1500	0.2000	0.2500	0.3000	0.3500	0.4000
0.0100	0.0193	0.1054	0.1746	0.2267	0.2603	0.2774	0.2760	0.2568	0.2358
0.0200	0.0379	0.1208	0.1871	0.2366	0.2663	0.2808	0.2798	0.2606	0.2401
0.0400	0.0731	0.1501	0.2109	0.2556	0.2773	0.2879	0.2874	0.2689	0.2483
0.0600	0.1061	0.1774	0.2331	0.2734	0.2874	0.2951	0.2946	0.2771	0.2568
0.0800	0.1370	0.2031	0.2542	0.2884	0.2971	0.3023	0.3017	0.2853	0.2648
0.1000	0.1660	0.2272	0.2739	0.3002	0.3063	0.3095	0.3082	0.2930	0.2727
0.1200	0.1934	0.2500	0.2926	0.3113	0.3153	0.3169	0.3149	0.3011	0.2811
0.1400	0.2192	0.2716	0.3104	0.3219	0.3241	0.3244	0.3215	0.3092	0.2894
0.1600	0.2437	0.2921	0.3273	0.3319	0.3327	0.3318	0.3282	0.3168	0.2976
0.1800	0.2669	0.3116	0.3413	0.3415	0.3412	0.3393	0.3351	0.3245	0.3053
0.2000	0.2890	0.3302	0.3520	0.3511	0.3496	0.3468	0.3420	0.3324	0.3135

ϕu.My/ϕy.Mi
lf/lw=1.50 g=0.95 fy=275.0 Mpa

Axial Load Ratio Nu/f'm.Ag

fy/f'm	0.0000	0.0500	0.1000	0.1500	0.2000	0.2500	0.3000	0.3500	0.4000
0.0100	38.5263	5.0758	2.3612	1.3867	1.0000	1.0000	1.0000	0.0000	0.0000
0.0200	18.0135	4.2949	2.1729	1.3083	1.0000	1.0000	1.0000	0.0000	0.0000
0.0400	8.7122	3.3301	1.8903	1.1700	1.0000	1.0000	1.0000	0.0000	0.0000
0.0600	5.6968	2.7399	1.6803	1.0000	1.0000	1.0000	1.0000	1.0000	0.0000
0.0800	4.2448	2.3363	1.5050	1.0000	1.0000	1.0000	1.0000	1.0000	0.0000
0.1000	3.4080	2.0544	1.3673	1.0000	1.0000	1.0000	1.0000	1.0000	0.0000
0.1200	2.8561	1.8420	1.2475	1.0000	1.0000	1.0000	1.0000	1.0000	0.0000
0.1400	2.4704	1.6686	1.0000	1.0000	1.0000	1.0000	1.0000	1.0000	0.0000
0.1600	2.1884	1.5304	1.0000	1.0000	1.0000	1.0000	1.0000	1.0000	0.0000
0.1800	1.9747	1.4072	1.0000	1.0000	1.0000	1.0000	1.0000	1.0000	0.0000
0.2000	1.8090	1.3027	1.0000	1.0000	1.0000	1.0000	1.0000	1.0000	0.0000

CASE 13 $g = 0.95$, $\ell_f/\ell_w = 1.50$ FLANGE IN COMPRESSION

Icr/Igross
1f/lw=1.50 g=0.95 fy=275.0 Mpa

Axial Load Ratio Nu/f'm.Ag

fy/f'm	0.0000	0.0500	0.1000	0.1500	0.2000	0.2500	0.3000	0.3500	0.4000
0.0100	0.0098	0.0766	0.1352	0.1866	0.2331	0.2737	0.3079	0.3399	0.3649
0.0200	0.0194	0.0850	0.1424	0.1933	0.2397	0.2803	0.3147	0.3445	0.3698
0.0400	0.0381	0.1014	0.1577	0.2081	0.2528	0.2915	0.3259	0.3562	0.3821
0.0600	0.0565	0.1182	0.1729	0.2229	0.2660	0.3047	0.3395	0.3678	0.3944
0.0800	0.0745	0.1348	0.1890	0.2364	0.2791	0.3179	0.3508	0.3794	0.4038
0.1000	0.0923	0.1509	0.2041	0.2511	0.2922	0.3311	0.3620	0.3910	0.4159
0.1200	0.1099	0.1673	0.2192	0.2646	0.3070	0.3422	0.3755	0.4025	0.4280
0.1400	0.1273	0.1832	0.2342	0.2793	0.3201	0.3554	0.3867	0.4166	0.4399
0.1600	0.1445	0.1995	0.2484	0.2927	0.3333	0.3686	0.4002	0.4280	0.4518
0.1800	0.1616	0.2152	0.2634	0.3074	0.3464	0.3818	0.4113	0.4394	0.4637
0.2000	0.1785	0.2308	0.2783	0.3208	0.3595	0.3929	0.4248	0.4507	0.4755

Mi/f'm.t.lw**2
1f/lw=1.50 g=0.95 fy=275.0 Mpa

Axial Load Ratio Nu/f'm.Ag

fy/f'm	0.0000	0.0500	0.1000	0.1500	0.2000	0.2500	0.3000	0.3500	0.4000
0.0100	0.0054	0.0319	0.0578	0.0831	0.1079	0.1321	0.1560	0.1792	0.2020
0.0200	0.0107	0.0371	0.0629	0.0880	0.1127	0.1368	0.1607	0.1839	0.2065
0.0400	0.0213	0.0475	0.0730	0.0978	0.1223	0.1465	0.1702	0.1934	0.2161
0.0600	0.0319	0.0578	0.0830	0.1076	0.1319	0.1559	0.1796	0.2029	0.2256
0.0800	0.0423	0.0680	0.0928	0.1172	0.1415	0.1654	0.1891	0.2124	0.2352
0.1000	0.0526	0.0780	0.1025	0.1269	0.1510	0.1751	0.1985	0.2219	0.2447
0.1200	0.0629	0.0879	0.1122	0.1364	0.1605	0.1845	0.2080	0.2313	0.2543
0.1400	0.0730	0.0975	0.1218	0.1461	0.1702	0.1940	0.2174	0.2408	0.2638
0.1600	0.0829	0.1073	0.1314	0.1556	0.1796	0.2034	0.2272	0.2503	0.2734
0.1800	0.0925	0.1168	0.1410	0.1651	0.1891	0.2129	0.2367	0.2598	0.2830
0.2000	0.1022	0.1265	0.1506	0.1748	0.1986	0.2223	0.2462	0.2693	0.2925

$\phi u.My/\phi y.Mi$
1f/lw=1.50 g=0.95 fy=275.0 Mpa

Axial Load Ratio Nu/f'm.Ag

fy/f'm	0.0000	0.0500	0.1000	0.1500	0.2000	0.2500	0.3000	0.3500	0.4000
0.0100	*******	197.044	115.794	72.5786	55.4815	44.1105	34.2153	28.8813	23.6440
0.0200	434.857	188.172	98.9164	71.0299	54.6253	43.6119	33.9433	28.5143	24.2871
0.0400	261.457	121.771	84.4622	63.3220	49.6485	40.0823	33.2077	28.0351	23.9904
0.0600	145.331	101.200	73.7524	57.1263	48.4596	39.3566	32.7715	27.5981	23.7140
0.0800	118.506	77.5027	65.8864	55.6107	44.5179	38.7137	32.1638	27.1955	23.2891
0.1000	99.9978	68.4670	59.2905	50.8252	43.6859	36.1388	31.6126	26.8241	23.0516
0.1200	76.2878	67.3653	58.1726	49.7969	43.1839	35.4465	31.3039	26.4803	22.8281
0.1400	68.1443	60.7699	53.0237	45.9317	40.0509	35.0190	30.8350	26.3281	22.6170
0.1600	61.6710	60.1248	52.1115	45.1972	39.4973	34.6311	29.1809	26.0243	22.4174
0.1800	56.5106	54.8354	51.4848	44.7289	38.9991	34.2777	28.7950	25.7405	22.2280
0.2000	56.4572	54.3180	47.4429	41.4324	38.5484	33.7813	28.5957	25.4747	22.0481

CASE 14 g = 0.95, ℓ_f/ℓ_w = 1.75 WEB IN COMPRESSION

Icr/Igross
1f/1w=1.75 g=0.95 fy=275.0 Mpa

Axial Load Ratio Nu/f'm.Ag

fy/f'm	0.0000	0.0500	0.1000	0.1500	0.2000	0.2500	0.3000	0.3500	0.4000
0.0100	0.0463	0.1921	0.2662	0.2382	0.3475	0.4492	0.4565	0.4350	0.4115
0.0200	0.0835	0.2122	0.2786	0.2568	0.3559	0.4509	0.4625	0.4414	0.4186
0.0400	0.1447	0.2481	0.2997	0.2908	0.3717	0.4552	0.4742	0.4541	0.4308
0.0600	0.1947	0.2795	0.3158	0.3160	0.3864	0.4602	0.4859	0.4651	0.4427
0.0800	0.2371	0.3070	0.3270	0.3374	0.4001	0.4662	0.4960	0.4774	0.4561
0.1000	0.2738	0.3313	0.2893	0.3573	0.4137	0.4731	0.5073	0.4895	0.4675
0.1200	0.3062	0.3516	0.3244	0.3753	0.4264	0.4809	0.5171	0.5015	0.4804
0.1400	0.3349	0.3672	0.3492	0.3921	0.4390	0.4887	0.5281	0.5149	0.4932
0.1600	0.3607	0.3783	0.3682	0.4080	0.4516	0.4975	0.5376	0.5266	0.5039
0.1800	0.3840	0.3861	0.3862	0.4230	0.4633	0.5062	0.5456	0.5381	0.5163
0.2000	0.4033	0.3567	0.4032	0.4378	0.4750	0.5150	0.5534	0.5496	0.5285

Mi/f'm.t.lw**2
1f/1w=1.75 g=0.95 fy=275.0 Mpa

Axial Load Ratio Nu/f'm.Ag

fy/f'm	0.0000	0.0500	0.1000	0.1500	0.2000	0.2500	0.3000	0.3500	0.4000
0.0100	0.0216	0.1175	0.1927	0.2474	0.2788	0.2926	0.2786	0.2582	0.2373
0.0200	0.0425	0.1344	0.2062	0.2577	0.2838	0.2957	0.2827	0.2624	0.2418
0.0400	0.0818	0.1665	0.2316	0.2761	0.2933	0.3021	0.2908	0.2708	0.2499
0.0600	0.1184	0.1962	0.2553	0.2901	0.3025	0.3086	0.2989	0.2786	0.2580
0.0800	0.1524	0.2240	0.2774	0.3026	0.3113	0.3153	0.3066	0.2869	0.2666
0.1000	0.1842	0.2499	0.2980	0.3139	0.3200	0.3222	0.3146	0.2951	0.2745
0.1200	0.2140	0.2742	0.3174	0.3245	0.3285	0.3293	0.3222	0.3032	0.2830
0.1400	0.2419	0.2970	0.3316	0.3347	0.3369	0.3364	0.3301	0.3118	0.2914
0.1600	0.2682	0.3185	0.3429	0.3444	0.3452	0.3437	0.3377	0.3199	0.2991
0.1800	0.2930	0.3388	0.3537	0.3540	0.3534	0.3510	0.3449	0.3279	0.3074
0.2000	0.3164	0.3579	0.3641	0.3632	0.3616	0.3583	0.3522	0.3360	0.3156

ϕu.My/ϕy.Mi
1f/1w=1.75 g=0.95 fy=275.0 Mpa

Axial Load Ratio Nu/f'm.Ag

fy/f'm	0.0000	0.0500	0.1000	0.1500	0.2000	0.2500	0.3000	0.3500	0.4000
0.0100	35.2296	4.5129	2.0890	1.0000	1.0000	1.0000	1.0000	0.0000	0.0000
0.0200	16.3885	3.8375	1.9160	1.0000	1.0000	1.0000	1.0000	0.0000	0.0000
0.0400	7.8367	2.9564	1.6587	1.0000	1.0000	1.0000	1.0000	0.0000	0.0000
0.0600	5.0819	2.4275	1.4559	1.0000	1.0000	1.0000	1.0000	0.0000	0.0000
0.0800	3.7827	2.0723	1.2895	1.0000	1.0000	1.0000	1.0000	0.0000	0.0000
0.1000	3.0430	1.8135	1.0000	1.0000	1.0000	1.0000	1.0000	0.0000	0.0000
0.1200	2.5402	1.6174	1.0000	1.0000	1.0000	1.0000	1.0000	0.0000	0.0000
0.1400	2.1960	1.4555	1.0000	1.0000	1.0000	1.0000	1.0000	0.0000	0.0000
0.1600	1.9422	1.3143	1.0000	1.0000	1.0000	1.0000	1.0000	1.0000	0.0000
0.1800	1.7494	1.1964	1.0000	1.0000	1.0000	1.0000	1.0000	1.0000	0.0000
0.2000	1.5922	1.0000	1.0000	1.0000	1.0000	1.0000	1.0000	1.0000	0.0000

CASE 15 g = 0.95, ℓ_f/ℓ_w = 1.75 FLANGE IN COMPRESSION

Icr/Igross
lf/lw=1.75 g=0.95 fy=275.0 Mpa

Axial Load Ratio Nu/f'm.Ag

fy/f'm	0.0000	0.0500	0.1000	0.1500	0.2000	0.2500	0.3000	0.3500	0.4000
0.0100	0.0095	0.0741	0.1313	0.1815	0.2269	0.2662	0.3037	0.3319	0.3581
0.0200	0.0188	0.0824	0.1384	0.1882	0.2335	0.2728	0.3081	0.3392	0.3659
0.0400	0.0369	0.0985	0.1535	0.2030	0.2466	0.2861	0.3193	0.3509	0.3753
0.0600	0.0547	0.1149	0.1686	0.2163	0.2597	0.2994	0.3331	0.3626	0.3877
0.0800	0.0722	0.1308	0.1836	0.2311	0.2728	0.3105	0.3443	0.3742	0.4000
0.1000	0.0895	0.1465	0.1986	0.2444	0.2860	0.3238	0.3554	0.3858	0.4122
0.1200	0.1066	0.1627	0.2136	0.2592	0.2991	0.3370	0.3692	0.3973	0.4211
0.1400	0.1235	0.1783	0.2276	0.2725	0.3122	0.3481	0.3803	0.4087	0.4331
0.1600	0.1403	0.1939	0.2424	0.2859	0.3254	0.3613	0.3940	0.4201	0.4451
0.1800	0.1570	0.2094	0.2573	0.3006	0.3385	0.3746	0.4050	0.4315	0.4570
0.2000	0.1735	0.2252	0.2721	0.3139	0.3516	0.3857	0.4161	0.4457	0.4688

Mi/f'm.t.lw**2
lf/lw=1.75 g=0.95 fy=275.0 Mpa

Axial Load Ratio Nu/f'm.Ag

fy/f'm	0.0000	0.0500	0.1000	0.1500	0.2000	0.2500	0.3000	0.3500	0.4000
0.0100	0.0054	0.0322	0.0584	0.0840	0.1089	0.1334	0.1575	0.1809	0.2036
0.0200	0.0108	0.0375	0.0635	0.0890	0.1137	0.1381	0.1622	0.1856	0.2084
0.0400	0.0216	0.0480	0.0739	0.0988	0.1235	0.1478	0.1717	0.1951	0.2180
0.0600	0.0322	0.0584	0.0839	0.1086	0.1332	0.1573	0.1812	0.2046	0.2276
0.0800	0.0428	0.0687	0.0938	0.1183	0.1427	0.1667	0.1906	0.2141	0.2372
0.1000	0.0532	0.0789	0.1036	0.1280	0.1522	0.1764	0.2001	0.2236	0.2464
0.1200	0.0635	0.0889	0.1132	0.1376	0.1619	0.1859	0.2095	0.2331	0.2559
0.1400	0.0739	0.0985	0.1229	0.1472	0.1714	0.1954	0.2190	0.2427	0.2655
0.1600	0.0839	0.1083	0.1325	0.1568	0.1809	0.2048	0.2285	0.2522	0.2750
0.1800	0.0938	0.1178	0.1422	0.1664	0.1904	0.2143	0.2379	0.2617	0.2846
0.2000	0.1032	0.1275	0.1518	0.1759	0.2001	0.2237	0.2474	0.2712	0.2941

ϕu.My/ϕy.Mi
lf/lw=1.75 g=0.95 fy=275.0 Mpa

Axial Load Ratio Nu/f'm.Ag

fy/f'm	0.0000	0.0500	0.1000	0.1500	0.2000	0.2500	0.3000	0.3500	0.4000
0.0100	*******	251.120	115.383	79.3794	59.5892	46.7522	36.3782	30.2121	25.6835
0.0200	431.159	187.186	111.823	70.9356	58.7205	46.2740	35.8252	30.0872	25.6429
0.0400	259.597	143.289	84.3533	68.9120	53.2175	42.7679	35.0883	29.6115	25.1421
0.0600	185.229	100.949	73.7867	61.5270	48.6208	42.0607	34.6908	29.1752	24.8780
0.0800	117.822	86.2673	65.7331	55.8698	47.6728	41.1412	34.0776	28.7730	24.6298
0.1000	99.5077	75.3817	64.3652	54.6565	46.8433	38.3518	33.5202	28.4010	25.3947
0.1200	86.1087	67.2632	58.2672	50.1732	43.2771	37.8936	33.2416	28.0557	24.9745
0.1400	67.8725	60.7770	57.1814	49.3298	42.6769	37.2431	32.7641	27.7339	24.7631
0.1600	61.4851	60.0898	52.3343	48.5892	42.1396	36.8768	32.5374	27.4333	24.5621
0.1800	61.4869	54.8800	51.7842	45.0284	41.6558	36.5429	32.1222	27.1518	24.3706
0.2000	56.4332	54.5534	51.2991	44.4812	38.8216	36.0307	31.7377	27.0658	24.1879

CASE 16 $g = 0.95$, $\ell_f/\ell_w = 2.00$ WEB IN COMPRESSION

Icr/Igross
1f/lw=2.00 g=0.95 fy=275.0 Mpa

Axial Load Ratio Nu/f'm.Ag

fy/f'm	0.0000	0.0500	0.1000	0.1500	0.2000	0.2500	0.3000	0.3500	0.4000
0.0100	0.0497	0.2011	0.2735	0.2706	0.3867	0.4663	0.4516	0.4288	0.4053
0.0200	0.0892	0.2217	0.2844	0.2882	0.3930	0.4718	0.4575	0.4352	0.4124
0.0400	0.1534	0.2579	0.3015	0.3157	0.4046	0.4813	0.4692	0.4477	0.4244
0.0600	0.2051	0.2890	0.3118	0.3389	0.4162	0.4895	0.4807	0.4601	0.4360
0.0800	0.2484	0.3159	0.2889	0.3598	0.4278	0.4975	0.4921	0.4706	0.4494
0.1000	0.2856	0.3372	0.3230	0.3778	0.4393	0.5029	0.5033	0.4826	0.4606
0.1200	0.3177	0.3528	0.3450	0.3948	0.4509	0.5080	0.5145	0.4962	0.4734
0.1400	0.3457	0.3626	0.3651	0.4106	0.4615	0.5140	0.5269	0.5078	0.4860
0.1600	0.3705	0.3270	0.3834	0.4262	0.4721	0.5210	0.5377	0.5194	0.4985
0.1800	0.3900	0.3659	0.4012	0.4402	0.4836	0.5289	0.5484	0.5308	0.5107
0.2000	0.4041	0.3847	0.4176	0.4547	0.4942	0.5356	0.5590	0.5420	0.5227

Mi/f'm.t.lw**2
1f/lw=2.00 g=0.95 fy=275.0 Mpa

Axial Load Ratio Nu/f'm.Ag

fy/f'm	0.0000	0.0500	0.1000	0.1500	0.2000	0.2500	0.3000	0.3500	0.4000
0.0100	0.0240	0.1293	0.2101	0.2660	0.2947	0.2994	0.2805	0.2595	0.2384
0.0200	0.0470	0.1477	0.2243	0.2752	0.2989	0.3034	0.2846	0.2637	0.2429
0.0400	0.0903	0.1823	0.2512	0.2904	0.3071	0.3110	0.2927	0.2722	0.2511
0.0600	0.1304	0.2143	0.2759	0.3033	0.3153	0.3184	0.3009	0.2805	0.2591
0.0800	0.1674	0.2438	0.2987	0.3150	0.3235	0.3257	0.3090	0.2883	0.2679
0.1000	0.2017	0.2712	0.3175	0.3258	0.3316	0.3325	0.3170	0.2965	0.2757
0.1200	0.2337	0.2966	0.3302	0.3360	0.3397	0.3392	0.3251	0.3053	0.2843
0.1400	0.2635	0.3204	0.3421	0.3458	0.3476	0.3461	0.3334	0.3134	0.2928
0.1600	0.2913	0.3425	0.3535	0.3552	0.3556	0.3532	0.3414	0.3216	0.3012
0.1800	0.3175	0.3632	0.3639	0.3646	0.3636	0.3604	0.3493	0.3296	0.3095
0.2000	0.3419	0.3745	0.3746	0.3735	0.3716	0.3675	0.3572	0.3377	0.3177

$\phi u.My/\phi y.Mi$
1f/lw=2.00 g=0.95 fy=275.0 Mpa

Axial Load Ratio Nu/f'm.Ag

fy/f'm	0.0000	0.0500	0.1000	0.1500	0.2000	0.2500	0.3000	0.3500	0.4000
0.0100	32.3960	4.0489	1.8546	1.0000	1.0000	1.0000	0.0000	0.0000	0.0000
0.0200	14.9990	3.4357	1.7033	1.0000	1.0000	1.0000	0.0000	0.0000	0.0000
0.0400	7.1013	2.6598	1.4510	1.0000	1.0000	1.0000	0.0000	0.0000	0.0000
0.0600	4.6049	2.1773	1.2563	1.0000	1.0000	1.0000	1.0000	0.0000	0.0000
0.0800	3.4175	1.8523	1.0000	1.0000	1.0000	1.0000	1.0000	0.0000	0.0000
0.1000	2.7389	1.6103	1.0000	1.0000	1.0000	1.0000	1.0000	0.0000	0.0000
0.1200	2.2870	1.4208	1.0000	1.0000	1.0000	1.0000	1.0000	0.0000	0.0000
0.1400	1.9744	1.2581	1.0000	1.0000	1.0000	1.0000	1.0000	0.0000	0.0000
0.1600	1.7431	1.0000	1.0000	1.0000	1.0000	1.0000	1.0000	0.0000	0.0000
0.1800	1.5511	1.0000	1.0000	1.0000	1.0000	1.0000	1.0000	0.0000	0.0000
0.2000	1.3953	1.0000	1.0000	1.0000	1.0000	1.0000	1.0000	0.0000	0.0000

CASE 17 g = 0.95, ℓ_f/ℓ_w = 2.00 FLANGE IN COMPRESSION

Icr/Igross
lf/lw=2.00 g=0.95 fy=275.0 Mpa

Axial Load Ratio Nu/f'm.Ag

fy/f'm	0.0000	0.0500	0.1000	0.1500	0.2000	0.2500	0.3000	0.3500	0.4000
0.0100	0.0092	0.0726	0.1276	0.1776	0.2216	0.2616	0.2976	0.3297	0.3540
0.0200	0.0183	0.0802	0.1356	0.1842	0.2282	0.2683	0.3046	0.3340	0.3621
0.0400	0.0359	0.0965	0.1506	0.1990	0.2414	0.2817	0.3159	0.3458	0.3713
0.0600	0.0533	0.1121	0.1645	0.2123	0.2545	0.2927	0.3271	0.3576	0.3838
0.0800	0.0704	0.1277	0.1794	0.2256	0.2677	0.3061	0.3382	0.3692	0.3963
0.1000	0.0873	0.1433	0.1943	0.2404	0.2808	0.3171	0.3522	0.3808	0.4051
0.1200	0.1040	0.1587	0.2082	0.2537	0.2939	0.3304	0.3633	0.3923	0.4173
0.1400	0.1206	0.1741	0.2230	0.2669	0.3071	0.3438	0.3744	0.4038	0.4294
0.1600	0.1371	0.1900	0.2378	0.2817	0.3202	0.3548	0.3882	0.4152	0.4414
0.1800	0.1534	0.2053	0.2516	0.2950	0.3334	0.3681	0.3993	0.4266	0.4534
0.2000	0.1696	0.2205	0.2664	0.3082	0.3465	0.3815	0.4103	0.4379	0.4617

Mi/f'm.t.lw**2
lf/lw=2.00 g=0.95 fy=275.0 Mpa

Axial Load Ratio Nu/f'm.Ag

fy/f'm	0.0000	0.0500	0.1000	0.1500	0.2000	0.2500	0.3000	0.3500	0.4000
0.0100	0.0055	0.0326	0.0590	0.0849	0.1101	0.1348	0.1589	0.1824	0.2053
0.0200	0.0110	0.0379	0.0642	0.0899	0.1149	0.1395	0.1636	0.1872	0.2101
0.0400	0.0218	0.0485	0.0746	0.0999	0.1245	0.1490	0.1731	0.1967	0.2198
0.0600	0.0326	0.0590	0.0849	0.1097	0.1343	0.1585	0.1825	0.2062	0.2294
0.0800	0.0433	0.0695	0.0949	0.1194	0.1438	0.1682	0.1920	0.2157	0.2385
0.1000	0.0538	0.0798	0.1046	0.1291	0.1535	0.1777	0.2015	0.2252	0.2481
0.1200	0.0642	0.0898	0.1144	0.1387	0.1630	0.1872	0.2109	0.2347	0.2577
0.1400	0.0746	0.0998	0.1240	0.1484	0.1726	0.1966	0.2204	0.2442	0.2672
0.1600	0.0848	0.1093	0.1337	0.1580	0.1823	0.2061	0.2299	0.2538	0.2768
0.1800	0.0948	0.1191	0.1433	0.1675	0.1918	0.2159	0.2397	0.2633	0.2864
0.2000	0.1041	0.1286	0.1529	0.1771	0.2013	0.2253	0.2492	0.2728	0.2960

ϕu.My/ϕy.Mi
lf/lw=2.00 g=0.95 fy=275.0 Mpa

Axial Load Ratio Nu/f'm.Ag

fy/f'm	0.0000	0.0500	0.1000	0.1500	0.2000	0.2500	0.3000	0.3500	0.4000
0.0100	*******	250.380	131.812	79.1408	59.3374	46.8406	38.2731	32.0202	26.9611
0.0200	427.318	185.483	111.632	77.5457	58.5380	46.4085	38.0438	31.6194	26.9460
0.0400	257.576	143.029	94.3044	68.9132	57.1245	45.6269	37.2912	31.1525	26.4219
0.0600	183.944	115.846	73.3720	61.5996	52.0373	44.5734	36.6127	30.7227	26.1687
0.0800	117.036	85.8610	71.5993	60.1298	51.0868	41.4156	35.9977	30.3253	27.0366
0.1000	98.9067	75.1065	64.2606	54.8833	46.9806	40.6175	35.7205	29.9564	26.5711
0.1200	85.6477	66.8977	62.9230	53.8956	46.3098	40.1889	35.1942	29.6127	26.3547
0.1400	75.5372	66.0435	57.2427	53.0360	45.7129	39.8017	34.7106	29.2916	26.1484
0.1600	61.2125	60.1190	56.6108	48.9501	42.3995	39.1840	34.5142	28.9907	25.9512
0.1800	61.2785	59.5918	51.7622	48.3293	41.9568	36.7203	32.3740	28.7079	25.7637
0.2000	56.3151	54.5766	51.3509	47.7755	41.5559	36.4546	32.0018	28.4416	25.3858

CASE 18 $q = 0.80$, $\ell_f/\ell_w = 0.00$ (RECTANGULAR) IN COMPRESSION

Icr/Igross
lf/lw=0.00 g=0.80 fy=275.0 Mpa

Axial Load Ratio Nu/f'm.Ag

fy/f'm	0.0000	0.0500	0.1000	0.1500	0.2000	0.2500	0.3000	0.3500	0.4000
0.0100	0.0208	0.1288	0.2014	0.2543	0.2929	0.3203	0.3370	0.2338	0.2756
0.0200	0.0387	0.1399	0.2098	0.2611	0.2985	0.3249	0.3416	0.2385	0.2796
0.0400	0.0703	0.1610	0.2258	0.2740	0.3095	0.3346	0.3504	0.2469	0.2855
0.0600	0.0981	0.1806	0.2410	0.2863	0.3205	0.3442	0.3592	0.2543	0.2913
0.0800	0.1234	0.1992	0.2558	0.2988	0.3308	0.3538	0.3682	0.2627	0.2982
0.1000	0.1466	0.2169	0.2702	0.3111	0.3416	0.3634	0.3769	0.2712	0.3051
0.1200	0.1683	0.2338	0.2839	0.3227	0.3517	0.3729	0.3857	0.2786	0.3119
0.1400	0.1887	0.2500	0.2976	0.3343	0.3623	0.3824	0.3945	0.2872	0.3187
0.1600	0.2080	0.2657	0.3107	0.3457	0.3723	0.3919	0.4034	0.2946	0.3254
0.1800	0.2264	0.2808	0.3236	0.3569	0.3823	0.4009	0.4122	0.3021	0.3321
0.2000	0.2440	0.2954	0.3360	0.3680	0.3923	0.4104	0.4209	0.3107	0.3400

Mi/f'm.t.lw**2
lf/lw=0.00 g=0.80 fy=275.0 Mpa

Axial Load Ratio Nu/f'm.Ag

fy/f'm	0.0000	0.0500	0.1000	0.1500	0.2000	0.2500	0.3000	0.3500	0.4000
0.0100	0.0049	0.0280	0.0483	0.0658	0.0806	0.0928	0.1021	0.1088	0.1128
0.0200	0.0098	0.0323	0.0519	0.0690	0.0834	0.0951	0.1042	0.1106	0.1144
0.0400	0.0191	0.0404	0.0591	0.0752	0.0887	0.0997	0.1082	0.1142	0.1175
0.0600	0.0280	0.0482	0.0658	0.0810	0.0939	0.1042	0.1121	0.1176	0.1206
0.0800	0.0363	0.0555	0.0723	0.0867	0.0988	0.1086	0.1160	0.1211	0.1238
0.1000	0.0443	0.0625	0.0784	0.0922	0.1037	0.1128	0.1199	0.1246	0.1270
0.1200	0.0518	0.0691	0.0844	0.0974	0.1083	0.1171	0.1236	0.1280	0.1303
0.1400	0.0590	0.0756	0.0901	0.1026	0.1129	0.1212	0.1274	0.1315	0.1335
0.1600	0.0659	0.0818	0.0957	0.1076	0.1174	0.1253	0.1311	0.1349	0.1367
0.1800	0.0725	0.0878	0.1011	0.1124	0.1218	0.1293	0.1348	0.1383	0.1400
0.2000	0.0789	0.0936	0.1063	0.1172	0.1262	0.1333	0.1385	0.1418	0.1433

$\phi u.My/\phi y.Mi$
lf/lw=0.00 g=0.80 fy=275.0 Mpa

Axial Load Ratio Nu/f'm.Ag

fy/f'm	0.0000	0.0500	0.1000	0.1500	0.2000	0.2500	0.3000	0.3500	0.4000
0.0100	69.8687	12.4418	6.2769	3.9945	2.8772	2.2170	1.7803	1.0000	1.0000
0.0200	32.0818	10.1831	5.6555	3.7765	2.7745	2.1639	1.7561	1.0000	1.0000
0.0400	15.1387	7.3958	4.7046	3.3772	2.5915	2.0695	1.7155	1.0000	1.0000
0.0600	9.6744	5.8890	4.1163	3.0914	2.4333	1.9943	1.6777	1.0000	1.0000
0.0800	7.2554	4.9807	3.6597	2.8564	2.3165	1.9351	1.6436	1.0000	1.0000
0.1000	5.8489	4.3502	3.3427	2.6888	2.2154	1.8806	1.6175	1.0000	1.0000
0.1200	4.9943	3.8919	3.0966	2.5388	2.1323	1.8302	1.5929	1.0000	1.0000
0.1400	4.4374	3.5499	2.8891	2.4201	2.0593	1.7914	1.5698	1.0000	1.0000
0.1600	3.9900	3.2640	2.7239	2.3137	1.9996	1.7552	1.5486	1.0000	1.0000
0.1800	3.6521	3.0629	2.5939	2.2293	1.9445	1.7193	1.5339	1.0000	1.0000
0.2000	3.3930	2.8865	2.4755	2.1521	1.8933	1.6873	1.5139	1.0000	1.0000

CASE 19 $g = 0.80\ \ell_f/\ell_w = 1.00$ WEB IN COMPRESSION

Icr/Igross
lf/lw=1.00 g=0.80 fy=275.0 Mpa

Axial Load Ratio Nu/f'm.Ag

fy/f'm	0.0000	0.0500	0.1000	0.1500	0.2000	0.2500	0.3000	0.3500	0.4000
0.0100	0.0362	0.1636	0.2366	0.2767	0.2473	0.3304	0.4067	0.4297	0.4300
0.0200	0.0661	0.1808	0.2483	0.2841	0.2596	0.3362	0.4087	0.4337	0.4335
0.0400	0.1162	0.2120	0.2700	0.1992	0.2824	0.3479	0.4137	0.4415	0.4430
0.0600	0.1582	0.2400	0.2897	0.2246	0.3008	0.3596	0.4185	0.4490	0.4521
0.0800	0.1947	0.2652	0.3079	0.2483	0.3179	0.3702	0.4242	0.4563	0.4608
0.1000	0.2270	0.2883	0.3242	0.2726	0.3331	0.3809	0.4299	0.4633	0.4693
0.1200	0.2561	0.3095	0.3385	0.2956	0.3479	0.3915	0.4377	0.4700	0.4789
0.1400	0.2825	0.3291	0.2429	0.3190	0.3618	0.4021	0.4443	0.4766	0.4867
0.1600	0.3066	0.3474	0.2665	0.3403	0.3748	0.4127	0.4519	0.4842	0.4957
0.1800	0.3290	0.3642	0.2897	0.3554	0.3876	0.4224	0.4596	0.4917	0.5030
0.2000	0.3498	0.3795	0.3124	0.3696	0.4003	0.4329	0.4672	0.4977	0.5115

Mi/f'm.t.lw**2
lf/lw=1.00 g=0.80 fy=275.0 Mpa

Axial Load Ratio Nu/f'm.Ag

fy/f'm	0.0000	0.0500	0.1000	0.1500	0.2000	0.2500	0.3000	0.3500	0.4000
0.0100	0.0138	0.0760	0.1273	0.1678	0.1973	0.2148	0.2227	0.2169	0.2058
0.0200	0.0271	0.0871	0.1364	0.1751	0.2032	0.2181	0.2251	0.2197	0.2085
0.0400	0.0524	0.1081	0.1537	0.1892	0.2139	0.2246	0.2300	0.2253	0.2145
0.0600	0.0759	0.1278	0.1700	0.2025	0.2231	0.2311	0.2350	0.2308	0.2204
0.0800	0.0978	0.1462	0.1853	0.2150	0.2315	0.2374	0.2401	0.2362	0.2262
0.1000	0.1184	0.1637	0.1999	0.2270	0.2395	0.2437	0.2453	0.2416	0.2319
0.1200	0.1379	0.1801	0.2136	0.2385	0.2471	0.2500	0.2507	0.2469	0.2379
0.1400	0.1562	0.1958	0.2269	0.2496	0.2544	0.2562	0.2561	0.2522	0.2435
0.1600	0.1737	0.2106	0.2395	0.2599	0.2616	0.2623	0.2615	0.2577	0.2493
0.1800	0.1903	0.2249	0.2516	0.2678	0.2686	0.2685	0.2670	0.2631	0.2548
0.2000	0.2062	0.2385	0.2633	0.2756	0.2754	0.2746	0.2726	0.2684	0.2605

ϕu.My/ϕy.Mi
lf/lw=1.00 g=0.80 fy=275.0 Mpa

Axial Load Ratio Nu/f'm.Ag

fy/f'm	0.0000	0.0500	0.1000	0.1500	0.2000	0.2500	0.3000	0.3500	0.4000
0.0100	42.6096	5.9147	2.8197	1.7213	1.0000	1.0000	1.0000	1.0000	1.0000
0.0200	20.0595	4.9799	2.5812	1.6400	1.0000	1.0000	1.0000	1.0000	1.0000
0.0400	9.1997	3.8322	2.2447	1.0000	1.0000	1.0000	1.0000	1.0000	1.0000
0.0600	6.0788	3.1314	1.9990	1.0000	1.0000	1.0000	1.0000	1.0000	1.0000
0.0800	4.5817	2.6934	1.8138	1.0000	1.0000	1.0000	1.0000	1.0000	1.0000
0.1000	3.7200	2.3689	1.6687	1.0000	1.0000	1.0000	1.0000	1.0000	1.0000
0.1200	3.1527	2.1292	1.5512	1.0000	1.0000	1.0000	1.0000	1.0000	1.0000
0.1400	2.7718	1.9476	1.0000	1.0000	1.0000	1.0000	1.0000	1.0000	1.0000
0.1600	2.4663	1.8078	1.0000	1.0000	1.0000	1.0000	1.0000	1.0000	1.0000
0.1800	2.2501	1.6840	1.0000	1.0000	1.0000	1.0000	1.0000	1.0000	1.0000
0.2000	2.0663	1.5853	1.0000	1.0000	1.0000	1.0000	1.0000	1.0000	1.0000

CASE 20 g = 0.80, ℓ_f/ℓ_w = 1.00 FLANGE IN COMPRESSION

Icr/Igross
1f/1w-1.00 g-0.80 fy-275.0 Mpa

Axial Load Ratio Nu/f'm.Ag

fy/f'm	0.0000	0.0500	0.1000	0.1500	0.2000	0.2500	0.3000	0.3500	0.4000
0.0100	0.0117	0.0879	0.1455	0.1934	0.2344	0.2692	0.3010	0.3267	0.3476
0.0200	0.0226	0.0962	0.1527	0.1993	0.2400	0.2746	0.3065	0.3304	0.3514
0.0400	0.0431	0.1122	0.1670	0.2121	0.2524	0.2871	0.3157	0.3417	0.3632
0.0600	0.0625	0.1280	0.1805	0.2248	0.2636	0.2980	0.3267	0.3510	0.3729
0.0800	0.0810	0.1433	0.1946	0.2376	0.2760	0.3090	0.3377	0.3623	0.3825
0.1000	0.0989	0.1587	0.2079	0.2502	0.2871	0.3199	0.3469	0.3715	0.3921
0.1200	0.1162	0.1735	0.2212	0.2629	0.2983	0.3308	0.3578	0.3828	0.4016
0.1400	0.1331	0.1883	0.2350	0.2755	0.3107	0.3417	0.3688	0.3920	0.4111
0.1600	0.1496	0.2028	0.2482	0.2871	0.3218	0.3526	0.3798	0.4032	0.4228
0.1800	0.1657	0.2172	0.2612	0.2997	0.3342	0.3635	0.3908	0.4124	0.4322
0.2000	0.1816	0.2315	0.2743	0.3122	0.3453	0.3745	0.3999	0.4236	0.4416

Mi/f'm.t.lw**2
1f/1w-1.00 g-0.80 fy-275.0 Mpa

Axial Load Ratio Nu/f'm.Ag

fy/f'm	0.0000	0.0500	0.1000	0.1500	0.2000	0.2500	0.3000	0.3500	0.4000
0.0100	0.0060	0.0347	0.0615	0.0865	0.1095	0.1309	0.1506	0.1685	0.1848
0.0200	0.0118	0.0402	0.0667	0.0910	0.1138	0.1349	0.1546	0.1725	0.1887
0.0400	0.0234	0.0510	0.0767	0.0999	0.1220	0.1430	0.1624	0.1802	0.1965
0.0600	0.0347	0.0615	0.0860	0.1085	0.1302	0.1509	0.1702	0.1881	0.2043
0.0800	0.0456	0.0717	0.0949	0.1171	0.1384	0.1589	0.1781	0.1957	0.2121
0.1000	0.0563	0.0813	0.1036	0.1254	0.1466	0.1668	0.1857	0.2034	0.2196
0.1200	0.0667	0.0901	0.1121	0.1337	0.1547	0.1746	0.1935	0.2113	0.2274
0.1400	0.0767	0.0988	0.1206	0.1420	0.1626	0.1825	0.2014	0.2190	0.2351
0.1600	0.0856	0.1074	0.1290	0.1502	0.1708	0.1904	0.2090	0.2267	0.2429
0.1800	0.0942	0.1159	0.1373	0.1583	0.1787	0.1982	0.2169	0.2343	0.2507
0.2000	0.1028	0.1243	0.1455	0.1664	0.1866	0.2061	0.2248	0.2423	0.2585

ϕu.My/ϕy.Mi
1f/1w-1.00 g-0.80 fy-275.0 Mpa

Axial Load Ratio Nu/f'm.Ag

fy/f'm	0.0000	0.0500	0.1000	0.1500	0.2000	0.2500	0.3000	0.3500	0.4000
0.0100	218.434	41.0652	21.3236	13.6665	10.2262	7.9523	6.4942	5.4307	4.5900
0.0200	97.6525	33.1101	18.8536	12.8247	9.7476	7.7659	6.3692	5.3112	4.5446
0.0400	45.3360	23.5585	15.2582	11.7140	9.2576	7.4618	6.1748	5.2596	4.5116
0.0600	29.1897	18.7660	13.3956	10.7997	8.7814	7.2465	6.0286	5.1261	4.4550
0.0800	21.4251	15.1276	12.2631	10.0281	8.3969	6.9522	5.8919	5.0838	4.4020
0.1000	16.8898	13.0423	11.2914	9.5284	8.0129	6.7732	5.8038	5.0174	4.3958
0.1200	14.3499	12.0246	10.6734	9.0844	7.6654	6.6069	5.6824	4.9277	4.3486
0.1400	12.1627	11.3925	9.9766	8.6853	7.4889	6.4516	5.5676	4.8698	4.3041
0.1600	11.4163	10.8374	9.6786	8.2953	7.1894	6.3061	5.5243	4.8399	4.2845
0.1800	10.9823	10.3419	9.2449	8.0937	7.0402	6.1692	5.4192	4.7882	4.2440
0.2000	10.5691	9.8941	8.8516	7.7837	6.8739	6.0399	5.2949	4.7111	4.2056

CASE 21 $g = 0.80$, $\ell_f/\ell_w = 2.00$ WEB IN COMPRESSION

Icr/Igross
1f/lw=2.00 g=0.80 fy=275.0 Mpa

Axial Load Ratio Nu/f'm.Ag

fy/f'm	0.0000	0.0500	0.1000	0.1500	0.2000	0.2500	0.3000	0.3500	0.4000
0.0100	0.0504	0.2011	0.2670	0.2888	0.4068	0.4385	0.4439	0.4363	0.4179
0.0200	0.0898	0.2204	0.1828	0.3024	0.4106	0.4428	0.4472	0.4402	0.4245
0.0400	0.1528	0.2540	0.2250	0.3260	0.4181	0.4499	0.4570	0.4515	0.4354
0.0600	0.2026	0.2818	0.2662	0.3453	0.4256	0.4582	0.4649	0.4606	0.4459
0.0800	0.2435	0.3038	0.2988	0.3624	0.4341	0.4651	0.4743	0.4695	0.4561
0.1000	0.2775	0.2256	0.3206	0.3783	0.4415	0.4732	0.4819	0.4800	0.4681
0.1200	0.3065	0.2651	0.3407	0.3923	0.4500	0.4812	0.4909	0.4884	0.4777
0.1400	0.3310	0.3043	0.3583	0.4061	0.4585	0.4892	0.4997	0.4985	0.4892
0.1600	0.3500	0.3363	0.3752	0.4189	0.4680	0.4970	0.5085	0.5083	0.4982
0.1800	0.2668	0.3545	0.3907	0.4316	0.4765	0.5061	0.5170	0.5161	0.5091
0.2000	0.3050	0.3716	0.4056	0.4442	0.4850	0.5138	0.5255	0.5255	0.5177

Mi/f'm.t.lw**2
1f/lw=2.00 g=0.80 fy=275.0 Mpa

Axial Load Ratio Nu/f'm.Ag

fy/f'm	0.0000	0.0500	0.1000	0.1500	0.2000	0.2500	0.3000	0.3500	0.4000
0.0100	0.0225	0.1200	0.1932	0.2402	0.2629	0.2607	0.2514	0.2379	0.2207
0.0200	0.0440	0.1367	0.2056	0.2466	0.2658	0.2637	0.2542	0.2408	0.2246
0.0400	0.0839	0.1676	0.2285	0.2577	0.2717	0.2694	0.2606	0.2478	0.2314
0.0600	0.1202	0.1956	0.2492	0.2673	0.2776	0.2754	0.2665	0.2541	0.2381
0.0800	0.1533	0.2212	0.2650	0.2761	0.2837	0.2810	0.2728	0.2603	0.2447
0.1000	0.1837	0.2446	0.2763	0.2844	0.2897	0.2870	0.2786	0.2670	0.2520
0.1200	0.2115	0.2660	0.2862	0.2923	0.2959	0.2929	0.2848	0.2730	0.2584
0.1400	0.2372	0.2857	0.2958	0.2999	0.3020	0.2988	0.2910	0.2796	0.2655
0.1600	0.2609	0.3013	0.3046	0.3073	0.3083	0.3047	0.2971	0.2860	0.2717
0.1800	0.2829	0.3110	0.3133	0.3146	0.3145	0.3108	0.3031	0.2919	0.2786
0.2000	0.3033	0.3202	0.3215	0.3216	0.3207	0.3167	0.3091	0.2982	0.2846

ϕu.My/ϕy.Mi
1f/lw=2.00 g=0.80 fy=275.0 Mpa

Axial Load Ratio Nu/f'm.Ag

fy/f'm	0.0000	0.0500	0.1000	0.1500	0.2000	0.2500	0.3000	0.3500	0.4000
0.0100	28.2889	3.6616	1.6536	1.0000	1.0000	1.0000	1.0000	1.0000	1.0000
0.0200	13.0336	3.0820	1.0000	1.0000	1.0000	1.0000	1.0000	1.0000	1.0000
0.0400	6.1392	2.3710	1.0000	1.0000	1.0000	1.0000	1.0000	1.0000	1.0000
0.0600	3.9966	1.9372	1.0000	1.0000	1.0000	1.0000	1.0000	1.0000	1.0000
0.0800	2.9849	1.6433	1.0000	1.0000	1.0000	1.0000	1.0000	1.0000	1.0000
0.1000	2.3978	1.0000	1.0000	1.0000	1.0000	1.0000	1.0000	1.0000	1.0000
0.1200	2.0137	1.0000	1.0000	1.0000	1.0000	1.0000	1.0000	1.0000	1.0000
0.1400	1.7444	1.0000	1.0000	1.0000	1.0000	1.0000	1.0000	1.0000	1.0000
0.1600	1.5342	1.0000	1.0000	1.0000	1.0000	1.0000	1.0000	1.0000	1.0000
0.1800	1.0000	1.0000	1.0000	1.0000	1.0000	1.0000	1.0000	1.0000	1.0000
0.2000	1.0000	1.0000	1.0000	1.0000	1.0000	1.0000	1.0000	1.0000	1.0000

CASE 22 g = 0.80, ℓ_f/ℓ_w = 2.00 FLANGE IN COMPRESSION

Icr/Igross
1f/1w=2.00 g=0.80 fy=275.0 Mpa

Axial Load Ratio Nu/f'm.Ag

fy/f'm	0.0000	0.0500	0.1000	0.1500	0.2000	0.2500	0.3000	0.3500	0.4000
0.0100	0.0103	0.0851	0.1399	0.1838	0.2227	0.2560	0.2850	0.3126	0.3326
0.0200	0.0200	0.0924	0.1469	0.1894	0.2283	0.2616	0.2909	0.3158	0.3393
0.0400	0.0384	0.1068	0.1598	0.2022	0.2394	0.2705	0.2999	0.3251	0.3494
0.0600	0.0560	0.1207	0.1716	0.2134	0.2505	0.2818	0.3116	0.3345	0.3593
0.0800	0.0728	0.1349	0.1844	0.2247	0.2616	0.2931	0.3206	0.3468	0.3657
0.1000	0.0892	0.1490	0.1972	0.2374	0.2727	0.3020	0.3295	0.3561	0.3755
0.1200	0.1052	0.1625	0.2090	0.2486	0.2818	0.3132	0.3411	0.3653	0.3851
0.1400	0.1208	0.1759	0.2218	0.2599	0.2929	0.3245	0.3500	0.3744	0.3947
0.1600	0.1361	0.1898	0.2345	0.2711	0.3040	0.3357	0.3617	0.3866	0.4077
0.1800	0.1511	0.2030	0.2462	0.2838	0.3151	0.3446	0.3705	0.3957	0.4172
0.2000	0.1660	0.2162	0.2589	0.2950	0.3262	0.3558	0.3821	0.4047	0.4265

Mi/f'm.t.1w**2
1f/1w=2.00 g=0.80 fy=275.0 Mpa

Axial Load Ratio Nu/f'm.Ag

fy/f'm	0.0000	0.0500	0.1000	0.1500	0.2000	0.2500	0.3000	0.3500	0.4000
0.0100	0.0070	0.0404	0.0715	0.1005	0.1267	0.1510	0.1731	0.1935	0.2113
0.0200	0.0138	0.0468	0.0775	0.1059	0.1313	0.1552	0.1773	0.1974	0.2154
0.0400	0.0273	0.0593	0.0891	0.1160	0.1404	0.1635	0.1852	0.2053	0.2236
0.0600	0.0404	0.0715	0.1005	0.1255	0.1492	0.1717	0.1933	0.2132	0.2313
0.0800	0.0531	0.0833	0.1108	0.1346	0.1577	0.1802	0.2014	0.2211	0.2395
0.1000	0.0654	0.0948	0.1202	0.1434	0.1663	0.1884	0.2093	0.2290	0.2476
0.1200	0.0775	0.1059	0.1292	0.1521	0.1746	0.1963	0.2174	0.2369	0.2553
0.1400	0.0891	0.1155	0.1381	0.1607	0.1829	0.2044	0.2253	0.2448	0.2634
0.1600	0.1005	0.1243	0.1469	0.1692	0.1912	0.2126	0.2331	0.2527	0.2715
0.1800	0.1109	0.1330	0.1554	0.1776	0.1994	0.2208	0.2413	0.2606	0.2791
0.2000	0.1195	0.1419	0.1640	0.1860	0.2076	0.2287	0.2491	0.2685	0.2872

ϕu.My/ϕy.Mi
1f/1w=2.00 g=0.80 fy=275.0 Mpa

Axial Load Ratio Nu/f'm.Ag

fy/f'm	0.0000	0.0500	0.1000	0.1500	0.2000	0.2500	0.3000	0.3500	0.4000
0.0100	195.024	48.5834	24.7119	15.9257	11.9051	9.3981	7.7210	6.4905	5.5879
0.0200	106.834	40.0372	22.2817	14.8020	11.5421	9.1891	7.5880	6.4253	5.5927
0.0400	49.5011	28.0343	17.9262	13.1259	10.6831	8.8775	7.4922	6.3617	5.5473
0.0600	31.9500	21.3149	14.8713	12.2635	10.1419	8.6653	7.3566	6.3017	5.5726
0.0800	24.8233	17.7876	13.1277	11.5405	9.8425	8.3284	7.1647	6.3013	5.4792
0.1000	19.4185	14.8400	12.3639	10.9872	9.3992	8.0850	7.0891	6.2457	5.4401
0.1200	15.9532	12.6987	11.6610	10.4361	9.0955	8.0478	6.9703	6.1930	5.4711
0.1400	13.5501	12.0159	11.1031	9.9455	8.8754	7.8853	6.9036	6.1429	5.4345
0.1600	11.7912	11.4978	10.8121	9.6781	8.6702	7.7307	6.8932	6.1452	5.4457
0.1800	11.0078	11.0056	10.3118	9.4808	8.4777	7.5312	6.7323	6.0982	5.4799
0.2000	10.7044	10.7571	10.0802	9.2495	8.2960	7.5092	6.7247	6.0535	5.4454

APPENDIX (b)

FORTRAN LISTING - FLANGED WALL ANALYSIS PROGRAM

```
c       ***** PROGRAM FOR ANALYSING FLANGED WALLS *****

c       ***** MAIN PROGRAM *****
        dimension vp(11),va(9)
        character*14 ma(6)
        character*21 mb(6)
        common e2,bt,p,g,pl,ep,gi
        common /c1/ r1,r2,zm
        common /c2/ el,fk,ak,an,en
        common /c3/ vr(6,100)
        common /c4/ ar,cu,cv(2,0:1),cv1(10,0:1),qv1(10,0:1)
        common /c5/ qv(2,0:1),cq(3,0:1),dt(10,0:1)
        type *,'rk,tk,zk,fm,fy,bt,zs,fh,hc,sh,ar,pd,ad'
        accept *,rk,tk,zk,fm,fy,bt,zs,fh,hc,sh,ar,pd,ad
        type *,'rk=',rk,'tk=',tk,'zk=',zk,'fm=',fm,'fy=',fy,
     6  'bt=',bt,'zs=',zs,'fh=',fh,'hc=',hc,'sh=',sh,'ar=',ar,
     6  'pd=',pd,'ad=',ad
        g=1.0-bt
        ak=1.0+rk*tk
        fk=rk*tk/bt
        en=0.5*(1.0+rk*tk*bt)/ak
        ep=fy/2.0e5
        gi=(0.5-en)**2+0.083333*(1.0+rk*tk*bt*bt)+rk*tk*(en-
     6  0.5*bt)**2
        r1=1.0+zs*fh/fm
        zm=0.5/((3.0+0.29*fm)/(145.0*fm-1000.0)-0.002*r1+
     6  0.75*zs*sqrt(hc/sh))
        if(r1.eq.1.0)  then
        r2=0.9375
        e1=0.0015
        e2=0.0025
        else
        r2=r1
        e1=0.002*r1
        e2=0.008
        end if
        ma(1)='  Icr/Igross  '
        ma(2)='Mi/f m.t.lw**2'
        ma(3)='  u.My/ y.Mi  '
        ma(4)=ma(1)
        ma(5)=ma(2)
        ma(6)=ma(3)
        mb(1)=' Web in compression  '
        mb(2)=mb(1)
        mb(3)=mb(1)
        mb(4)='Flange in compression'
        mb(5)=mb(4)
        mb(6)=mb(4)
        if(ar.eq.1.0) then
        p=pd
        pl=p*rk*tk*zk
        an=ad
        call coft(0.0)
        call coft(1.0)
        goto 25
        end if
        k=0
        p=0.01
  5     k=k+1
        vp(k)=p
        j=0
        i=9*(k-1)
        pl=p*rk*tk*zk
        do 20 an=0.0,0.4,0.05
        j=j+1
        va(j)=an
        type *,'k=',k,'j=',j,'i+j=',i+j
        call relt(0.0,i+j)
        call relt(1.0,i+j)
  20    continue
        if(p.eq.0.01) then
        p=p+0.01
        else
        p=p+0.02
        end if
        if(p.le.0.2) goto 5
  25    open(unit=1,file='limin.relt',form='formatted',status='new')
        if(ar.eq.1.0) goto 50
        write(1,40) (ma(k),mb(k),rk,g,fy,
     6  (va(i),i=1,9),(vp(i),(vr(k,9*(I-1)+j),j=1,9),i=1,11),k=1,6)
  40    format(////////,17x,'Table',4x,a14,2x,a21,/,
     6  25x,'lf/lw=',f4.2,2x,'g=',f4.2,2x,'fy=',f5.1,' Mpa',//,
     6  28x,'Axial Load Ratio Nu/f m.Ag',/,2x,'fy/f m',9f8.4,//,10f
     6  8.4,/,10f8.4,/,10f8.4,/,10f8.4,/,10f8.4,/,10f8.4,/,
     6  10f8.4,/,10f8.4,/,10f8.4,/,10f8.4,///////)
        if(ar.eq.0.0) goto 70
```

```
 50     write (1,60) (i,pd,ad,zs,fh,hc,sh,rk,tk,zk,fm,fy,g,(cv(j,i)
     6  ,j=1,2),(qv(j,i),j=1,2),(cq(j,i),j=1,3),(dt(j,i),j=1,10),
     6  (cv1(j,i),j=1,10),(qv1(j,i),j=1,10),i=0,1)
 60     format(///,28x,'R=',i2,4x,'pd=',f5.3,4x,'ad=',f5.3,/,
     6  20x,'zs=',f5.3,4x,'fh=',f5.1,4x,'hc=',f5.1,4x,'sh=',f5.1,
     6  /,12x,'k1=',f4.2,4x,'kt=',f4.2,4x,'kz=',f4.2,4x,'fm=',f4.1,
     6  4x,'fy=',f5.1,4x,'g=',f4.2,//,10x,'CURVATURE',2f20.5,/,
     6  10x,'MOMENT',3x,2f20.5,//,10x,'COEFFICINT',3e15.5,//,
     6  10x,'Di=',/,5f16.5,/,5f16.5,//,10x,'Cv=',/,5f16.5,/,5f16.5,
     6  //,10x,'Qv',/,5f16.5,/,5f16.5)
 70     type *,'The End of Calculation'
        stop
        end
c       ***** Subroutine for Result *****
        subroutine relt(r,ij)
        external spy,spu
        common e2,bt,p,g,pl,ep,gi
        common /c3/ vr(6,100)
        cn=root(spy,r)
        if(cn.eq.1.0) then
        vr(3+3*r,ij)=1.0
        cn=root(spu,r)
        if(cn.ge.1.0) vr(3+3*r,ij)=0.0
        vr(2+3*r,ij)=squ(cn,r)
        vr(1+3*r,ij)=9.375e-4*vr(2+3*r,ij)*cn/gi/e2
        return
        end if
        vt=sqy(cn,r)*(1.0-cn-0.5*bt)/ep
        vr(1+3*r,ij)=9.375e-4*vt/gi
        cm=root(spu,r)
        vr(2+3*r,ij)=squ(cm,r)
        vr(3+3*r,ij)=e2*vt/cm/vr(2+3*r,ij)
        return
        end
c       ***** Functions for P-D curve *****
        subroutine coft(r)
        external spy,spu
        common e2,bt,p,g,pl,ep,gi
        common /c4/ ar,cu,cv(2,0:1),cv1(10,0:1),qv1(10,0:1)
        common /c5/ qv(2,0:1),cq(3,0:1),dt(10,0:1)
        ar=0.0
        cn=root(spy,r)
        cm=root(spu,r)
        cv(2,r)=e2/cm
        qv(2,r)=squ(cm,r)
        a=9.375e-4/gi
        cq(1,r)=a
        if(cn.eq.1.0) then
        ar=1.0
        cv(1,r)=0.75*cv(2,r)
        cu=cv(1,r)
        cm=root(spu,r)
        qv(1,r)=squ(cm,r)
        else
        cv(1,r)=ep/(1.0-cn-0.5*bt)
        qv(1,r)=sqy(cn,r)
        end if
        ar=1.0
        do 10 i=1,5
        cv1(i,r)=i*0.2*cv(1,r)
 10     cv1(i+5,r)=cv(1,r)+i*0.2*(cv(2,r)-cv(1,r))
        do 20 i=1,10
        cu=cv1(i,r)
        cm=root(spu,r)
 20     qv1(i,r)=squ(cm,r)
        do 30 i=1,10
        if(i.eq.1) then
        dt(1,r)=0.33333*cv1(i,r)
        else
        t=qv1(i-1,r)/qv1(i,r)
        s=(cv1(i,r)-cv1(i-1,r))/(qv1(i,r)-qv1(i-1,r))
        dt(i,r)=dt(i-1,r)*t*t+0.5*(1.0-t*t)*(cv1(i-1,r)-
     6  s*qv1(i-1,r))+0.33333*s*qv1(i,r)*(1.0-t**3)
        end if
 30     continue
        t=0.0
        do 40 i=5,10
        if(dt(i,r).gt.t) then
        t=dt(i,r)
        k=i
        end if
 40     continue
        cq(2,r)=dt(k,r)-dt(5,r)*qv(2,r)/qv(1,r)
        cq(3,r)=cv1(k,r)-cv(1,r)*qv(2,r)/qv(1,r)
        cq(2,r)=cq(2,r)/cq(3,r)
        cq(3,r)=1.0-sqrt(1.0-2.0*cq(2,r))
        ar=1.0
```

```
      return
      end
c     ***** Function for CN *****
      function root(cyu,r)
      x0=0.0001
      y0=cyu(x0,r)
 10   x0=x0+0.09999
      if(y0.eq.1000.0) then
      type *,'NO ROOT'
      root=1.0
      return
      end if
      y1=cyu(x0,r)
      type *,'x0=',x0,'y1=',y1
      if(y1*y0.lt.0.0.or.y1.eq.0.0) goto 20
      y0=y1
      goto 10
 20   x1=x0-0.1
      x2=x0
      y0=cyu(x1,r)
 30   x=0.5*(x1+x2)
      y=cyu(x,r)
      if(y*y0.gt.0.0) x1=x
      if(y*y0.lt.0.0) x2=x
      if(x2-x1.gt.0.001) goto 30
      root=x
      type *,'x=',x
      return
      end
c     ***** function for Axial Forces ******
      function p1(e)
      common /c1/ r1
      p1=533.33*e*e-88888.9*e**3/r1
      return
      end
      function p2(e)
      common /c1/ r1,r2,zm
      common /c2/ e1
      p2=1.067*r2*((1.0+e1*zm)*(e-e1)-0.5*zm*(e*e-e1*e1))
      return
      end
      function py(cn,r)
      common e2,bt,p,g,p1
      et=1.0-cn-0.5*bt
      ct=cn-0.5*bt
      if(cn.le.0.5) then
      py=0.5*p*ct*ct/g/et+p1*r*ct/et
      else
      py=0.5*p*et/g+p*(2.0*cn-1.0)/g+p1*r
      end if
      return
      end
      function pu(e2,cn,r)
      common e0,bt,p,g,p1,ep
      cc=cn*ep/e2
      ct=cn-0.5*bt
      if(cc.le.ct) then
      pu=p1*r+p*(ct-0.5*cc)/g
      else if(cn.ge.0.5*bt/(1.0+ep/e2)) then
      pu=e2*p1*r*ct/cn/ep+0.5*e2*p*ct*ct/g/cn/ep
      else
      pu=-p1*r-p+p*(1.0-cn-0.5*bt-0.5*cc)/g
      end if
      return
      end
      function pt(e2,cn,r)
      common e0,bt,p,g,p1,ep
      et=1.0-cn-0.5*bt
      cc=cn*ep/e2
      if(cc.le.et) then
      pt=p1*(1.0-r)+p*(et-0.5*cc)/g
      else if(cc.le.cn-1.0+0.5*bt) then
      pt=p*(cn-0.5*bt-0.5*cc)/g-p-p1*(1.0-r)
      else
      pt=e2*p1*(1.0-r)*et/cn/ep+0.5*e2*p*et*et/g/cn/ep
      end if
      return
      end
      function spy(cn,r)
      common e2,bt,p,g,p1,ep
      common /c2/ e1,fk,ak,an
      et=1.0-cn-0.5*bt
      re=ep/et
      ce=(cn-bt)*re
      ct=cn*re
      ek=1.0+fk*r
      sum=ak*an+p1*(1.0-r)+0.5*p*et/g
      t1=p1(cn*re)/re
      t2=p2(cn*re)/re
      if(ct.le.e1) then
      continue
```

```
      if(cn.ge.bt) then
      pm=t1*ek-r*fk*p1(ce)/re
      else
      pm=t1*ek
      end if
      continue
      else if(ct.le.e2) then
      continue
      if(ce.ge.e1) then
      pm=p1(e1)/re+t2*ek-r*fk*p2(ce)/re
      else
      pm=(p1(e1)/re+t2)*ek-r*fk*p1(ce)/re
      end if
      continue
      else
      spy=1000.0
      return
      end if
      spy=sum-pm-py(cn,r)
      return
      end
      function spu(cn,r)
      common e0,bt
      common /c2/ e1,fk,ak,an
      common /c4/ ar,cu
      if(ar.eq.0.0) then
      e2=e0
      else
      e2=cn*cu
      end if
      re=e2/cn
      ce=(cn-bt)*re
      if(e2.ge.e1) then
      t=(p1(e1)+p2(e2))/re
      else
      t=p1(e2)/re
      end if
      ek=1.0+fk*r
      cet=(cn-1.0+bt)/cn
      ceo=(cn-1.0)/cn
      if(ce.ge.e1) then
      pm=(p1(e1)+p2(e2)*ek-r*fk*p2(ce))/re
      else if(cn.ge.bt) then
      pm=t*ek-r*fk*p1(ce)/re
      else
      pm=t*ek
      end if
      if(cn.ge.1.0) pm=pm-p1((cn-1.0)*e2/cn)/re
      if(r.eq.0.0.and.cn.ge.1.0-bt) then
      continue
      if(ceo.ge.e1/e2) then
      pm=(p2(e2)+p2(cet*e2)*fk-(1.0+fk)*p2(ceo*e2))/re
      else if(cet.ge.e1/e2) then
      pm=(p2(e2)+p2(cet*e2)*fk+(1.0+fk)*(p1(e1)-p1(ceo*e2)))/re
      else if(cn.ge.1.0) then
      pm=t+(p1(cet*e2)*fk-(1.0+fk)*p1(ceo*e2))/re
      else
      pm=t+p1(cet*e2)*fk/re
      end if
      continue
      end if
      spu=ak*an+pt(e2,cn,r)-pm-pu(e2,cn,r)
      return
      end
c     ***** Function for Moments *****
      function q1(e)
      common /c1/ r1
      q1=355.56*e**3-66666.7*e**4/r1
      return
      end
      function q2(e)
      common /c1/ r1,r2,zm
      common /c2/ e1
      q2=1.067*r2*(0.5*(1.0+e1*zm)*(e*e-e1*e1)-0.33333*zm*(e**3-
     6 e1**3))
      return
      end
      function qy(cn,r)
      common e2,bt,p,g,p1
      ct=cn-0.5*bt
      et=1.0-cn-0.5*bt
      if(cn.le.0.5) then
      qy=0.33333*p*ct**3/g/et+p1*r*ct*ct/et
      else
      qy=0.33333*p*et*et/g+p*(cn-0.5)+p1*r*ct
      end if
      return
      end
```

```
      function qu(e2,cn,r)
      common e0,bt,p,g,pl,ep
      ct=cn-0.5*bt
      cc=cn*ep/e2
      if(cc.le.ct) then
      qu=pl*r*ct+0.5*p*(ct*ct-0.33333*cc*cc)/g
      else if(cn.ge.0.5*bt/(1.0+ep/e2)) then
      qu=r*e2*pl*ct*ct/cn/ep+0.33333*p*e2*ct**3/g/cn/ep
      else
      qu=pl*r*(0.5*bt-cn)-0.5*p*((1.0-cn-0.5*bt)**2-cc*cc/3.0)/g
     6 +p*(0.5-cn)
      end if
      return
      end
      function qt(e2,cn,r)
      common e0,bt,p,g,pl,ep
      et=1.0-cn-0.5*bt
      cc=cn*ep/e2
      if(cc.le.et) then
      qt=pl*(1.0-r)*et+0.5*p*(et*et-0.33333*cc*cc)/g
      else if(cc.le.cn-1.0+0.5*bt) then
      qt=-0.5*p*((cn-0.5*bt)**2-0.33333*cc**2)/g+p*(cn-0.5)+pl
     6 *(cn-1.0+0.5*bt)*(1.0-r)
      else
      qt=pl*(1.0-r)*et*et*e2/cn/ep+0.33333*p*et**3*e2/g/cn/ep
      end if
      return
      end
      function sqy(cn,r)
      common e2,bt,p,g,pl,ep
      common /c2/ e1,fk,ak,an,en
      et=1.0-cn-0.5*bt
      re=ep/et
      ct=cn*re
      ce=(cn-bt)*re
      ek=1.0+fk*r
      sum=ak*an*((1.0-en-cn)*(1.0-r)+(en-cn)*r)+pl*(1.0-r)*et
     6 +0.33333*p*et*et/g
      t1=q1(cn*re)/re/re
      t2=q2(cn*re)/re/re
      if(ct.le.e1) then
      continue
      if(cn.ge.bt) then
      qm=t1*ek-r*fk*q1(ce)/re/re
      else
      qm=t1*ek
      end if
      continue
      else
      continue
      if(ce.ge.e1) then
      qm=q1(e1)/re/re+t2*ek-r*fk*q2(ce)/re/re
      else
      qm=(q1(e1)/re/re+t2)*ek-r*fk*q1(ce)/re/re
      end if
      continue
      end if
      sqy=sum+qm+qy(cn,r)
      return
      end
      function squ(cn,r)
      common e0,bt
      common /c2/ e1,fk,ak,an,en
      common /c4/ ar,cu
      if(ar.eq.0.0) then
      e2=e0
      else
      e2=cn*cu
      end if
      re=e2/cn
      ce=(cn-bt)*re
      ek=1.0+fk*r
      ceo=(cn-1.0)/cn
      cet=(cn-1.0+bt)/cn
      if(e2.ge.e1) then
      t=(q1(e1)+q2(e2))/re/re
      else
      t=q1(e2)/re/re
      end if
      if(ce.ge.e1) then
      qm=(q1(e1)+q2(e2)*ek-r*fk*q2(ce))/re/re
      else if(cn.ge.bt) then
      qm=t*ek-r*fk*q1(ce)/re/re
      else
```

```
      qm=t*ek
      end if
      if(cn.ge.1.0) qm=qm-ql((cn-1.0)*e2/cn)/re/re
      if(r.eq.0.0.and.cn.ge.1.0-bt) then
      continue
      if(ceo.ge.el/e2) then
      qm=(q2(e2)+q2(cet*e2)*fk-(1.0+fk)*q2(ceo*e2))/re/re
      else if(cet.ge.el/e2) then
      qm=(q2(e2)+q2(cet*e2)*fk+(1.0+fk)*(ql(el)-ql(ceo*e2)))/re/re
      else if(cn.ge.1.0) then
      qm=t+(ql(cet*e2)*fk-(1.0+fk)*ql(ceo*e2))/re/re
      else
      qm=t+ql(cet*e2)*fk/re/re
      end if
      continue
      end if
      squ=ak*an*((1.0-cn-en)*(1.0-r)+(en-cn)*r)+qt(e2,cn,r)
     6 +qm+qu(e2,cn,r)
      return
      end

c     ***** The End of Program *****
```